The lithospheric structure of Africa: Mapping crustal and lithospheric thickness using geoid and elevation constraints together with a thermal analysis

Jan Globig

The lithospheric structure of Africa: Mapping crustal and lithospheric thickness using geoid and elevation constraints together with a thermal analysis.

Submitted by:

Jan Globig[1]

Dissertation submitted to the Faculty of Geology of the University of Barcelona

to obtain the Degree of Doctor of Philosophy (PhD) in Earth Sciences

Supervisors:

Prof. Dr. Manel Fernàndez Ortiga [1]

Dr. Montserrat Torné Escasany[1]

Tutor:

Dr. Juan José Ledo Fernández [2]

UNIVERSITAT DE BARCELONA

This thesis was written at the Institute of Earth Sciences Jaume Almera (ICTJA)

Consejo Superior de Investigaciones Científicas (CSIC)

1 Institute of Earth Sciences Jaume Almera

2 Department of Geodynamics and Geophysics of the University of Barcelona

June 2016

To my family,

friends, and sincere supporters.

"Was lange währt, braucht seine Zeit." - Jafar Globán

Acknowledgments

First of all I have to admit that this thesis probably would never have come to existence without the ambitious and enthusiastic engagement of Claudio Faccenna and Francesca Funiciello, and of course all the PIs involved, who took the unique initiative to launch the innovative TOPOMOD project.

Special thanks are dedicated to my first supervisor Manel Fernandez, who had the courage to accept me as his PhD student and who guided me, together with my second supervisor Montserrat Torne, with patience and diligence through a live changing period of my carrier.

Furthermore, I want to acknowledge my fellow students from the TOPOMOD project and my Almera colleagues for all the social energy that was created and shared among us inside a vibrant and inspiring young researcher's environment. Special thanks are delivered to Alberto Carballo and Lavinia Tunini, my first office mates in the beginning. I always looked up to you, because you were constantly a step ahead of me. Thanks to Alexandra Robert, who successfully brokered between ME and GMT and my warmest gratitude to my dear friend, TOPOMOD fellow and flatmate Siddique Akthar Ehsan, who was the most fascinating character that I was allowed to experience throughout my time as a PhD student.

But how would my period as PhD student and this thesis have looked like without the beauty of Barcelona and the incredible support of my friends and my family? Well, the answer is obsolete, because you were all there, always next to me all along my way, regardless of whether you could follow it or not. Thank you so much for this truly amazing time. You made my live complete and I am looking forward with optimism to continue in future what we started yesterday. Fröhlichste Grüsse to my best Barna friends Arnau, Laura, Xavi, Nadine, Yohann, Dimmi and Roman and to my entourage Martin, Toni, Raik, Frank, Erik, Robert, Anton, Mami, Papi, Omi, Kai, natürlich auch an alle, die ich nicht aufgezählt habe (ihr wisst schon wer), und vorallem Fäulein Sophia, die wahrlich faszinierendenste Entdeckung während meines Studienaufenhaltes in Barcelona. Danke Cariño ;)

Funding:

From 2011 to 2014, the author of this thesis was an Early Stage Researcher (ESR) in the ITN TOPOMOD project “Sculpting the Earth’s topography: Insights from modelling deep-surface processes”, and was funded by the European Commission grant Marie Curie Actions (264517-TOPOMOD-FP7-PEOPLE-2010-ITN).

Table of Contents

Summary

Summary

The African continent preserves a >3.7 Ga long geological record, which comprises stabilization of oldest crust in the Archean, late Proterozoic joining of first cratonic units that lead to the formation of Gondwana and later the supercontinent Pangea, and post-breakup Mesozoic and Cenozoic continental rifting with transition to active oceanic spreading in the Afar and Red Sea region. Today, most of Africa's basement consists of Archean cratons and blocks flanked by Proterozoic mobile belts and is considered to be tectonically stable, as it largely escaped tectonothermal deformation since the late-Precambrian Pan-African orogeny. Yet, Africa is affected by a number of active processes, many of them as young as the Cenozoic Era, including widespread hotspot volcanism, active rifting in East Africa, large-scale doming in eastern and sub-equatorial Africa and intracratonic subsidence in the Congo. The link between old Precambrian stable basement and recent tectonic activity makes Africa an ideal laboratory to study the role of the crustal and lithospheric mantle structure on the observed deformation within the continent.

The main goal of this thesis is to provide new crustal and lithospheric thickness maps of the African mainland based on integrated modelling of elevation and geoid data and thermal analysis. The approach assumes local isostasy, thermal steady-state, and linear density increase with depth in the crust and temperature-dependent density in the lithospheric mantle. The obtained results are constrained by a new comprehensive compilation of seismic Moho-depth data consisting of 551 data points from active and passive source seismic experiments, and by published tomography models relative to lithosphere thickness.

The calculated crustal thickness map shows a north-south bimodal distribution with higher thickness values in the cratonic domains of southern Africa (38 - 44 km) relative to those beneath northern Africa (33 - 39 km). The most striking result is the crustal thinning (28 - 30 km thickness) imaged along the Mesozoic West and Central African Rift Systems. The crustal model shows noticeable differences when compared to previous global and continent-scale models, especially for regions to the north of the equator. After excluding the Afar

plume region, where the modeling assumptions are not fulfilled, the model shows the best fit with the available seismic data (76.3% fitting; RMSE=4.3 km). The new crustal thickness map correlates better with geological structures and tectonic provinces as well as gravity anomalies, and shows a higher spatial resolution.

The resulting lithospheric thickness map shows large spatial variability (90 to 230 km), with thicker lithosphere related to cratonic domains and shallower LAB related to Mesozoic and Cenozoic rifting domains, which is in good agreement with seismic tomography models. Though the crustal and lithosphere thickness maps show similar regional patterns, major differences are found in the Atlas Mountains, the West African Rift System, and the intracratonic basins, i.e., the Taoudeni and Congo Basin, indicating strong strain partitioning most probably due to intra-lithospheric decoupling along the crust-mantle boundary. The effects of lateral variations in crustal density as well as the non-isostatic contribution to elevation in the Afar plume region, was estimated to be ~1.8 km, and are also discussed.

Chapter 1. Introduction

Chapter 1. Introduction

1.1 Motivation

The current crust and lithosphere mantle structure of the African continent results from a complex >3.7 billion year old geodynamic history involving: i) juvenile crust formation and craton stabilization during the Archean; ii) extensive crustal reworking during the Proterozoic; iii) Pan-African assemblage followed by Mesozoic break-up of the Gondwana supercontinent; and iv) Cenozoic widespread volcanism, uplift and continental rifting. The African lithospheric structure has been the target of various continental and global studies, but large parts of the continent still remain unknown because of the lack of seismic studies in vast regions of the continent.

Since the first seismic experiments in the Kaapvaal Craton (Willmore et al., 1952) and the East African Rift System (Dopp, 1964), investigation of the crustal and upper mantle structure focused on hotly debated processes shaping the African continent, such as the formation of crust and craton stability during the Archean, the anomalous swell topography (e.g., the African Superswell), the crust/mantle strain partitioning related with the successive tectonic episodes, and the Cenozoic hotspot volcanism and active rifting. The precise knowledge of the current variations of the average density and thickness of the crust and the lithospheric mantle of the different tectonic units throughout the African continent is a major contribution in understanding these processes.

Thanks to an increased number of seismic experiments (e.g., KRISP, EAGLE, MAMBA, Africa-Array, SASE) information on the African crustal structure and its diverse characteristics has improved significantly in some regions. However, available seismic data come from stations that are regionally concentrated in four regions, namely the Rif-Tell-Atlas in northern Africa, the East-Africa Rift System, the Kaapvaal-Zimbabwe Craton, and the Cameroon region in west Africa. To bridge data-sparse areas, different regional and continental-scale crustal models exist for Africa or can be developed by extracting this information from global models. The existing crustal models, mainly seismological, gravity-

based, or some combination of the two, provide homogeneous coverage but show significant differences depending on the modelling technique, the resolution, and the data-type used to extrapolate the seismic estimates to the vast unsampled regions (van der Meijde et al., 2015). Nevertheless, they share the advantage of incorporating a variety of information of crustal properties with high spatial resolution, allowing the depth of subsurface discontinuities, such as the Moho and the LAB, beneath data-absent regions to be estimated.

Interestingly, a comparison between existing crustal models for Africa shows remarkable variations in regions were no seismic data are available, especially between global and continental models. Recently, van der Meijde et al. (2015) pointed out that these differences may be up to 28 km in Moho depth, and that gravity-based models actually show less variation between them than that seen when comparing seismic models or combined gravity-based and seismic models. As there is almost no control on the quality of the resulting structure in sparse seismic regions, these authors warn that the impact of these differences for geodynamic interpretation might be significant.

Looking deeper, the structure of the sub-crustal lithosphere beneath Africa is even less well understood. Similar to the Moho maps, the choice of data and approach used has a strong influence on the final model when trying to resolve the poorly constrained topography of the LAB (Eaton et al., 2009).

The purpose of this thesis is to present new insights into the present-day structure of the crust and lithosphere beneath the African continent. In the absence of seismic information alternative high-resolution data sets sensitive to the density structure of the lithosphere are available for the entire continent and can be used to gain additional knowledge on sub-surface structures to bridge these off-data regions. Therefore, in this work joint modelling of elevation and geoid anomaly data together with a thermal analysis under the assumption of local isostasy will be used to map lateral variations in the geometry of the crust-mantle boundary and the lithosphere-asthenosphere boundary (Fullea et al., 2007). The resulting thickness maps will be compared with recent continental and global scale models of crustal and lithospheric thickness to discuss the differences in terms of their geodynamic implications.

1.2. Objectives

The main goal of this thesis is to provide crustal and lithospheric thickness maps of the African continent that are consistent with the available seismic estimates and tomography models, as well as with elevation and geoid data, to ensure their validity on the vast unexplored regions (~80% of Africa), where existing crustal and lithospheric models predict contradicting results.

In this respect the following main objectives were defined:

I. *To carry out a comprehensive compilation of seismic crustal thickness:* Gathering information on Moho depth in Africa from available deep seismic sounding (DSS) and receiver function (RF) studies in order to tie and better evaluate the accuracy of the crustal thickness model.

II. *To derive crustal and lithospheric thickness maps via 1D joint modelling of elevation and geoid anomaly data together with thermal analysis:*

   a) Determining the appropriate lithospheric reference column for continen-tal Africa and definition of the physical input parameters (density, thermal conductivity and radiogenic heat production).

   b) Investigating the influence of sediment thickness and 2D lateral density variations by incorporating information on sediment thickness and crustal densities from the global model CRUST1.0 to improve the crustal thickness model.

III. *Comparison with previous models to discuss the differences and their geodynamic implications:*

   a) Comparing the obtained crustal thickness model with most recent gravity-based models for Africa and the global model CRUST1.0.

   b) Comparing the obtained LAB geometry with continental and global-scale estimates of lithospheric thickness from surface-wave tomography and heat flow measurements.

1.3. Structure of the thesis

The contextual framework of this thesis is organized as follows:

Chapter 2 summarizes the geological history of the African continent from the Archean to the Cenozoic and provides an overview about the distribution and location of Precambrian tectonic units such as cratons and surrounding mobile belts and younger to recent features such as volcanism and active rifts.

Chapter 3 provides an introduction into the fundamental parameters under study and presents the applied methodology together with the basic geophysical assumptions. In a first part the different definitions of the main lithospheric discontinuities, the *crust-mantle boundary* (CMB) and the *lithosphere-asthenosphere boundary* (LAB), are reviewed to provide an overview of their physico-chemical properties and the existing ambiguities regarding their nature, especially in the case of the LAB. Furthermore, a brief introduction into the necessary geophysical concepts and assumptions, such as *local isostasy*, *geoid*, and the *thermal state* of the lithosphere is given to connect to the second part in which the applied methodology is presented.

Chapter 4 introduces the set of input data, geoid and elevation, that are used in the modelling procedure. Furthermore, available crustal parameters such as sediment thickness and crustal densities are presented together with an extensive review of the actual knowledge of the crustal structure and available point estimates of crustal thickness in Africa from seismic experiments.

Chapter 5 gives a summary of previous studies, who attempted to model the lithospheric structure beneath the African continent. For this purpose, all available continental and global-scale *crustal* and *lithospheric thickness models* based on different datasets are presented to highlight the existing differences in resolution and predicted structures.

Chapter 6 presents the obtained *crustal* and *lithospheric thickness maps* from the 1D joint modelling of elevation and geoid anomaly data. In a first step, the choice of an optimal lithospheric reference column for Africa and the influence of sediments and lateral changes in density distribution will be explained. In the

following, the final model parameter setup will be presented and the obtained crustal model will be compared with the available seismic data across Africa to evaluate its accuracy and the regional trend in data fitting. Finally, the modelled variations in Moho and LAB geometry are presented and locally compared where knowledge on crustal and lithospheric thickness is available.

Chapter 7 discusses the significance of the obtained results within a critical comparison with existing crustal and lithospheric thickness models. Furthermore, observed misfits with seismic data will be discussed in terms of processes that influence the crustal density structure and cause departure from local isostasy.

Chapter 8 summarizes the main findings and concluding remarks obtained throughout the course of the presented study and also provides some recommendations for further work in future.

This PhD thesis is a contribution to the Innovative Training Network project TOPOMOD and was funded by the European Commission grant Marie Curie Actions (264517-TOPOMOD-FP7-PEOPLE-2010-ITN). During the course of this project a manuscript has been submitted for publication to the Journal of Geophysical Research (JGR) - Solid Earth and is currently under revision: Globig, J., Fernandez, M., Torne, M., Vergés, J., Robert, A. and Faccenna, C. (2016). "New insights into the crust and lithosphere mantle structure of Africa from elevation, geoid and thermal analysis."

During my Ph.D. project, I also spent a three-month long secondment at the laboratory of experimental tectonics (LET) at the University of Roma Tre in 2013, during which the transfer of normal stresses through the lithosphere, caused by a rising sublithospheric density anomaly was investigated by the use of analogue models. Results obtained from the conducted experiments were summarized in a manuscript for possible publication, which was submitted to Geophysical Research Letters (GRL) and is currently under revision: A. Sembroni, A. Kiraly, C. Faccenna, F. Funiciello, J. Globig and M. Fernandez (2016) “Impact of the lithosphere on the dynamic topography: Insights from analogue modeling.”

Chapter 2. Geological setting

Chapter 2. Geological setting

The African continent as it exists today is the results of a complex >3.7 billion year old history from juvenile crust formation and craton stabilization in the Archean, extensive crustal reworking during the Proterozoic, Pan-African accretion followed by Mesozoic break-up of the Gondwana supercontinent and Cenozoic widespread volcanism, uplift and continental rifting (Fig. 2.1).

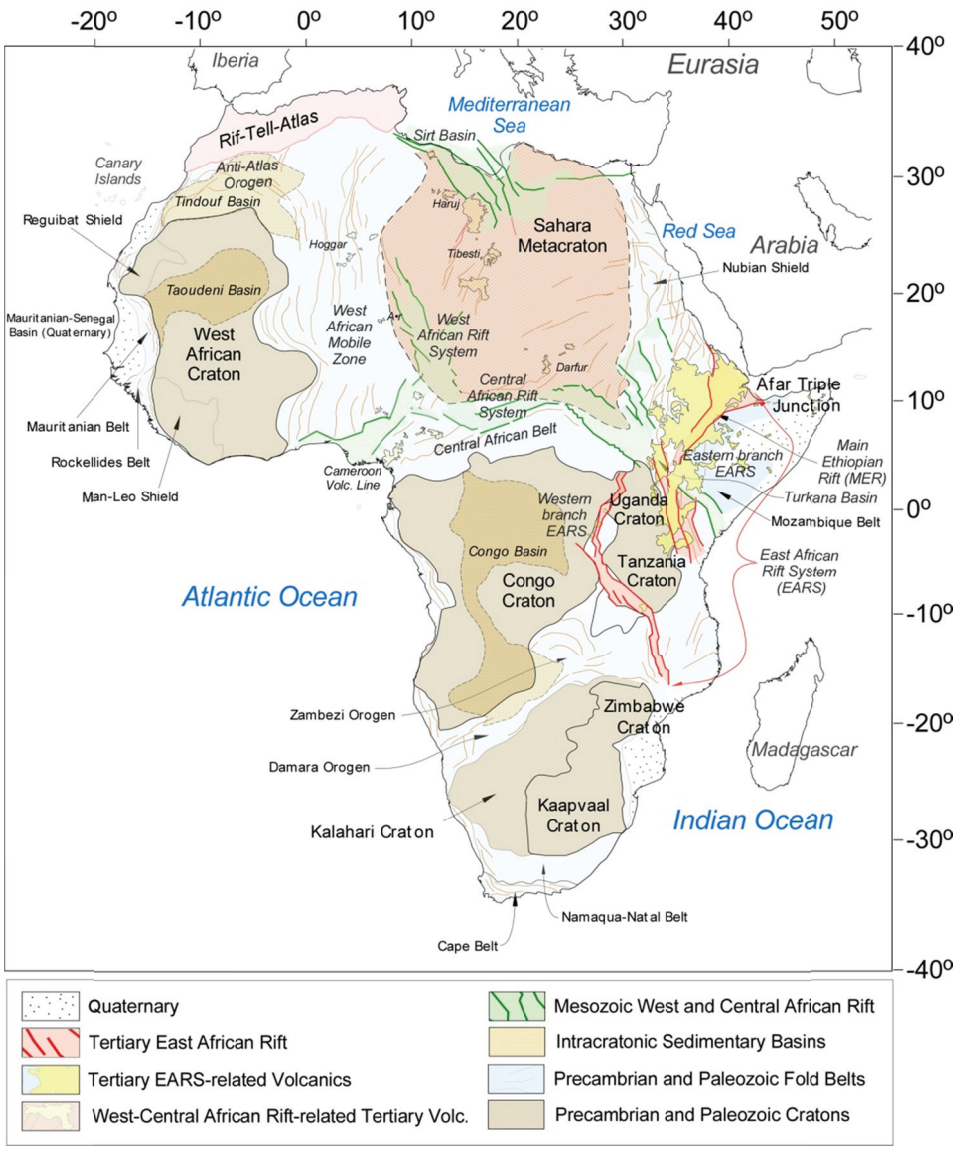

Figure 2.1. Simplified tectonic map of Africa based on Milesi et al. (2010) showing the location and extent of the Archean Cratons, intracratonic basins and the surrounding Precambrian and Paleozoic fold belts, which were affected by rifting processes during Mesozoic and Cenozoic times and Cenozoic volcanism. Figure was taken from Globig et al. (2016).

Africa is an assemblage of Precambrian cratons and fragments separated by Proterozoic and Palaeozoic mobile belts. Apart from oblique conversion between Eurasia and northern Africa at 2 to 6 mm/yr (Nocquet and Calais, 2003; McClusky et al., 2003) the continent is surrounded by divergent plate boundaries, predefined during Mesozoic break-up of Gondwana and the coeval opening of the Southern and Central Atlantic. Currently, continental break-up and rifting occurs along the boundary between the Nubian and Somalian plates, marked by the 5000 km long East African Rift System (EARS). In the following subsections I will briefly describe the most remarkable tectonic features, highlighting their significance in relation to Africa's current lithospheric structure and anomalous topographic features.

2.1 Archean cratons

The Precambrian history of Africa can be divided into Archean crust formation and the stabilization of the first cratonic cores followed by their Proterozoic assemblage, which created the surrounding collisional fold belts. The continent's core is mainly composed of the West African and Saharan Metacraton, located in northern Africa, Congo Craton, Kaapvaal plus Zimbabwe Cratons and some smaller Archean fragments, such as the Tanzania and Uganda Cratons and the Bangweleu and Limpopo microcontinents, located in southern Africa (Fig. 2.2).

The Archean core of Northern Africa is made up of the West African Craton (WAC) and the Saharan Metacraton separated by the West African Mobile Zone (WAMZ). Archean rocks of the WAC are exposed in the north-western Reguibat (3.52 - 2.84 Ga) and south-western Man Leo Shield (>3.0 Ga). The centre of the less rigid portion of the craton, is overlain by the Neoproterozoic Taoudeni Basin (Fig. 2.1), which is a typical intracratonic depression (MacGregor, 1998) filled with ~3 km of Neoproterozoic to Palaeozoic deposits. The basin is partly underlain by cratonic basement of the Reguibat Shield and shows regional-scale Pan-African tilting (Mann et al., 2003) with two periods of large-scale depression: the infra-Cambrian and the Palaeozoic depression (Mann et al., 2003). Apart from confined contact-metamorphism during Mesozoic diabase intrusions the sediments were

not affected by tectonism and show continuous succession (Waters and Schofield, 2004).

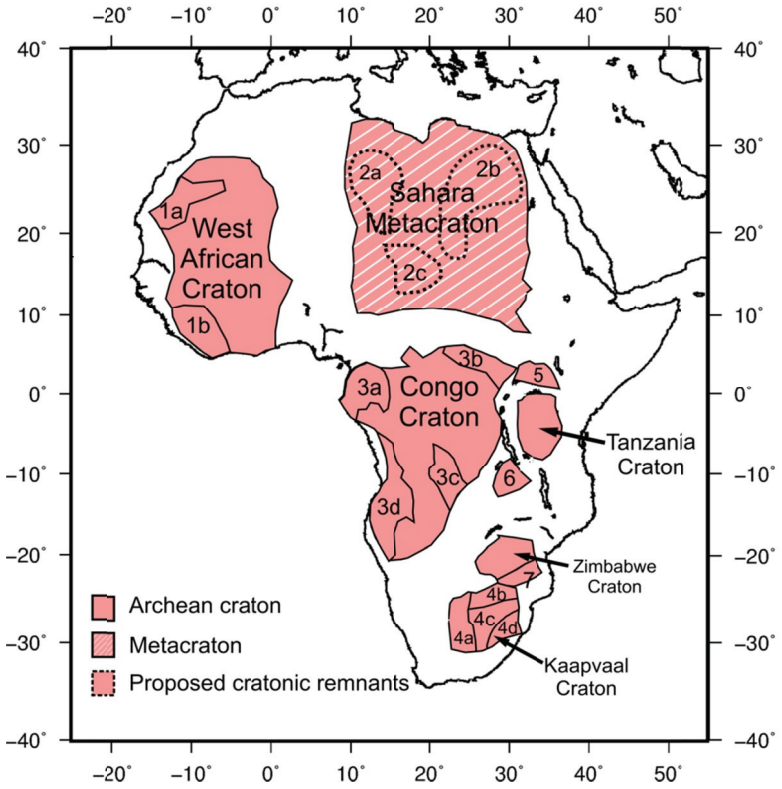

Figure 2.2. Simplified map of African Archean cratons and blocks. West African Craton (1a-Reguibat Shield; 1b- Man Leo Shield); Sahara Metacraton (2a-Murzuq Craton; 2b-Al Kufrah Craton; 2c-Chad Craton); Congo Craton (3a-Gabon Cameroon Shield; 3b-Bomu-Kibalian Shield; 3c-Kasai Shield; 3d-Angolan Shield); 5-Uganda Craton; 6- Bangweleu Block; 7-Limpopo Block; Kaapvaal Craton (4a-Kimberley Terrain; 4b-Pietersburg Terrain; 4c-Witwatersrand Terrain, 4d-Swaziland Terrain).

The Saharan Metacraton (Abdelsalam et al., 2002) to the east of the WAC is a poorly known ~5,000.000 km^2 tract of continental crust. The pre-Neoproterozoic character of its cratonic units (Murzuq, Al Kufrah and Chad Cratons, Fig 2.2) suggests a pre-existing Saharan Craton that was remobilized by surrounding Neoproterozoic collision, possibly leading to delamination or convective removal of negativly buoyant metasomatised cratonic lithosphere (Lucassen et al., 2008; Begg et al., 2009; Shang et al., 2010; Fezaa et al., 2010; Abdelsalam et al., 2011).

In Central Africa the Congo Craton comprises most of the landmass and is almost entirely surrounded and partly indented by Pan-African foreland belts. It amalgamated between 2.1 Ga and 1.8 Ga and the four Archean blocks (Fig. 2.2),

located at its margins were extensively affected during the Paleoproterozoic.

Big parts of the Craton are covered by the Proterozoic Congo Basin (~1.2 million km^2), an intracontinental depression, filled up with 4 to 9 km of Proterozoic to Neogene sediments. The basin is related with a long-wavelength negative gravity anomaly and experienced very slow subsidence since the Pan-African event, probably due to moderate extension of thick lithosphere (Crosby et al., 2010; Kadima et al., 2011). The long subsidence history (~0.5 Ga) of the Congo Basin, which differs from other sag basins and is not well understood, yet it but might be associated either with a downwelling mantle plume (Hartley and Allen, 1994) or with a high-density anomaly within the lithosphere (Downey and Gurnis, 2009). Wide areas of the southern Congo Craton are covered by Cretaceous to Cenozoic sediments of the vast Kalahari Basin.

The ~2.6 Ga Tanzania Craton is located between the Eastern and Western branches of the East African Rift System. Whereas the craton remained stable, the surrounding lithosphere was reworked during several Mesoproterozoic tectonothermal events (Kokonyangi et al., 2006). During the last 80 My kimberlite volcanism has affected the craton (Chesler, 2012).

The Uganda Craton, made up of a central Mesoarchean (~3 Ga) and an eastern Neoarchean terranes (~2.5 Ga; Link et al., 2010; Mänttäri et al., 2013), contains Neoproterozoic units that cover the north-eastern boundary with the Congo Craton and were reworked together with its Archean basement at 635 - 570 Ma.

The Archean nucleus of southern Africa consists of the Kaapvaal and Zimbabwe Cratons separated by the Limpopo Block, a zone of thickened Archean crust (3.3 - 3.1 Ga), reworked during the collision of the two cratons at ~2.6 Ga. The Kaapvaal Craton formed and stabilized by accretion of Paleo- to Neo-Archean terranes between 3.7 Ga and 2.7 Ga (de Wit et al., 1992; Schoene et al., 2008) and it is subdivided into four tectono-stratigraphic terrains (Fig. 2.2). Throughout the Precambrian the craton was affected by tectonothermal events (e.g. emplacement of the Bushveld Complex at ~2.05 Ga) and the lithosphere of the south-western Kimberley Terrain has been strongly metasomatised during Mesozoic intervals of kimberlitic intrusions at ~110 Ma and ~90 Ma (Pearson et al.,

1995; Bell et al., 2005; Kobussen et al., 2008).

To the north the Kaapvaal is separated from the Zimbabwe Craton by the Limpopo Block, a zone of thickened Archean crust consisting of 3.3 - 3.1 Ga gneisses, that were affected by granulite-metamorphism during the collision of the Kaapvaal with the Zimbabwe Craton at around 2.7 - 2.6 Ga. The Limpopo Block comprises reworked Zimbabwe Craton in the Northern Marginal Zone, platform sediments (3.5 Ga) in the Central Zone and reworked Kaapvaal craton in the South Marginal Zone.

Formation of oldest crust in the Zimbabwe Craton occurred between 3.5 to 3.2 Ga, followed by main craton-forming events in the Neoarchean. The Zimbabwe Craton is underlain by Paleoarchean lithosphere suggesting that isolation from the convective mantle already occurred during the initial phase of craton formation. The last major tectonothermal event that affected the craton was the Great Dike emplacement at ~2.58 Ga (Jelsma and Dirks, 2002).

2.2 Proterozoic fold belts

African Archean cratons are surrounded by a number of younger Paleoproterozoic, Mesoproterozoic and Neoproterozoic mobile belts (Fig. 2.3), formed dominantly by obduction. These tectonic sutures and polycyclic mobile zones caused structural basement anisotropies, which often acted as weak zones that were later reactivated during the Phanerozoic and controlled the locus of igneous activity, extension and initiation of rifting (e.g., Black and Girod, 1970; Thorpe and Smith, 1974; Roberts and Bally, 2012).

Paleoproterozoic belts (i.e., the belts surrounding the Tanzania Craton) comprise passive-margin metamorphosed supra-crustal and metasedimentary rocks. Examples include the ~ 2.5 Ga West Central African Belt bounding the Congo Craton to the West, the ~2.1 Ga Magondi Belt of the Zimbabwe Craton, the belts surrounding the Tanzania craton, the 800 km long ~2.0 Ga Ubendian Belt (southwest), the ~2 Ga Ruwenzori Belt (north), the ~1.92 Ga Usagaran Belt (east) and the ~1.96 Ga Kheis Belt along the western margin of the Kaapvaal Craton.

Mesoproterozoic belts include volcanic arcs and island arc docking, mainly consisting of volcano-sedimentary sequences and gneisses intruded by Meso- and Neoproterozoic post-tectonic granites (Begg et al., 2009; and references therein). Examples include the ~1.86 Ga Kibaran Belt between the Congo and Tanzania cratons, the Irumide Belt to the south of the Tanzania craton and the Bangweulu Block and the Namaqua Natal belt around the southern margin of the Kaapvaal Craton.

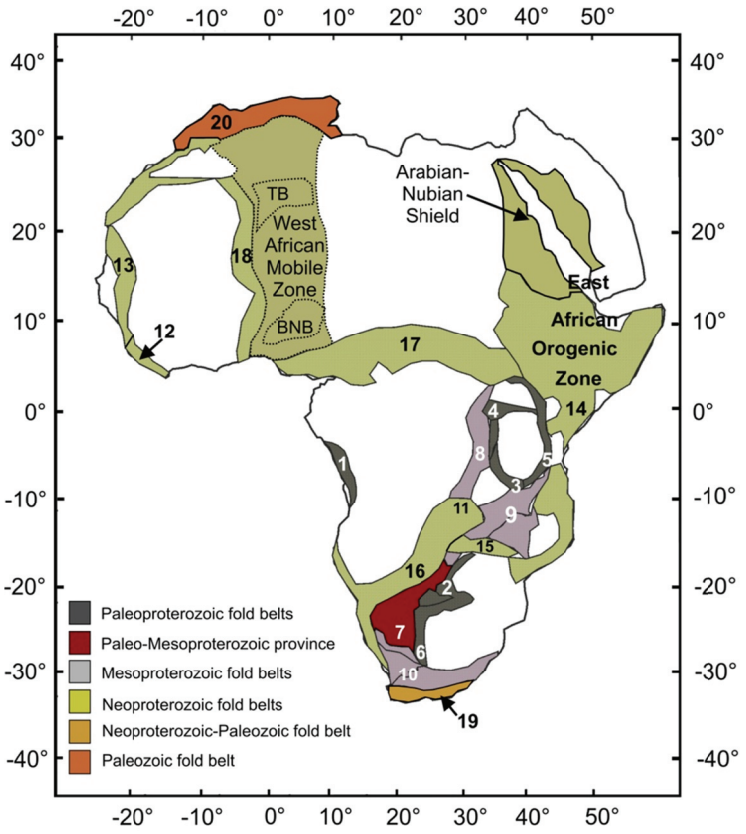

Figure 2.3. Simplified map showing the African Proterozoic mobile belts. Paleoproterozoic belts: 1-West Central African Belt; 2-Magondi Belt; 3-Ubendian Belt; 4-Ruwenzori Belt; 5-Usagaran Belt; 6-Kheis Belt. Paleo-Mesoproterozoic Province: 7-Rehoboth. Mesoproterozoic Belts: 8-Kibaran Belt; 9-Irumide Belt; 10-Namaqua Natal Belt. Neoproterozoic Belts: 11-Lufilian Arc; 12-Rokelide Belt; 13-Mauretanian Belt, 14-Mozambique Belt; 15-Zambezi Belt; 16-Damara Belt; 17-Central African Belt; 18-Pharusian Belt; West African Mobile Zone (TB-Tuareg Block; BNB-Benin-Nigeria Block). Neoproterozoic-Paleozoic Belt: 19-Cape Fold Belt. Paleozoic Belt: 20-Atlas Mountain Belt.

Neoproterozoic belts were formed between ~870 and ~550 Ma during the continent-wide Pan-African orogenic cycle that terminated with the amalgamation of Gondwana (~ 550 Ma). Two types of Pan-African mobile belts of which many represent complete Wilson cycles, can be distinguished (Kröner and Stern, 2004). Younger belts containing Neoproterozoic supracrustal and magmatic materials,

that expose upper to middle crustal levels linked with ophiolites, subduction- or collision related granitoids, island-arc or passive continental margin assemblages. Such belts are the Arabian-Nubian Shield, the Lufilian Arc, and the West Central African Belt and the Rokelides and the Mauretanian belt along the western boundary of the West African Craton. The West African Mobile Zone (WAMZ) comprises several Archean and Proterozoic fragments, such as the ~3.5 Ga Benin-Nigeria Shield, the ~2.65 Ga Tuareg Shield (including the Hoggar domain) that were intensively reworked and intruded during the Pan-African orogeny. The second type consists of generally polydeformed high-grade metamorphic Mesoproterozoic to Archean middle to lower continental crustal assemblages, strongly reworked during the Neoproterozoic. Examples of these belts are the Mozambique Belt, the Zambezi Belt and, possibly, the little known migmatitic terranes of Chad and the Tibesti Massif (see Begg et al., 2009; and references therein for a more complete description).

2.3 Palaeozoic tectonics

By the end of the Pan-African orogeny (~550 Ma) the African plate formed the interior part of the Gondwana supercontinent with the modern South American plate to the west and Arabia, Madagascar, India, and Antarctica to the east. Post Pan-African, early Palaeozoic molasse-related deposits cover vast areas from west to east Africa and into southern Africa, filling the Tindouf and Taudeni basins in the WAC and along the east coast of South Africa (e.g., Cavaroc et al., 1976; Villeneuve, 2005; Milani and De Wit, 2008). During the Ordivician, Silurian, and Devonian, plate motion driven latitude dependent sedimentation in Africa included glacial deposits and post-glacial transgressive shallow marine sedimentation throughout northern Africa and along the southern African coastline.

After a period of Cambrian to Silurian tectonic quiescence the continent was subject to mainly extensional forces and the formation of the Karoo-aged basins across Africa. Their locus was controlled by the inherent structures in the underlying Precambrian basement (Cantuneanu et al., 2005) and the combined effect of compression and accretion along the southern margin of Gondwana together with the existence of a tensional/transtensional regime, which propagated

into the supercontinent from the Thethyan margin from the North (Wopfner, 2002). During the final amalgamation of Pangea in the Late Proterozoic, convergent activity was limited to the north-western and southern margins of the African plate leading to eastward thrusting of the Mauritanian belt (~300 Ma) onto the West African Craton and the formation of both the Variscan orogenic belts (Meseta, Anti-Atlas) in Morocco and the Cape Fold Belt (~250 Ma) in South Africa. By the end of the Palaeozoic the relief of the continent is supposed to have been relatively flat and low-lying (Doucour and Wit, 2003), except for the orogenic areas along the margins and broad regions in central and southern Africa, that were affected by mid-Palaeozoic deglaciation uplifts (Visser, 1997).

2.4 Mesozoic rift systems

The Mesozoic history of Africa is dominated by episodes of continental rifting related with the break-up of Gondwana. Jurassic-Cretaceous crustal extension affected huge portions of the African lithosphere (e.g., Burke and Whiteman, 1973; Frizon de Lamotte et al., 2015) mainly along a large-scale system of aborted rifts and pre-existing basement lineaments. These lineaments initially evolved during Karoo times and resulted in the development of two major rift systems, the West and the Central African Rift systems (Fairhead, 1988; Fig. 2.4).

The African eastern margin was shaped by the fragmentation of East Gondwana in the mid-Jurassic (Royer and Coffin, 1922; König and Jokat, 2010) associated with the opening of the southern Indian Ocean and the southward drift of Madagascar. The breaking-up of Gondwana left the African continent encompassed by passive margins, leading to slow plate rotation and the relative stationary position of Africa since the Mesozoic. Exposed to the effects of episodic deep-mantle upwellings of Mesozoic origin (Nyblade and Sleep, 2003), portions of African lithosphere underwent thermal and chemical modification, which probably already induced the bimodal character of Cretaceous African topography (Doucour and Wit, 2003).

2.5 Cenozoic hotspots, rifts and anomalous swells

During the Cenozoic widespread volcanism affected the African continent, mainly related with Pan-African crustal reactivation (Ashwal and Burke, 1989), continental rifting (Thorpe and Smith, 1974) and hotspots beneath north-central Africa (Hoggar, Tibesti, Darfur), the Cameroon Volcanic Line (CVL), and the EARS (Fig. 2.4). The Eocene to Quaternary volcanic fields of Hoggar, Tibesti and Darfur are marked by topographic swells of broad uplifted Precambrian basement weakened by Mesozoic rifting. Their alkaline volcanism might be fed by unconnected plumes (Wilson and Guiraud, 1992; Burke, 1996), the Afar plume (Ebinger and Sleep, 1998) or adiabatic upwelling of asthenosphere in response to the Africa-Europe collision (Bailey, 1992).

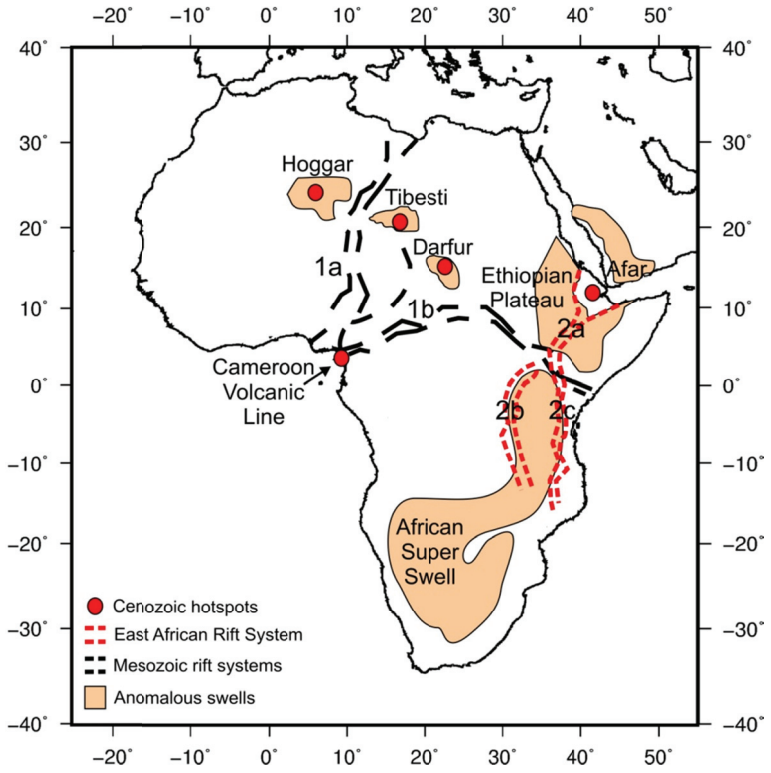

Figure 2.4. Simplified map showing African hotspots, rifts and anomalous swells. Big Mesozoic Rift Systems (1a-West African Rift System; 1b-Central African Rift System); East African Rift System (2a-Main Ethiopian Rift; 2b-Western Branch; 2c-Eastern Branch).

The continental interior of West Africa is marked by the onshore section of the ~1600 km long CVL. Occurrence of mono- and polygenetic volcanoes, sporadic magma rise and the lack of age progression along the volcanic centres suggest fossil plume remelting (Halliday et al., 1990), plume-plume interaction

(Ngako et al., 2006), decompression melting beneath reactivated shear zones (Fairhead, 1988) or edge-driven convective flow at the north-western corner of the Congo Craton (Meyers et al., 1998; King and Anderson, 1995; Reusch et al., 2010).

The most prominent feature of Africa's topographic landscape is the "African Superswell" (Nyblade and Robinson, 1994; Fig. 2.4), which comprises the ~1 km elevated eastern and southern African plateau. Compared to global mean elevation of continents, the long-wavelength topographic anomaly exerts a residual elevation of ~500 m. Bouguer anomaly studies (Brown and Girdler, 1980; Ebinger et al., 1989) showed that the broad uplift in Africa is not a crustal feature, but rather sublithospheric in origin. Whereas seismic low-velocity anomalies at 250 km depth could explain the anomalous topography in East Africa by recent thermal perturbation of the lithosphere (Nyblade et al., 2000; Ritsema and van Heijst, 2000; Debayle et al., 2001; Nyblade, 2002; Weerarantne et al., 2003), the recent thermal uplift is not supported by the upper mantle seismic structure below the Southern African plateau. Its uplift history is maybe pre-Mesozoic in age and a result of combined effects of multiple plume events and processes involving dynamic topography induced by mantle upwelling from the core mantle boundary (Lithgow-Bertelloni and Silver, 1998; Gurnis et al., 2000; Conrad and Gurnis, 2003), phase change induced chemical anomalies within the upper mantle (Smith, 1982), dynamic rebound after slab detachment (Pysklywec and Mitrovica, 1999), lingering plume tails (~25 - 30 Ma) beneath the lithosphere (Nyblade and Sleep, 2003), buoyant depleted lithospheric mantle (Ashwal and Burke, 1989) and mid-Paleozoic post-glacial rebound (Visser, 1997).

The most striking tectonic and geomorphologic feature in East Africa is the seismically and volcanically active East African Rift System (EARS), a large zone of ongoing crustal extension from the Afar triangle, the triple junction between the Nubian, Arabian and Somalian plates, in the north through Ethiopia, Kenya and Tanzania (McConnell, 1972; Morley, 1999; Chorowicz, 2005). Continental break-up in the EARS occurs as rupture of weakened Proterozoic lithosphere (Ring, 1994; Burke, 1996) above a major mantle upwelling (Grand et al., 1997; Nyblade and Langston, 2002; Ritsema et al., 1999; Simmons et al., 2007; Hansen et al.,

2012; Hansen and Nyblade, 2013). Two large north-south trending branches circumvent the resistant Tanzania Craton (Fig. 2.1). The eastern branch cuts through Pan-African lithosphere in the Mozambique belt and is connected to the Afar triangle via the Main Ethiopian Rift (MER). The MER transects the Ethiopian Plateau, a 1000 km-wide Palaeogene flood basalt province at 2500 m elevation (e.g., Mohr and Zanettin, 1988), which was uplifted after the impingement of the Afar mantle plume on the base of the lithosphere at ~30 Ma (Ebinger and Sleep, 1998). The western branch cuts through Archean basement in the north (Link et al., 2010), and developed along the western border of the Tanzania craton. The EARS is an archetypal example of an active rift system (Şengör and Burke, 1980), whose geodynamic origin is under debate. Some studies advocate for one (Afar) plume as the origin of the EARS (e.g., Ebinger and Sleep, 1998; Furman et al., 2004), some advocate for multiple plumes (George et al., 1998; Rogers et al., 2000), and still others advocate for a connection to the African Superplume (e.g., Ritsema et al., 1999; Benoit et al., 2006; Pik et al., 2006; Bastow et al., 2008; Forte et al., 2010; Hilton et al., 2011; Hansen and Nyblade, 2013). Regardless the acting process, any of these mechanisms is causing thermal erosion of the lithosphere, updoming, and dynamic topography.

From late Cretaceous until recent time, the relative motion between Africa and Eurasia caused transpressive convergence in the northern margin of Africa. As a consequence, the Atlas System, extending from Morocco to Tunisia, was developed during the Cenozoic along zones of crustal weakness inherited from rifting episodes related with the opening of the Atlantic and Tethys oceans (Frizon de Lamotte et al., 2000). The Rift-Tell Mountains correspond to accretionary wedges with fragments of stacked thrust sheets incorporating high-grade metamorphic rocks and occasionally peridotites (Frizon de Lamotte et al., 2000). The Rif-Tell Mountains resulted from the closure of the Tethys Ocean by subduction and further slab(s) retreating, whose polarity and geodynamic evolution is highly debatable (e.g., Vergés and Sàbat, 1999; Faccenna et al., 2004; Rosenbaum and Lister, 2004; Vergés and Fernandez, 2012).

Chapter 3.

Fundamentals and Methodology

Chapter 3. Fundamentals and Methodology

In this thesis the crustal and lithospheric thickness beneath the African continent is modelled combining geophysical observables that provide complementary information on the internal density distribution of the lithosphere: elevation and geoid anomalies. The integration of these datasets into a coherent model that enables to investigate the lithospheric structure requires a numerical framework that is based on certain geophysical concepts and assumptions. The main concepts are *local isostasy* and the *thermal lithosphere*, in which a set of assumptions is applied to calculate the density and temperature profiles in the crust and lithospheric mantle. Within these concepts elevation reflects the average density of the lithospheric column, whereas geoid anomalies depend on the density moment. The fundamentals, the setup of the lithospheric model and the physical parameters used are explained in the following.

3.1 General definitions: Earth’s crust and lithosphere

3.1.1 Crust-mantle boundary (CMB)

The boundary between the Earth's crust and the underlying upper mantle, termed Mohorovic discontinuity (short "Moho"), is a first order lithospheric discontinuity, which was discovered by the Croatian seismologist Andrija Mohorovic, whilst he detected two distinct pairs of compressional (P) and shear (S) waves in the seismograms of the 8 October, 1909 earthquake in the Kulpa Valley in Croatia (Mohorovic, 1910). Mohorovic interpreted the two sets of arrivals as the existence of a sharp seismic discontinuity with P-wave velocities of 5.60 km/s above and 7.75 km/s below the detected boundary surface.

Since then, the Moho was found to be a worldwide boundary that defines the base of the crust separating lithospheric domains with fundamentally different physical properties, i.e. seismic wave velocities or densities. The observed differences in velocities of seismic waves in crust and upper mantle led to the seismological definition of the Earth's crust as the outer shell of our planet, in

which the velocity of P waves is smaller than about 7.6 km/s, and S-wave velocity is smaller than about 4.4 km/s (Meissner, 1986), where the average seismic velocity of P-waves changes to values approaching 8.0 km/s. Today, seismologist use typical velocity contrasts at the Moho of 6.6 - 7.3 km/s versus 7.6 - 8.3 km/s for P-waves and 3.3 - 41 km/s versus 4.3 - 4.5 km/s for S-waves (Rabbel et al., 2013).

From its discovery in the early 90's of the past century, the Moho has been mapped out either by passive (earthquake) or active (controlled source) seismic methods, which has resulted in a variety of Moho signatures generally dependent on the bandwidth of the seismic source. As pointed out by Carbonell et al. (2013), a variety of seismic signatures can be obtained at different scales, which sometimes complicates a single universal interpretation of the seismic Moho. It is widely accepted that the obtained seismic images are highly dependent on the source frequency content, on the angles of illumination, and on the density of the source and geometry and density of the recording array. Thus, it is not surprising that in the literature the Moho is referred to as the "refraction" or "reflection" Moho to indicate how the Moho signature has been obtained. In this study I refer basically to the "refraction/wide angle reflection" Moho that has been obtained either by Receiver Function analyses (passive) or Deep Seismic Soundings (active/source controlled) experiments.

The Receiver Function (RF) technique is a relatively new method that uses the teleseismic body waveforms to image the crustal structure under isolate or permanent/temporary arrays of seismic stations. The basics are that seismic energy at teleseismic distances arrives at the receiver array as a plane wave, which when impacts the Moho interface partitions into reflected and transmitted waves. Part of the P-wave signal is converted to S-waves (Ps) that arrive at the receiver within the P wave coda directly after the P-wave. Thus, the depth to the Moho can be estimated from the difference between the arrival times of the P phase (direct wave) and the converted Ps phase, providing the velocity model is known, whereas the relationship of the amplitudes of the two phases allows for an estimation of the contrast of the physical properties at the interface. Its main limitation is that RF models are assumed to be one-dimensional, which implies horizontal layers.

Controlled source seismic methods include refraction and/or wide-angle reflection and normal incidence reflection experiments, where the seismic energy is generated, onshore, usually by the use of controlled explosions or vibroseis, and then recorded along 2D or 3D sensor deployment geometries. The recorded seismic data allow imaging 2D and 3D variations in the velocity structure of the crust and upper mantle, with the Moho being the depth at which the P-wave velocity first increases rapidly or discontinuously to values above 7.6 - 8.3 km/s. Refraction and reflection data not only provide detailed knowledge on the Moho depth and Moho topography, but also on the internal structure of the crust and the crust-mantle transition.

In general, the frequency content in passive source records is very low compared to controlled source seismic data. For RF studies, useful teleseismic waves have frequencies in the range of 0.1 Hz to 1.0 Hz, with differences at least of one or two orders of magnitude when compared to the frequency content of the active seismic sources (Carbonell et al., 2013). For this reason, RF studies are not able to provide high resolution images of the CMB as refraction/reflection data do, but rather provide good constraints on its location at depth. For a detailed summary of the different seismic techniques, their accuracies and seismic constraints on the CMB beneath continents the reader is referred to Carbonell et al. (2013) and the references herein. Furthermore, as not only technical parameters, but also differences in the chemico-physical nature of the CMB in various tectonic settings influence the detection of the Moho interface, the reader is additionally referred to Rabbel et al. (2013).

In any case, the velocity contrast at the Moho or the presence of velocity transition zones in the vicinity of the CMB indicate a change in elastic parameters, which mainly correlate with a compositional change between the rocks of the crust and the uppermost mantle. Thus petrologically, the base of the crust is defined as the boundary between the felsic/mafic rocks of the crust, and the dominantly ultramafic rocks of the upper mantle (O'Reilly and Griffin, 2013). Separating two chemically and physically distinct layers, active in the theory of plate tectonics, makes the CMB an important key element in geodynamics.

However, xenolith data suggest, that the CMB is a lithological transition

zone with interlayering of mafic and ultramafic rocks, commonly over a thickness range of about 5-20 km in off-craton areas. This zone is producing velocity gradients, rather than sharp seismic discontinuities (Griffin and O'Reilly, 1987), which cause significant offsets (5-25 km) between the "Seismic Moho" and the petrological base of the crust. In addition, as the CMB is exposed to continuous mantle-crust interaction, it likely acts as a dynamic feature over geological time spans, that is repeatedly altered and reset (Carbonell et al., 2013). As a consequence, O'Reilly and Griffin (2013) warn that the seismic Moho may lie significantly deeper than the CMB, and that detecting the base of the continental crust by seismic techniques alone (without considering petrological aspects) may lead to an overestimation of actual crustal thickness by 15-30 % beneath off-craton areas.

Nevertheless, apart from the complex nature of the CMB and its internal architecture, for the sake of clarity it should be mentioned, that throughout the course of this thesis, and where seismic data are available, the crustal thickness and depth to the CMB is referred to the measured distance from the Earth's surface down to the seismically determined base of the crust.

3.1.2 Lithosphere-asthenosphere boundary (LAB)

The lithosphere-asthenosphere boundary in plate tectonics divides the cold rigid lithosphere from the hotter and weaker asthenosphere. In this context the LAB acts as a detachment zone allowing for differential motion between lithospheric plates, and the underlying convecting mantle (Karato and Wu, 1993). However, as several physical parameters change at the LAB, its nature is debatable in terms of its rheological, chemical, electrical and seismological characteristics (Eaton et al., 2009), which is why detection of the absolute depth of the base of the lithosphere by means of geophysical techniques still remains challenging.

Here I want to give a brief overview about the multi-disciplinary concept of the lithosphere, the properties under study and the related techniques used to determine its base. For a comprehensive insight into the complexity of the topic the reader is referred to Chapter 1 in Artemieva (2011) or Eaton et al. (2009).

Unlike the Moho, it is difficult to define the base of the lithosphere petrologically, since there are no bulk compositions known, that explicitly represent asthenospheric mantle material (O'Reilly and Griffin, 2010). Usually, changes from depleted (lithospheric) to undepleted or fertilized (asthenospheric) composition are used to determine the base of the petrological lithosphere. Thermobarometric studies on direct rock samples of the LAB environment provide xenolith-based geotherms that suggest minimum estimates of the thermal thickness of the lithosphere of 170-225 km (e.g., Boyd and Nixon, 1978; Finnerty and Boyd, 1987). In the thermal approach the base of the lithosphere is usually defined by the depth to an isotherm (e.g., 1300 ºC) or by the depth at which a downward continuing conductive geotherm intersects with a pre-defined fraction of the ambient mantle temperature or mantle solidus (Artemieva, 2011). It should be noted, that this interface does not correspond to any physical boundary (Priestley and McKenzie, 2013). In general, the lithospheric geotherms are constructed using different constraints coming from surface heat flow measurements, pressure-temperature estimates of equilibrium conditions in minerals from xenoliths, or from conversion of seismic velocities into temperatures.

Within the concept of the elastic (flexural) lithosphere, the LAB defines the base of a single-layer plate with elastic rheology that provides isostatic response to plate loading (surface and subsurface loads). This base corresponds to the elastic-plastic transition (Bodine et al., 1981) which, in the upper mantle, occurs at temperatures from 600 - 750 °C (Chen and Molnar, 1983). Compared to the base of the thermal lithosphere that is controlled by temperatures close to the mantle adiabat (~1300 °C) the thickness of the elastic lithosphere is approximately half of the thermal and also of the seismological and electrical lithosphere.

Beneath cratonic regions changes in elastic and non-elastic properties of mantle rocks are used to define the base of the seismological lithosphere, which is commonly characterized as a layer of high shear wave velocity from the Moho to ~100 - 300 km depth. In this sense the presence of a low-velocity zone (LVZ) beneath the high-velocity layer can be taken as an indication of the LAB (Pontevivo and Thybo, 2006). Anyhow, a clear LAB signal is often absent, as a variety of mechanisms can cause the existence of the LVZ (e.g., partial melting, high-temperature relaxation, contrasts in volatile content), which imply that the

base of the seismological lithosphere is diffuse and transitional over tens of kilometres in depth. A summary of seismic techniques used to map the LAB and their related technical challenges can be found in Eaton et al. (2009).

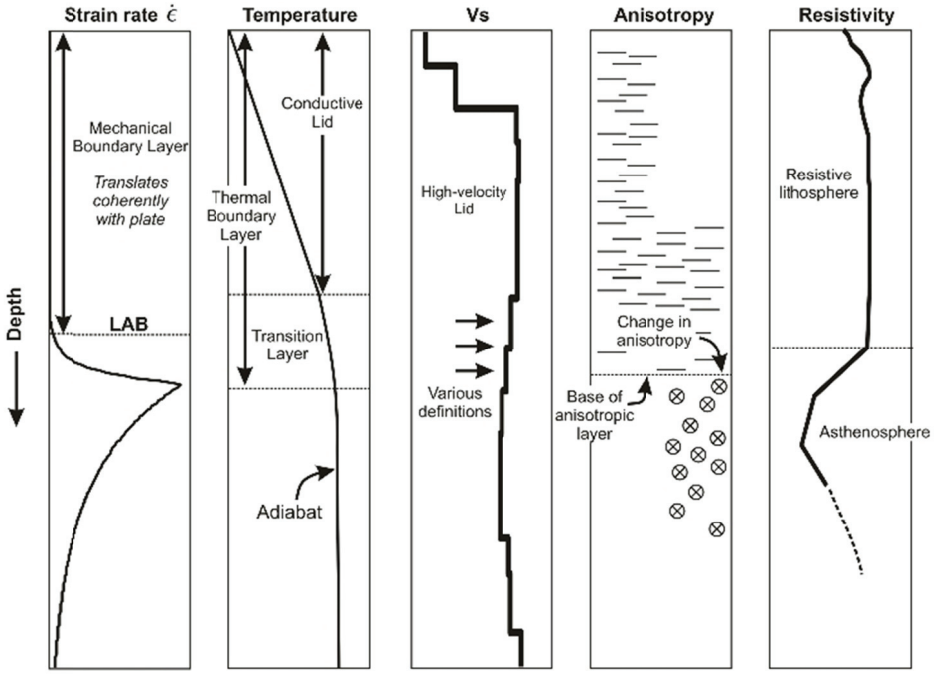

Figure 3.1. Definitions of the lithosphere and common proxies to estimate its thickness. The lithosphere, sensu stricto, is a mechanical boundary layer (left). The LAB coincides with the top of a zone of decoupling between the lithosphere and asthenosphere, marked by an increased strain rate. The thermal boundary layer, containing a conductive lid and a transition layer, represents a near-surface region where temperature deviates from the adiabat. A zone of low seismic shear-wave velocity (Vs) is sometimes detected beneath a high-velocity lid; various definitions have been used to correlate this zone with the LAB. The LAB may also correlate with a downward extinction of seismic anisotropy or a change in the direction of anisotropy. The electrical LAB is marked by a significant reduction in electrical resistivity. Figure and figure caption are taken from Eaton et al. (2009).

Variations in seismic anisotropy are another indicator of the LAB (Debayle et al., 2005; Sebai et al., 2003). They can help to detect the base of the rheological lithosphere, as present-day differential motion between the lithosphere and asthenosphere is dominantly accommodated by dislocation creep (Korenaga and Karato, 2008), which leads to lattice-preferred orientation of olivine, within a ~50 km thick region of high strain rate near and beneath the LAB (Eaton et al., 2009). Similarly, asthenospheric flow also causes anisotropic diffusivity of hydrogen in olivine crystals which leads to direction-dependent electrical conductivity in the mantle. Electromagnetic profiles of the lithosphere-asthenosphere system show regions of electrical anisotropy that can be attributed

to mantle deformation due to relative plate motion (Karato, 2012) and which, in a joint analysis together with seismic anisotropy, might coincide with the base of the rheological lithosphere.

The electrical LAB is usually defined as the base of the highly resistive lithosphere above the highly conducting asthenosphere, which is marked by a sharp change in mantle conductivity (or its inverse, resistivity) due to the presence of an interconnected conducting phase such as melt (1 - 3% of melt fraction) or graphite. The depth to the base of the resistive lithosphere is relatively well constrained by magnetotelluric observations (Jones, 1999) and was found to vary between ~205 km and 230 km beneath cratonic lithosphere (Eaton et al., 2009). Generally, these depth estimates are in good agreement with lithospheric thickness estimates from seismic anisotropy, xenolith thermobarometry and the top of the seismically-defined low-velocity zones.

Following this brief overview, the reader should notice that the presented lithospheric thickness map in Chapter 6 compares to LAB depth estimations as defined within the concept of the thermal lithosphere, because the method applied in this thesis, implements a pure thermal approach to calculate the depth-density profile in the lithospheric mantle.

3.1.3 Geoid height

The geoid is described as the equipotential surface of Earth's gravity that best correlates with global mean sea level over the oceans, excluding the effects of semi-dynamic sea surface topography. It defines the shape of the Earth and is a fundamental reference surface in geodesy and geophysics.

Being an equipotential surface the force of gravity is everywhere perpendicular to the geoid. Deviations of the geoid from the international reference ellipsoid are called geoid height anomalies ΔN (Fig. 3.2). They result from lateral density variations in the Earth's interior and provide valuable information on deep-Earth structures (e.g., the topography of the LAB) and mass density anomalies (Bowin, 1983).

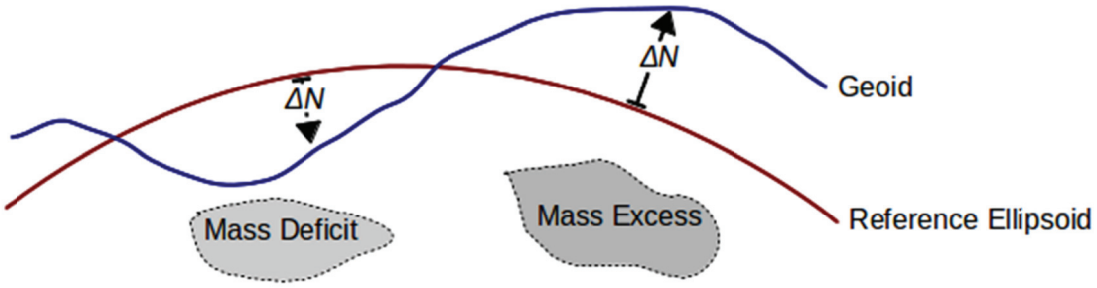

Figure 3.2. Relationship between the reference ellipsoid and measured geoid and the effect of density variations (mass anomalies) on the geoid anomaly *ΔN*. A negative deflection of the geoid occurs over regions of mass deficit, a bulge or a positive geoid anomaly occurs in regions of excess mass.

In isostatically compensated regions the geoid anomalies (after spectral filtering) are associated with the density moment and can be used to constrain the density distribution within the lithosphere. If the horizontal scale of the density variation is large compared to its location at depth, an isostatic density anomaly is directly proportional to the vertical dipole moment of the local density distribution (Ockendon and Turcotte, 1977; Haxby and Turcotte, 1978; Turcotte and Schubert, 1982).

3.1.4 Isostasy

Derived from the Greek words "iso" and "stasis" the term isostasy means "equal standing" and was introduced by Dutton (1882) to describe “the flotation of the Earth's crust upon a liquid or highly plastic substratum.” Within the concept of isostasy variations in surface topography can be explained by assuming that the lithosphere and the asthenosphere are in gravitational equilibrium, if external dynamical forces are absent. A simple analogue of isostasy is the Archimedes principle of hydrostatic equilibrium, in which columns of lighter lithospheric material (solid) would float on the denser underlying mantle (liquid), where equilibrium is achieved at a given depth of compensation, the depth below which the generated pressures are hydrostatic (constant). Deviations from hydrostatic equilibrium (e.g. due to surface loading or unloading) would lead to lateral pressure gradients, that cause the mantle material to flow until constant pressure

conditions are restored.

According to the local isostasy principle, the extra mass of a mountain in isostatic equilibrium is compensated by a mass deficit between the surface and the compensation depth, while the mass deficit at an ocean basin is compensated by an extra mass at depth. This assumption dates back to the middle of the 19th century, when the two widely used compensation mechanisms for gravitational equilibrium were proposed.

1. The Airy model (Fig. 3.3a), where densities are constant and variations in topography are compensated by changes in the lithospheric thickness and equilibrium is achieved at the base of the lithospheric root (Airy, 1855; Heiskanen, 1958).

2. The Pratt model (Fig. 3.3b), where variations in topography are compensated by lateral changes in the lithospheric density and equilibrium is achieved at the base of the lithosphere, which is assumed to be flat (Pratt, 1855; Hayford, 1909; Hayford and Bowie, 1912).

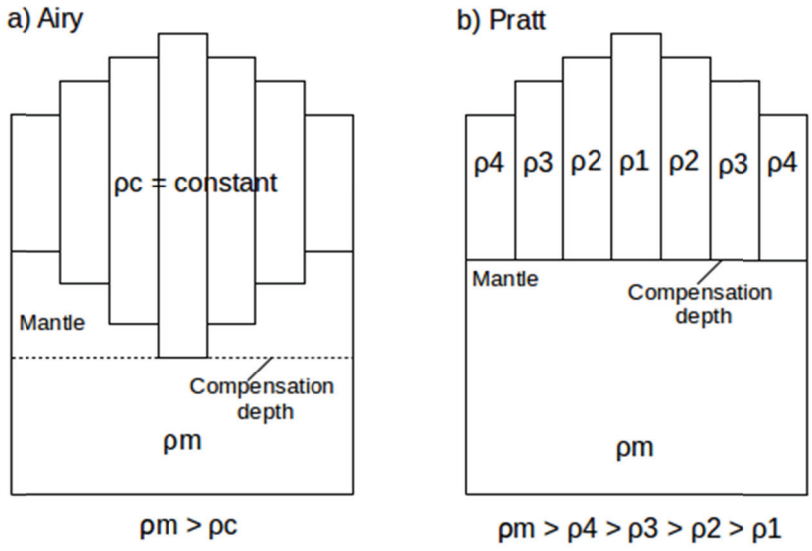

Figure 3.3. Classic end-member models of hydrostatic equilibrium (a) Airy isostatic model (b) Pratt isostatic model with homogeneous mantle density ρm. In the Airy-case crustal density is constant and changes in topography need to be compensated by changes in lithospheric thickness. The Pratt-case assumes topography variations being compensated by changes in crustal density

Both Airy and Pratt isostatic models assume that compensation is local and takes place along vertical columns, which move independently of each other. Whereas Pratt's model successfully explains isostatic equilibrium in oceanic

domains by variations in the lithosphere density due to lateral density variations with age, seismic experiments indicate that the topography of continents rather depends both on crustal densities and thickness variations (Artemjev et al., 1994). A comprehensive review of the development of the concept of isostasy can be found in Watts (2001).

The concept of “local” isostasy (incorporating the Airy and Pratt end member cases) requires that hydrostatic equilibrium of all masses from the surface t down to the level of compensation *H* is achieved in such way, that the vertical sum of masses is the same everywhere:

$$\int_{t}^{H} \rho(z)dz = const$$

where $\rho(z)$ is the density (mass) distribution with depth (including topography and water). Consequently, the sum of mass anomalies produced by density variations in the crust and upper mantle located within a vertical column above the compensation level should equal zero:

$$\int_{t}^{H} \Delta\rho(z)dz = 0$$

Note that in contrast to the classic isostatic models the level of isostatic compensation is taken at the base of the lithosphere, because subcrustal density variations within the lithosphere are expected to contribute to the isostatic equilibrium (Kaban et al., 1999; Panasyuk and Hager, 2000).

Local isostasy is a simplification of the real Earth’s structure and considering that geodynamic processes cause isostatic disturbances by modifying the internal structure of the lithosphere (depth to CMB/LAB and density), isostatic models should be treated with caution. Nevertheless, although “regional” compensation models (including elastic stresses in the lithosphere) are considered to be more realistic (Vening-Meinesz, 1931; 1940), for large wavelength topography variations, “local” isostasy in its classical sense can provide a good first order approximation of the structure of the lithosphere, especially where detailed knowledge of the lithospheric properties (e.g., rheology, temperature, density) is not available.

3.1.4 Lithospheric thermal regime

In the solid earth, heat is transferred by four mechanisms: conduction, advection, convection and radiation. Conduction is a diffusive process wherein heat is transported within a material in form of kinetic energy via atomic or molecular interaction. Heat transfer by convection involves the motion of material from hot (lighter) to cold (denser) regions, a process that is dominant in the Earth's sublithospheric mantle. Advection is a special form of convection, where heat is physically advected by tectonic processes (e.g., erosion/sedimentation, isostatic rebound, and magmatic ascent). Radiation describes the direct transfer of heat by electromagnetic radiation, which in the Earth is of minor importance and can be included into the definition of heat conduction.

The heat transfer processes within the Earth can be expressed by the heat transport equation (e.g., Fowler, 2005):

$$\frac{\partial T}{\partial t} = \frac{k}{\rho c_P} \nabla^2 T + \frac{A}{\rho c_P} - u \nabla T$$

where T is the temperature, t is the time, k is the thermal conductivity (W m^{-1} K^{-1}), ρ is the density, c_P is the specific heat at constant pressure (J kg^{-1} K^{-1}), ∇^2 is the Laplace operator, A is the radiogenic heat production per unit volume (W m^{-3}) and u is the velocity vector. In this sense the variation of temperature with time is described by the three terms to the right hand side of the above equation, which correspond to the diffusion of heat by conduction, the presence of heat producing elements and the advective/convective transfer of heat, respectively.

The latter term can be neglected, as advection/convection is considered not to take place in the lithosphere, which leads to the heat-conduction equation:

$$\frac{\partial T}{\partial t} = \frac{k}{\rho c_P} \nabla^2 T + \frac{A}{\rho c_P}$$

As previously mentioned, within the thermal definition the lithosphere is described as the conductive *thermal boundary layer* through which the heat loss from the Earth's interior is balanced by radioactive heat production and incoming heat flow from the underlying convecting asthenosphere.

In this thesis, the temperature distribution within the lithosphere is calculated using a steady-state conductive heat transport model, which can be applied to stable continental regions. Jaupart and Mareschal (2007; and references herein) have shown that the thermal relaxation time for continental lithosphere depends on its thickness and the thermal boundary conditions fixed at its base. For a 200 km thick lithosphere with a constant heat flux at the base, quasi steady-state conditions are reached after ~300 My. Thus, the temperature distribution with depth can be considered as constant, with radiogenic heat production and conductive heat transport being the dominant thermal processes and can be calculated by solving the 1D heat transport equation in steady-state:

$$k \cdot \nabla^2 T + A = 0$$

The radiogenic heat generation describes a substantial part of the Earth's internal heat budget, which is produced by the decay of the radioactive elements uranium, thorium and potassium. The radioactive isotopes ^{235}U, ^{238}U, ^{232}Th and ^{40}K are highly concentrated in the continental crust compared to the mantle, where they are some two orders of magnitude less abundant. On average, radiogenic heat generation of undepleted mantle is very low, whereas crustal rocks (e.g. granites) have a greater internal heat production. Nevertheless, as the volume of the Earth's mantle is much greater than the total crustal volume, only one-fifth of radioactive heat is produced in the crust. In this thesis, a simple "block model", in which the average heat production H_S is constant from the surface to the base of the crust, was selected:

$$H(z) = H_S$$

For the lithospheric mantle, the heat production was considered to be negligible and a linear temperature-depth profile (geotherm) was chosen (Lachenbruch and Morgan, 1990), meaning that the heat flow q_m (mW/m^2) within the mantle lithosphere is constant and equal to:

$$q_m = k_m \frac{T_a - T_{mh}}{Z_L - Z_C}$$

where k_m is the thermal conductivity of the lithospheric mantle, T_a is the

temperature at the LAB, T_{mh} is the temperature at the CMB and Z_L and Z_C describe the depth to the base of the lithosphere and the crust, respectively. For detailed information on the temperature distribution in the lithosphere the reader is referred to Lachenbruch and Sass (1977), Morgan (1984), Morgan and Sass (1984), Lachenbruch and Morgan (1990), Artemieva and Mooney (2001), and Michaut and Jaupart (2004).

3.2 Method: Combined geoid and elevation 1D modelling

To image lateral variations in crustal and lithospheric thickness elevation and geoid anomaly data are combined and coupled with a thermal analysis following the 1D approach by Fullea et al. (2007). The observed elevation and geoid height are simultaneously fitted assuming local isostasy and considering a four-layer model composed of water, crust, lithospheric mantle and asthenosphere (see Figure 3.4). In this context, elevation is proportional to $\int \rho_{(z)}\, d_z$, where $\rho_{(z)}$ is the density at a given depth *z*. The integral extends from the Earth's surface to the compensation level, which is located below the deepest point of the LAB over the entire modelled region. In this way, elevation *E* with respect to sea level can be expressed as (Lachenbruch and Morgan, 1990):

$$E = (\rho_a - \rho_L)/\rho_a \ * L - L_0 \qquad (E \geq 0)$$

$$E = \rho_a/(\rho_a - \rho_w) * ((\rho_a - \rho_L)/\rho_a * L - L_0) \qquad (E < 0)$$

where *L* is the total lithospheric thickness, ρ_a is the density of the asthenosphere (set to 3200 kg/m^3), ρ_w is the density of seawater (1030 kg/m^3), ρ_L is the average density of the lithosphere, and L_0 is the depth of the free (unloaded) asthenospheric level (2320 m; Fullea et al., 2007).

Under local isostasy and when lateral density gradients are moderate, the geoid anomaly is proportional to the dipolar moment of the vertical density distribution and, therefore is proportional to $\int z\ \rho_{(z)}\ d_z$. The geoid anomaly N is calculated by (e.g., Haxby and Turcotte, 1978):

$$N = -2\pi G/g \int z * \rho(z) dz + N_0$$

where G is the universal gravity constant ($m^3\ s^{-2}\ kg^{-1}$) and g is the gravitational acceleration at the Earth's surface (ms^{-2}) and $\rho(z)$ the local density at depth z. The integration constant N_0, which serves to adjust the zero level of the geoid anomalies, is calculated considering a reference column, where N and the crustal and lithosphere thickness and their respective densities are known.

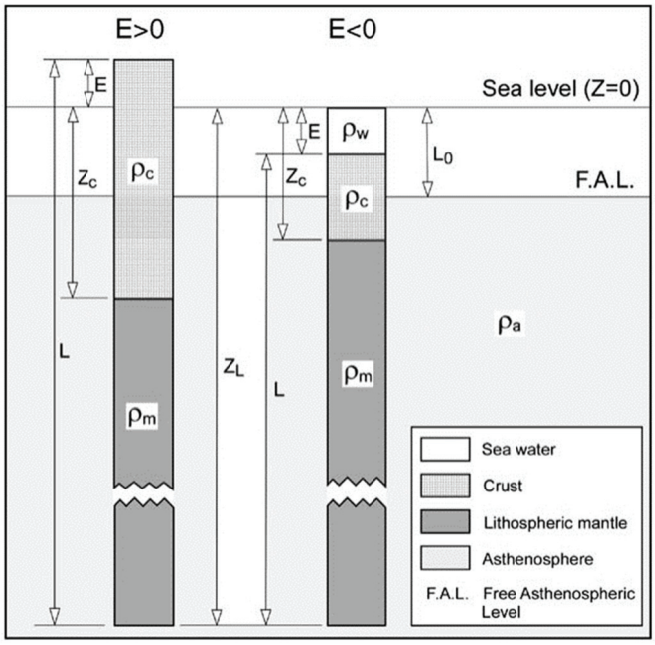

Figure 3.4. Schematic view of the lithospheric model by Fullea et al. (2007) used in this work. The model is composed of four layers; i) the crust with density ρ_c, ii) the lithospheric mantle with density ρ_m, iii) sea water column with density ρ_w and iv) the asthenosphere with the density ρ_a. E is the elevation (E>0 topography, E<0 bathymetry), z_c and z_L are the depths of the crust/mantle and lithosphere/asthenosphere boundaries, respectively, referred to the sea level. L is the total thickness of the lithosphere and $L0$ is the depth of the free asthenospheric level, i.e. without any lithospheric load. Figure and figure caption are taken from Fullea et al. (2007).

For the crust a laterally homogeneous density ρ_C is assumed that increases linearly with depth between predefined values, ρ_S at surface and ρ_B at the base of the crust. The density in the lithospheric mantle ρ_m is considered to be temperature dependent (e.g., Lachenbruch and Morgan, 1990) such that:

$$\rho_m(\mathrm{z}) = \rho_a\,(1 + \alpha[T_a - T_m\,(\mathrm{z})])$$

where α is the coefficient of thermal expansion, T_a is the temperature at the base of the lithosphere and T_m(z) is the temperature at depth z in the lithospheric mantle. For the African continent we can assume that the average mantle is of Archean age, therefore I have set α = 3.2 x 10^{-5} K^{-1} according to Afonso et al.

(2005). The temperature distribution with depth is calculated by solving the 1D heat transport equation in steady-state:

$$k \cdot \nabla^2 T + A = 0$$

where k is the scalar thermal conductivity, ∇^2 is the Laplace operator, and A the volumetric heat production. I consider a thermal conductivity of 2.5 W m^{-1} K^{-1} for the crust and 3.2 W m^{-1} K^{-1} for the lithospheric mantle (e.g., Fernandez et al., 1998). The radiogenic heat production is considered to be constant, with values of 0.5 and 0 μW m^{-3} (Vilà et al., 2010; Robert et al., 2015) for the crust and the lithospheric mantle, respectively. The above equation is solved with boundary conditions of fixed temperature at the surface T_s=0 °C and at the base of the lithosphere T_a=1350 ºC (see eqs. 4-32 and 4-33 in Turcotte and Schubert, 2002). For a detailed derivation of the generalized isostasy equation that includes the thermal field in a consistent way, the reader is referred to Fullea et al. (2007).

The choice of thermal parameters influences the calculated Moho temperature, which in turn modifies the density of the lithospheric mantle. According to Fullea et al. (2007), the calculated LAB depth decreases almost linearly with increasing the thermal expansion coefficient and crustal thermal conductivity, and by decreasing the radiogenic heat production. The calculated LAB depth can vary by ±6 km for a wide range of thermal parameters, whereas the crustal thickness is barely affected (~1 km). The inaccuracy of the calculated crustal and lithospheric thickness associated with the RMSE of the used input datasets is less than 2 and 10 km, respectively, as calculated by Fullea et al. (2007) for the older ETOPO2 (Sandwell and Smith, 1997) and EGM96 (Lemoine et al., 1998) datasets.

In order to improve the initial constant average crustal density distribution, the occurrence of large sedimentary basins in Africa will also be considered at a later stage during the modelling (Chapter 6.2) by using a 2D density distribution with lateral variations in surface density. Since sediment infill should decrease the average density of the crustal column and the approach requires the density values at surface and at the base of crust, the equivalent surface density that would result from considering a sedimentary layer of thickness h_s and average

density ρ_S was calculated. In addition, it is assumed that densities within sediments and crystalline crust increase linearly with depth and coincide at the base of the sedimentary layer. Therefore, to calculate the influence of sediment infill in decreasing the average density of the crustal column, the following scheme was applied to adjust the crustal density at the surface of the model, according to the local thickness of the sediment pile.

The density at depth z of the crustal column without sediments is defined by:

$$\rho(z) = \rho_0 + (\rho_M - \rho_0) * z / h_c$$

for $0 \leq z \leq h_C$ with ρ_0 and ρ_M being the densities fixed at the surface and the bottom of the crust, respectively, and h_c the crustal thickness. The crustal density at the base of the sedimentary layer is then given by:

$$\rho_{hs} = \rho_0 + (\rho_M - \rho_0) * h_s / h_c$$

where h_s is the total sedimentary thickness. Assuming a linear density increase with depth within the sedimentary layer and assuming that there are no discontinuities in the density profile of the whole crust, the average density ρ_s of the sediment layer is determined by:

$$\rho_s = (\rho_{s0} + \rho_{hs}) / 2$$

where ρ_{s0} is the surface density of the sedimentary layer. The average density of the crustal column, including sediments is given by

$$\rho_{cs} = (\rho_s * h_s + (\rho_{hs} + \rho_M)/2 * (h_c - h_s))/h_c$$

Thus, the equivalent surface density for a crustal column including sediments will be

$$\rho'_0 = 2 * \rho_{cs} - \rho_M$$

Note that the new surface crustal density yields the same average density of a crustal column with sediments, assuming a linear increase with depth from ρ'_0 *to* ρ_M.

As described above, the applied method is not accounting for absolute

density values, but is using a lateral density distribution, which provides a useful tool to describe first-order variations in topography and potential fields. This approach has been successfully applied to image variations in crustal and lithospheric thickness beneath the Atlantic-Mediterranean transition (Fullea et al., 2007), the Arabia-Eurasia collision (Jiménez-Munt et al., 2012), the Iberian Peninsula (Torne et al., 2015), central Asia (Robert et al., 2016), and to build a starting model to investigate the 3D lithospheric density structure of the southern Indian Shield (Kumar et al., 2014).

Chapter 4. Data

Chapter 4. Data

In this chapter I will introduce the type of data, the applied processing and their particular integration into the explained modelling procedure as explained in Chapter 6. The purpose of the data sets is basically threefold: i) *Elevation* and *geoid anomaly* are the main input data to invert the lithospheric structure; ii) Crustal parameters such as *sediment thickness* and *mean crustal densities* are used to improve the initially average constant density distribution of the model for lateral changes in crustal density and iii) *Seismic Moho estimates* serve to choose the best reference column, to define the best fitting crustal model and to compare the modelled crustal thickness map in order to discuss its strong and weak points.

4.1 Elevation

Digital elevation data for Africa were taken from the 1 arc-minute global relief model ETOPO1 (Amante and Eakins, 2009). The high frequency components were removed from the data-setusing a Gaussian low-pass filter with a wavelength of 100 km in order to avoid unrealistic short-wavelength signals into the modelled Moho and LAB topography associated with flexural support of topographic loads. Figure 4.1 shows the filtered ETOPO1 data, used as input elevation in the modelling procedure. Locally, small-scale high-amplitude signatures in topography occur in uplifted, mountainous and volcanic regions (e.g. Atlas, Tibesti, EARS) and are expressed as multiple peaks and troughs at the shortest range of spatial scales. The effect of the filtering on the raw ETOPO1 elevation data is shown along three profiles (Fig. 4.2), crossing the main African topographic features to demonstrate i) the alteration of the topography signal for locations where the vertical component is very high compared to the horizontal one (removal of nonrelevant short-wavelengths considering lithosphere isostasy calculations) and ii) the maintenance of relief information in terms of regional trend and characteristics of the elevation profile.

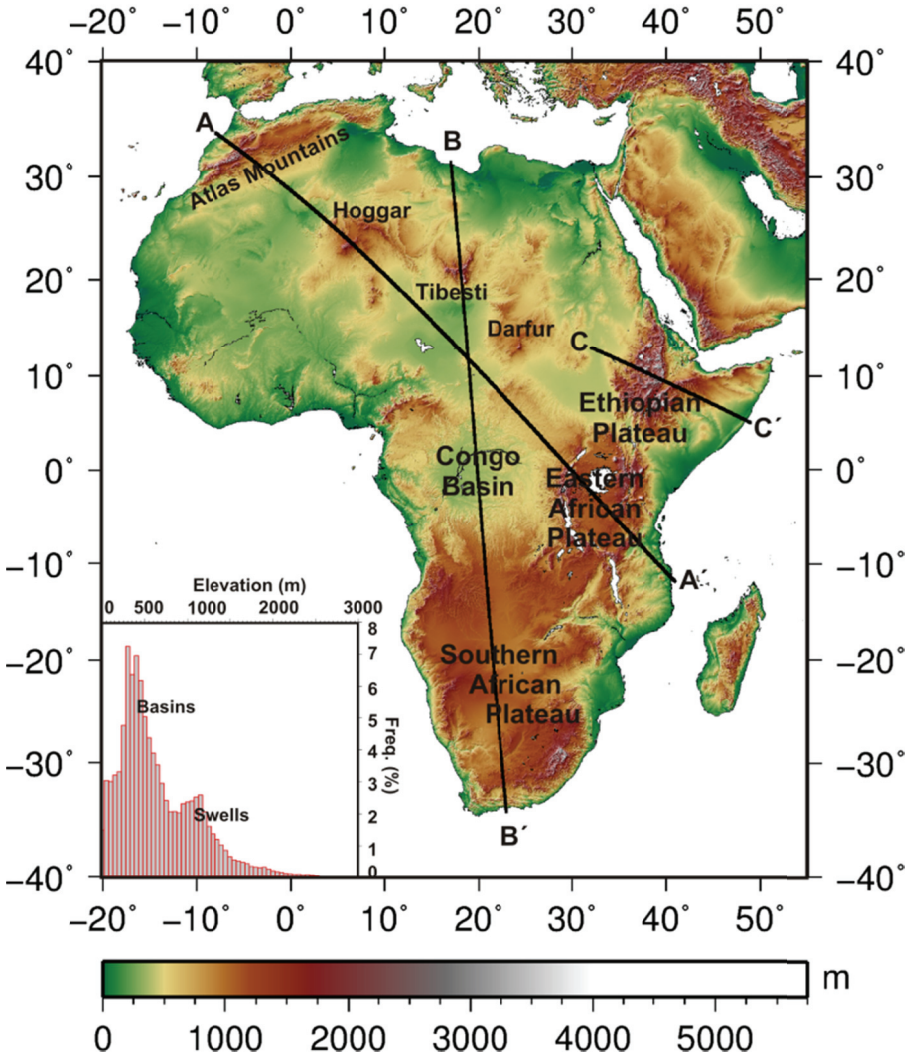

Figure 4.1. Elevation map showing filtered elevation from global relief model ETOPO1 (Amante and Eakins, 2009) after application of a low-pass filter to eliminate the short wavelengths (< 100 km) and gridding to 10-arc minutes. Profiles A, B and C cross the most important topographic features of African landscape. Inset shows the bimodal distribution of elevation as result of the long-wavelength basin and swells topography

Although included in the calculations, I will not discuss the offshore elevation and bathymetry data further, as the following observations and investigations rather focus on the land surface of the African continent. The physiography of African topography is distinctly bimodal and dominated by high elevations of >1000 m in eastern and sub-equatorial Africa, related with the African Superswell, and by average to moderate elevations of <500 m in Central, North Africa. Long-wavelength (>1000 km) topographic highs in eastern Africa are related with the Ethiopian Plateau and the East African Plateau, both with average elevation of ~1500 m, and to the highest rift-related withpography >3000 m along the flanks of the East African Rifts System.

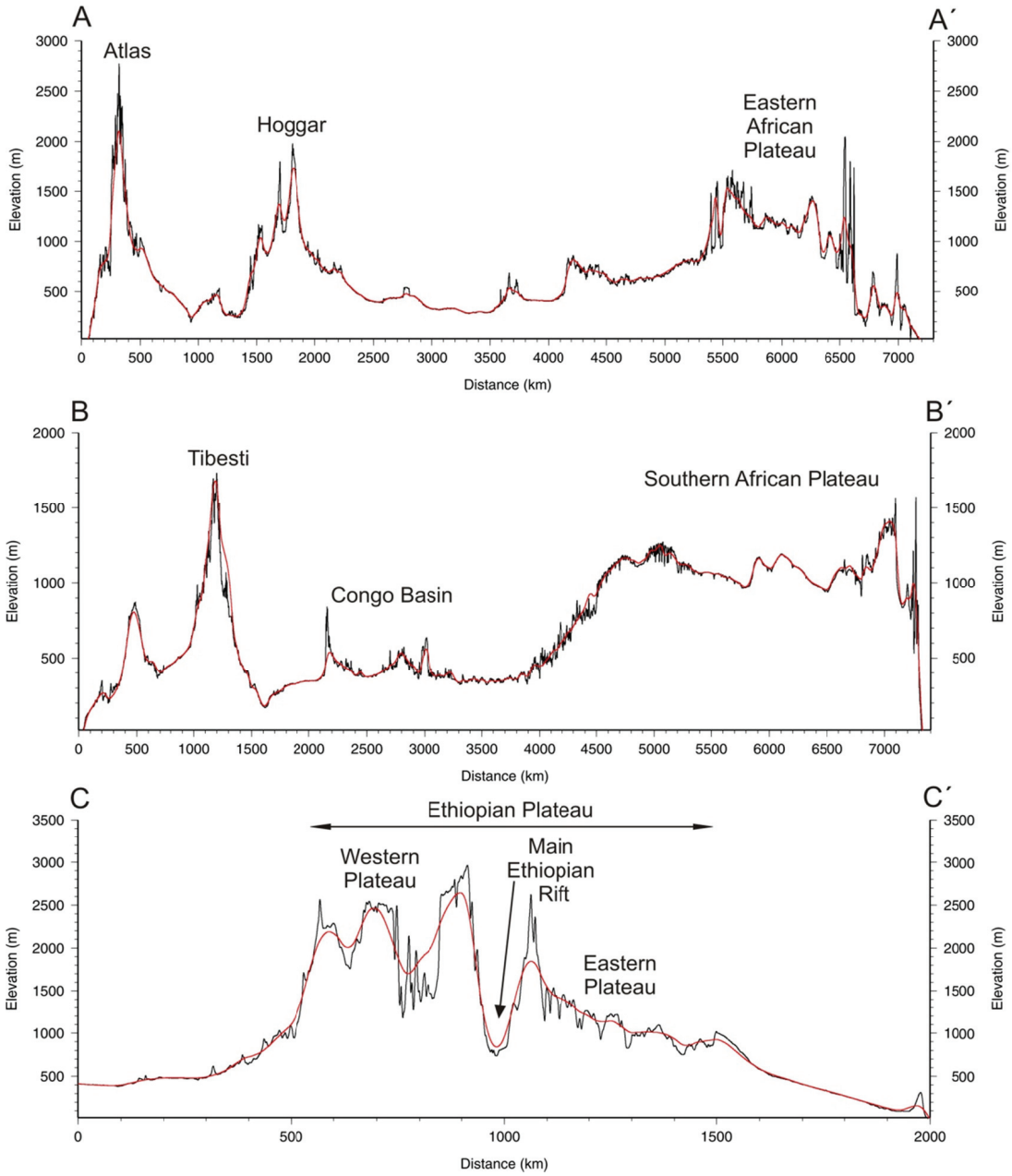

Figure 4.2. Visualization of the filtering of ETOPO1 elevation data along the profiles A, B and C as located in Fig. 4.1. Raw ETOPO1 data are plotted in black and the red lines show the input elevation after applying a linear low-pass filter with λ=100 km.

In southern Africa, a broad uplifted region surrounds the Cenozoic Kalahari Basin,. which is marked by a marginal escarpment related with the highest elevations of >2500 m.

In contrast, central and northern Africa is dominated by low topographic relief ~500 m, which is mainly related with large-scale depressional features in the cratons of Congo (Congo Basin), West Africa (Taoudeni Basin) and the Sahara Metacraton (Chad Basin). To the north this smooth topography is interrupted by a

number of shorter wavelength swells and uplifted regions, such as the Hoggar Massif (~1000 m), the Tibesti Mountains (~ 2000 m) and Darfur (~1200 m, see Fig. 4.1 for locations), giving Africa its typical basin and swell topography (Holmes, 1944). The transition to the passive continental margins of the Atlantic and Indian oceans is marked by coastal areas characterized by low relief (~150 m), with the exception of the northwest corner of Africa, where convergence between Africa and Europe is marked by high topography (~2000 m) along the Rif-Tell-Atlas orogenic system, and the southeast and south regions of Africa, where steep topographic gradients mark the transition to the continental shelf (Fig. 4.1).

4.2 Geoid anomaly

Geoid anomaly data were extracted from the EGM2008 global model (Pavlis et al., 2012). Global studies show that geoid anomalies with wavelengths greater than 4000 km are produced by density anomalies located at sublithospheric levels (Bowin, 1983). To only retain the signature of mass distribution related with the lithospheric structure, those wavelengths exceeding ~4000 km were filtered by removing the lower harmonic coefficients up to degree and order 10 (see Root et al., 2014 for a detailed sensitivity analysis of spherical harmonic degrees). Figure 4.3 below shows the full resolution geoid (a) and the geoid signal used as input during the modelling procedure, after filtering of the sublithospheric long-wavelength sources (b). The resulting geoid anomalies range from -16 to 16 m and largely follow the distribution of high and low topography in Africa, except for some regions to the north of the Kaapvaal Craton (Fig. 4.3b).

The most striking features are the circular geoid low with a wavelength of > 750 km and minimum values of -16 m in the centre of Africa, related with the Congo Basin and a widespread and elongated negative anomaly, with minimum values of -9 m that crosses the West African Craton trending NE-SW parallel to the Atlas. The SW end of this geoid low extends to the northern and central regions of the Taoudeni Basin, where values less than -4 m are observed. The northeasternmost part of the east Saharan Metacraton is marked by a -6 m geoid low located in the Nile Delta region.

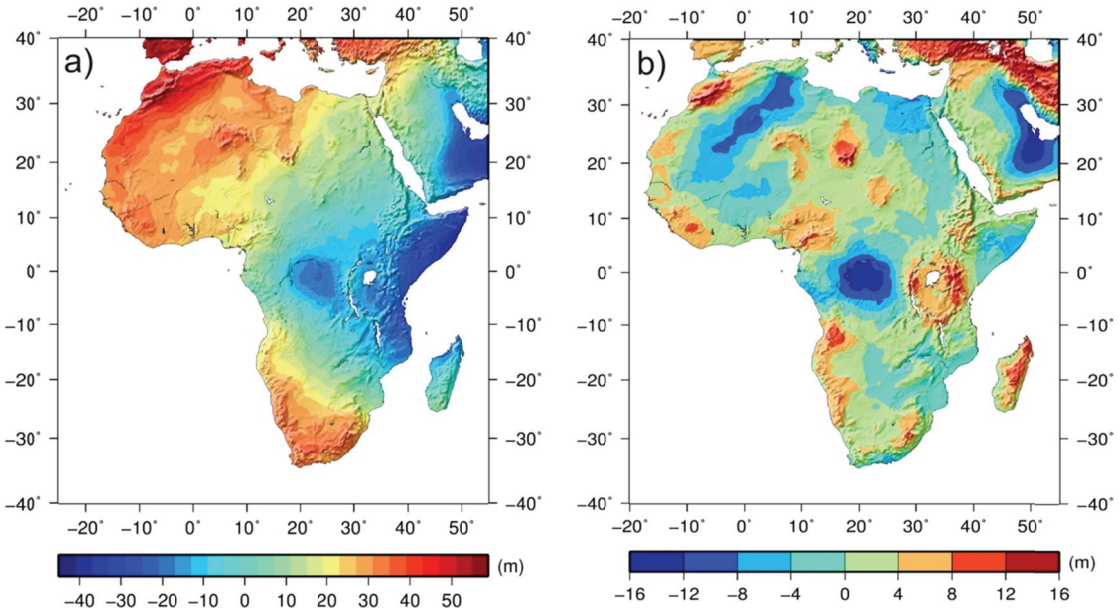

Figure 4.3. Geoid anomalies. a) Geoid anomaly map for Africa extracted from EGM2008 global model (Pavlis et al., 2012). b) Filtered geoid to degree and order 10

Negative anomalies are generally related with big basins and coastal plain depressions, whereas positive anomalies are to mountain ranges, domes and plateaus.

Maximum positive geoid anomalies with values >12 m coincide with the regions of highest topography (e.g., Atlas Mountains, EARS, Tibesti). The largest long wavelength geoid high coincides with the EARS. With a NNE-SSW direction and a length of > 3000 km, this maximum extends from the Afar Triple Junction along the Main Ethiopian Rift and increases from ~6 m to ~14 m in the Tanzania Craton. The volcanic centres (Hoggar, Tibesti, Darfur, and the CVL) are throughout related with positive anomalies showing maximum values of >10 m in the Tibesti centre and up to 6 m in Hoggar and Darfur. In contrast, the African Superswell is characterized by moderate geoid anomaly values (-4 to +4 m), except in the southwestern border of the Congo Craton and the eastern border of the Kaapvaal Craton, where values of >8 m coincide with high elevation ranges (Fig. 4.3b).

Maximum geoid gradients occur in northwest Africa, from >15 m in the Atlas to -12 m towards the WAC, and in Central Africa, from >12 m in the western branch of the EARS to -16 m in the Congo Craton. In Southern Africa positive anomalies are related with the Zimbabwe Craton (0 m to 4 m), the south-western

terranes of the Kaapvaal Craton (from 4 m to 8 m, and very locally above 8 m), the NE and SW ends (Namibia highlands) of the Namaqua-Natal belt (from 0 m to 4 m and from 4 m to 8 m, respectively) and the Angolan Shield, where values of up to 12 m are reached.

The transition to the continent's margins are characterized by negative anomalies along the eastern coast (Red Sea and Indian Ocean) and positive anomalies along the western coast (Atlantic Ocean), with the exception of the Gabon and Congo coastlines, where negative values of -4 m to -8 m are recorded. Remarkable are the regional low of -4 m in average extending along the Nubian Shield and the lows located in the Somalia coastline (up to -6 m) and along the almost entire Mozambique coast, which shows average values in the range of -2 m. To the west, maximum values are recorded in the Angola-Kaapvaal Craton and in the Man Leo Shield locally (up to 8 m) and in the SW termination of the Damara Belt (up to 6 m). Values in the range of 0 to 4 m are observed in the Rokelide and Mauritanian belts. To the north, the transition to the west Mediterranean is characterized by a geoid high with values ranging from 0 to 4 m, whereas the transition to the Central and Eastern Mediterranean is marked by geoid lows with mean values of -2 m and -6 m, respectively. In the southernmost region a local low (mean value of -4 m) is observed at the eastern segment of the Great Escarpment and in the Limpopo Belt (0 to -2 m) between the Zimbabwe and Kaapvaal cratons.

4.3 Crustal parameters

4.3.1 Sediment thickness

Information on the sediment cover in Africa were extracted from the updated 1ºx1º global sediment thickness map from Laske and Masters (1997) and gridded to 10 arc-min using a surface interpolation algorithm. Across the continent thickness of sediments ranges from zero to 14 km, with significant accumulations (>4 km) occurring in the margins of the eastern Mediterranean, North Atlantic and Indian Ocean as well as in the big African basins.

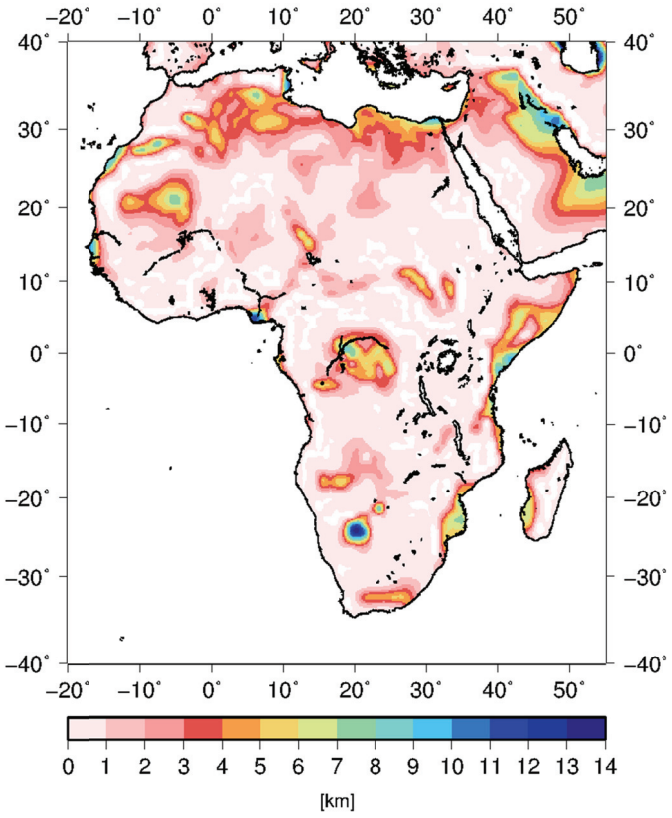

Figure 4.4. Thickness of sediments in Africa, the data were extracted from the global sediment thickness map from Laske and Masters (1997).

Up to 8 km of sediments cumulated in the North African basins of the Sahara, the Taoudeni Basin in the WAC and the intracratonic Congo Basin in Central Africa. Maximum sediment thickness of 14 km is related with the Lower Kalahari Basin in Southern Africa. For the biggest part of the continent the sediment model provides thickness values of less than 1 km. As the degree of compaction and the age of sediments strongly influence their density it is assumed that for very thick and old (>500 Ma) sediment piles (e.g., the Proterozoic basins and the Kalahari Basin) the contrast to basement density is negligible at depths greater than 6 km.

4.3.2 Crustal densities

Information on the crustal density structure in Africa was taken from the CRUST1.0 global dataset (Laske et al., 2013). The model includes estimated density values for sediments (soft and hard) and consolidated crystalline crust (upper, middle and lower crust) on a grid with a resolution of 1° x 1°. Figure 4.5 a)

shows the lateral density variations for the African continent.

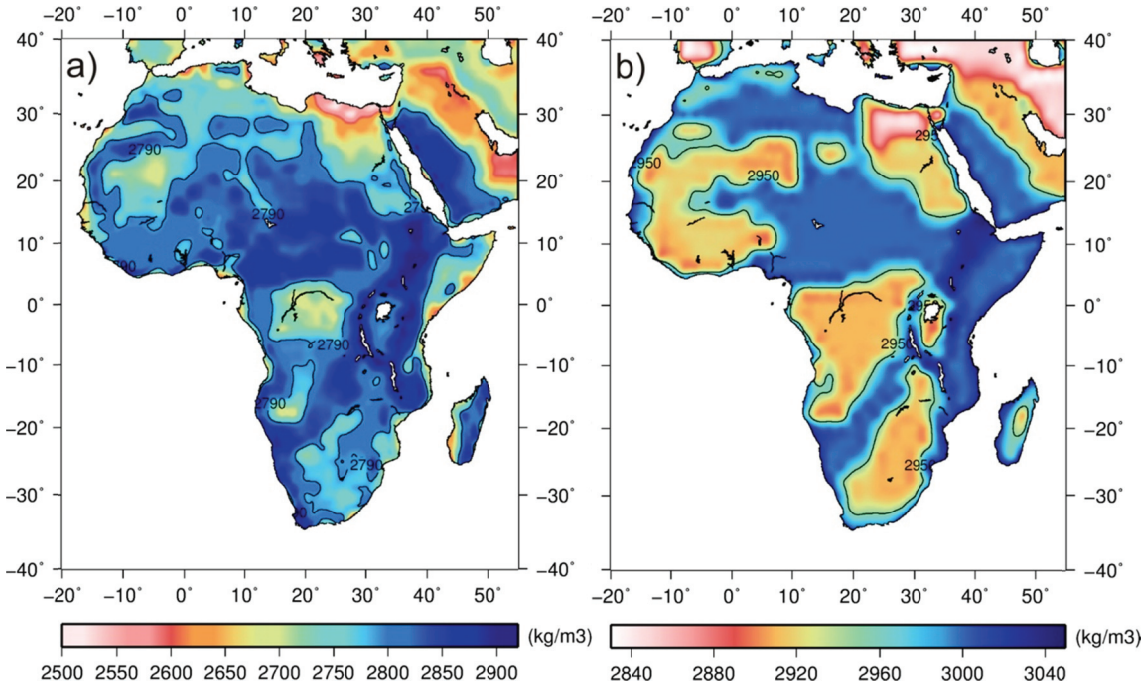

Figure 4.5. Lateral density variations. The density data from CRUST1.0 were used as input to account for the heterogeneous density structure within the crust related with the different types and ages of African tectonic settings. a) Mean crustal density and b) density at the base of the crust. The 2790 kg/m^3 (a) and the 2950 kg/m^3 (b) contour lines denote regions that approach crustal density values used in this thesis. Both datasets were gridded to 10 arc-min.

Additionally, CRUST1.0 provides densities at the base of the crust, ranging from 2840 to 3040 kg/m^3 (see Fig. 4.5b), with higher density values assigned to Phanerozoic basement (~3000 kg/m^3) and to Cenozoic rifts (~3040 kg/m^3). In this dataset average crustal densities away from the margins vary in accordance with the different crustal types (e.g., continental plateaus, rifts, orogenic regions, etc.) from about 2700 to 2910 kg/m^3 with lowest densities in the big basins (~2700 kg/m^3), intermediate densities in the Archean cratons (2780 - 2810 kg/m^3) and collisional belts (~2840 kg/m^3) and highest densities in the East African Rift Systems (>2870 kg/m^3). A particular low density region with values lower than 2600 kg/m^3 is visible around the north-eastern African margin, which is probably due to the contribution of the thick “soft sediment” layer as visible in the sediment thickness map from Laske and Masters (1997), see Figure 4.5b.

4.4 Seismic Moho estimates

I compiled a comprehensive set of Moho depth estimates throughout Africa and the adjacent Arabian Peninsula from available deep seismic sounding (DSS), as well as from receiver functions (RF) studies in order to better evaluate the accuracy of the crustal thickness model. The total database includes 551 data points, 139 from DSS and 412 from RF, which are regionally concentrated in northwest Africa (Morocco), Arabia, East Africa, Cameroon and Southern Africa. Though the focus of this study is clearly on the crustal and lithospheric structure of the African continent, Moho estimates from Arabia were also considered in the evaluation process since throughout most of geological history, the Arabian peninsula formed part of the pan-Afro-Arabian continent until separation took place around 30 Ma. The compiled seismic data and current knowledge of crustal thickness in Africa is presented in Figure 4.6, which displays very well their uneven distribution and absence of seismic coverage for vast areas of the continent (e.g., WAC, Sahara Metacraton, Congo Craton). For a brief review of passive-source seismic studies in Africa the reader is referred to Fishwick and Bastow (2011). Additional references for both active and passive seismic studies are listed in Table 4.1.

Crustal thickness estimates from DSS usually have uncertainties ranging from ±3.5 to ±6 km, depending on data quality, modelling, and interpolation techniques (Waldhauser et al., 1998). According to Spada et al. (2013) the vertical error for crustal thickness estimates derived from RF studies ranges from ±3 km to ±10 km with highest uncertainties expected for complex tectonic areas. Therefore, a threshold of ±4 km for Moho estimates from DSS and ±5 km for those derived from RF to benchmark the crustal thickness model is used.

Decades of seismic investigations revealed the distinctive characteristics of crustal thickness beneath Africa and the non-unique pattern of Moho depth variations related with the various cratons, mobile belts, Cenozoic volcanism, paleo-rifts and recent continental rifting. Summarized, thickest crust in Africa is observed beneath the cratons and belts (>38 km) and thinnest crust (<25 km) beneath the rifts of western and eastern Africa, as well as in the coastal plains (~28 km).

a) Deep Seismic Sounding (DSS)		b) Receiver Functions (RF)	
Region	**Moho depth (km)**	**Region**	**Moho depth (km)**
		Northern Africa	
Rif	29 - 42[d]	Rif	21.6 - 44.4[1,3]
Atlas	33 - 41[a,b,c]	Atlas	23 - 44.7[1,2,14,15,16]
Meseta	~30[c]	Meseta	30.7 - 37.6[1]
Tell (E)	29 - 37[e,f]	Lybian Margin	~27[3]
Saharan Platform	~35[e]	Algerian Margin	30 - 31[3]
Morocco Margin (NW)	34 - 35[x]	Hoggar	~38[2]
Morocco Margin (SW)	27 - 29[y]	Egypt	32 - 33[2,3]
Red Sea	29 - 32[m]	Mauritanian Belt	~26.3[4]
Dead Sea Transform	29 - 38[n,o,p]	West African Craton	41 - 42.6[2,4,17]
Turkana Depression	20 - 21[l]	Afar Depression	15 - 30[6,7]
Afar Depression	~15[h]	Main Ethiopian Rift	27 - 38[6]
Main Ethiopian Rift	25 - 45[g]	Ethiopian Plateau	34 - 44[6]
		Cameroon Volcanic Line	25.5 - 40.5[5]
		Southern Africa	
Zimbabwe Craton	~40[q]	Zimbabwe Craton	35 - 50.5[10,11]
Limpopo Belt	35 - 37[q,r]	Limpopo Belt	39.5 - 46[10]
Namaqua-Natal Belt	40 - 45[s,t,v,w]	Namaqua-Natal Belt	30 - 49[10,12]
Cape Fold Belt	39.5 - 42[u,v]	Kenya Rift	34 - 44[6]
Namibian Margin	28 - 33[β]	Albertine Rift	24 - 38[8]
South African Margin	~34[z]	Mozambique Belt	38 - 40[6]
(W) South	31 - 36.5[s,v]	Ruwenzory Belt	21 - 28[8]
African Margin (S)		Kibaran Belt	36.7 - 44.4[9]
		Ubendian Belt	40 - 49.2[9]
		Usagaran Belt	32.3 - 39.6[9]
		Congo Craton	43 - 48[2,5]
		Tanzania Craton	37 - 44.4[9]
		Irumide Belt	~42.5[13]
		Kaapvaal Craton	33 - 53.5[10,13]
		Cape Fold Belt	33.5 - 48[10,12]
		Kheis Belt	35 - 48[10,11,12]

Table 4.1. Crustal thickness estimates for distinct tectonic terrains in Africa from DSS (a) and RF (b) studies: a) [a] Ayarza et al. (2014), [b] Wigger et al. (1992), [c] Makris et al. (1985), [d] Gil et al. (2014), [e] Buness et al. (2003), [f] Morelli and Nicolech (1990), [g] Maguire et al. (1994), [h] Prodehl et al. (1997b), [l] Kahn et al. (1989), [j] Achauer et al. (1992), [k] Braile et al. (1994), [l] Gajewski et al. (1994), [m] Rihm et al. (1991), [n] Mechie et al. (2005), [o] Weber et al. (2004), [p] El-Isa et al. (1987), [q] Stuart and Zengeni (1987), [r] Durrrheim et al. (1992), [s] Lindeque et al. (2007), [t] Green and Durrheim (1990), [u] Parsiegla et al. (2009), [v] Stankiewicz et al. (2008), [w] Wright and Hall (1990), [x] Contrucci (2004a), [y] Klingelhoefer et al. (2009), [z] Hirsch et al. (2009), [β] Bauer et al. (2000). b) [1]Mancilla et al. (2012), [2]Sandvol et al. (1998), [3]van der Meijde et al. (2003), [4]Kosarian (2006), [5]Tokam et al. (2010), [6]Dugda et al. (2005), [7]Hansen et al. (2009), [8]Woelbern et al. (2010), [9]Tugume (2011), [10]Yousuff et al. (2013), [11]Nair et al. (2006), [12]Kagaswane et al. (2009), [13]Midzi and Ottemoeller (2001), [14]Miller and Becker (2013), [15]Spieker et al. (2014), [16]Cooper and Miller, [17]Di Leo et al. (2015).

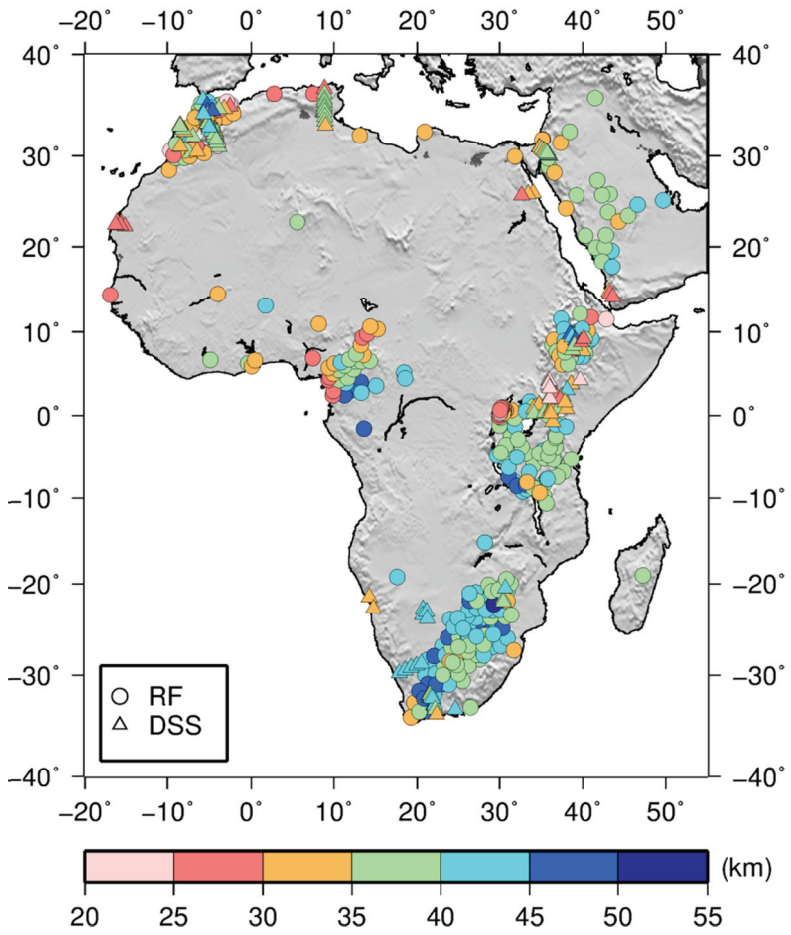

Figure 4.6. Available seismic Moho estimates from active (triangles) and passive (circles) seismic experiments. For details see Table 2. Note the irregular and local distribution of point estimates. Regional knowledge on crustal thickness is restricted to Morocco, Cameroon and Eastern and Southern Africa. Note that for the majority of continental areas data are absent

The distribution of measured crustal thickness from seismic studies in Africa and Arabia is displayed in Figure 4.7 and shows a mean crustal thickness is 36.58 km and a standard deviation of 5.79 km with a clear preponderance of values ranging from 34 to 44 km.

For the sake of simplicity and to facilitate the description of observations from geophysical studies and later also of the obtained results from this work, I will refer to northern Africa as the continental region extending north from a line between the Central Africa Rift System to the Afar Triple Junction, which coincides offshore with the Atlantic Romanche Fracture Zone that separates the Central and South Atlantic regions. Also, I will refer to southern Africa as the continental region

extending south from this line (see Fig. 2.1).

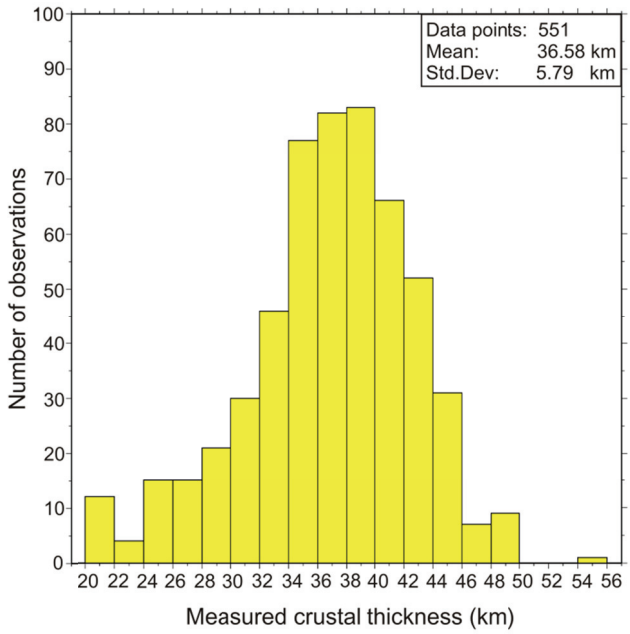

Figure 4.7. Histogram plot showing the distribution of measured crustal thickness from seismic data in Africa. The data compilation shows a mean crustal thickness of 36.58 km and a standard deviation of 5.79 km.

In Northern Africa the crustal structure was imaged during the Topoiberia experiment (Mancilla et al., 2012) showing that crustal thickness beneath northern Morocco is highly variable (Diaz et al., 2016). In the Rif domain crust is between 35 and 44 km thick. Thinner crust from 30 to 22 km is observed beneath north-eastern Morocco, and the southern Atlas foreland is underlain by intermediate thick crust of around 31 km. Crustal thickness along the SIMA transect (Ayarza et al., 2014), crossing the Atlas, varies from 32 km in the middle Atlas to ~40 - 41 km in the root zone and ~ 35 km in the high Atlas. In Tunisia crust is on average 30 to 35 km in the Tell area (Morelli and Nicolich, 1989). In Algeria Moho depth is available beneath a single GEOSCOPE station close to the Hoggar swell showing ~34 km thick crust (Liu and Gao, 2010).

The crustal structure beneath Cameroon was revealed during the Cameroon Broadband Seismic Experiment (Tokam et al., 2010). The authors found crustal thickness of ~28 km in the coastal plains, a decrease in crustal thickness from 33 to 26 km in the Garoua Rift and thickness values of 36 to 43 km in the Oubanguides Belt. For the vast regions comprising detailed knowledge on

crustal thickness beneath the West African Craton, the WAMZ and the Sahara Metacraton does not exist.

Receiver function studies in the East African Rift System (e.g., Dugda et al. 2005; Stuart et al. 2006; Cornwell et al. 2010) showed that crustal thickness within the Ethiopian Rift is 32 - 36 km, circa 40 km away from the flanks in the Nubian and Somalian plates and 39 - 42 km in the Kenya Rift. Controlled-source seismic investigation during the Kenya Rift International Seismic Project (KRISP Working Group 1987) imaged crustal thickness variations from 20 km in the northern part of the Kenya rift in the Turkana depression to 35 km beneath the southern Kenya Dome. Crustal thickness beneath the rift shoulders of the western branch is ~30 km. Thinner crust (20 - 28 km) is observed in the Rwenzori Block in the Western Branch of the EARS, whereas the adjacent Tanzania craton (~40 km) and the surrounding Ubendian (>40 km) and Mozambique Belts (~38 km) are underlain by thick crust.

In southern Africa the crustal structure has been intensively investigated beneath the array of the Southern African Seismic Experiment (Nguuri et al., 2001; Niu and James 2002; Stankiewicz et al., 2002, 2013; Nair et al., 2006; Kgaswane et al., 2009) located in Zimbabwe, Botswana and South Africa. Average crustal thickness is ~36 and ~38 km beneath the Zimbabwe and Kaapvaal Cratons with thicker crust of ~41 km in the northern Kaapvaal, the Pietersburg Terrain. Partly, the surrounding Proterozoic belts show increased thickness of up to 45 km in the Okwa/Magondi Belt and 50 km in the Namaqua-Natal Belt. Depth to the Moho in the Limpopo Belt is ~41 km, in the Kheis Belt ~40 km and shows large variations in the Cape Fold Belt from 26 to 45 km. Seismic data in the Congo Craton are only available for the north western edge of the craton, where the cratonic root reaches depths of 43 to 48 km (Tokam et al., 2010).

The compilation of seismic crustal thickness estimates and related references used in this study to benchmark the crustal model are stored in the digital appendix.

Chapter 5.

Previous continental and global models

Chapter 5. Previous continental and global models

Despite the increased number of (temporary) seismic networks during the last decades the lithospheric structure beneath Africa is still unknown for big parts of the continent, which are among the least understood continental regions in the world. Therefore, the geometry of the most fundamental subsurface boundaries, such as the Moho and LAB, is poorly constrained over large areas. Nevertheless, a number of existing continental and global models provide crustal and lithospheric thickness information for Africa. These models are based on different datasets and methodologies showing large lateral variations in resolution, which in turn lead to significant differences in the resulting structures. In this chapter I want to give an overview of the existing crustal and lithospheric models with focus on the underlying approaches and main structural differences, as the latter have significant influences on our understanding of African geodynamics.

5.1 Crustal models

5.1.1 Seismological models

First estimates of crustal thickness beneath Africa were taken from global models, based on seismic data compilation (Soller et al., 1982; Cadek and Martinec, 1991). Later, Nataf and Ricard (1996) presented the more developed global 3SMAC model, a tomographic model of the upper mantle, which included a crustal model combined with geophysical and chemical information.

The most noteworthy model is the recently published CRUST1.0 global crustal model from Laske et al. (2013), an upgraded version of the previous models CRUST2.0 (Bassin et al., 2000) and CRUST5.1 (Mooney et al., 1998). CRUST1.0 is more complex and provides thickness, densities and compressional and shear velocities for eight layers: water, ice, three sediment layers and upper, middle and lower crust. The model is based on 1º x 1º averages of crustal thickness from DSS and RF studies, and depth to Moho is calculated from gravity constraints, where no seismic data exist. In regions lacking both, seismic and

gravity constraints (e.g., in Africa, Antarctica, South America), crustal thickness is extrapolated based on statistical averages of crustal properties such as basement age and crustal type (e.g., orogen, rift, platform). In recent years CRUST2.0 was the most frequently used model in geodynamic and gravity modelling, and it has also been extensively used for crustal corrections in seismic wave studies (e.g., Zhou et al., 2006).

As the resolution of the CRUST2.0 and CRUST1.0 models is high for regions with good data coverage, but poor in off-data areas, their application in crustal corrections to surface wave measurements is far from errorless, which gave motivation to Meier et al. (2007) to construct a crustal thickness model (Meier07) with a resolution similar to the data sets used in surface wave tomography. Their 2º x 2º global Moho model is based on a neural network approach to invert surface wave data from global phase (Trampert and Woodhouse 2003) and group velocity (Ritzwoller et al., 2002) maps and comes with a global error standard deviation of around 3 km and a maximum absolute error of circa 8 km.

A continental-scale surface wave analysis model for Africa was presented by Pasyanos and Nyblade (2007) (Pasyanos07). Their top to bottom lithospheric study is based on surface wave dispersion measurements with increased data coverage (for tens of thousands of paths) relative to previous studies, especially in North Africa. Including short period group velocities allowed the authors to also investigate the shallow structure of the lithosphere and to develop a crustal thickness map with a 1º x 1º resolution.

The described crustal thickness models CRUST1.0, Meier07, and Pasyanos07 are displayed in Figure 5.1. A comparison between these models shows that biggest differences in terms of lateral thickness variations occur north of the equator, the data poorest region in Africa. Despite the quantitative differences in Meier07 and Pasyanos07, both models contradict the crustal thickening observed in CRUST1.0 related with the Mesozoic West African Rift System.

5.1.2 Gravity based models

Recently, a number of gravity based Moho models were presented, which take advantage of the high accuracy and high spatial resolution measurements of the Earth's gravity field and geoid provided by the GOCE and GRACE satellite missions (e.g., Pail et al., 2010). Inverting gravity data for crustal thickness has been used to generate models that are only based on those gravity observations, such as the Veining Meinesz's model (VMM) by Babherbandi et al. (2013), as well as models that combine gravity observations with seismic data, such as the Delft Moho model (Hamayun, 2014) and the GEMMA model (Reguzzoni et al., 2013). Certainly, these global models have increased our knowledge about crustal structure, but their associated resolution is still too coarse to be applied to regional studies.

The VMM model is based on the Vening Meinesz's inverse problem of isostasy based on generating the isostatic gravity disturbances which equal zero. Depth to the Moho ("mean Moho depth") is computed from Bouguer gravity anomalies and under the assumption of varying Moho depths and the use of a constant Moho density contrast. After correcting the gravity signal for topography, bathymetry, ice and sediments, the computed isostatic disturbances are taken as the sum of the crust stripped gravity disturbances plus the gravitational attraction of isostatic compensation masses. For gravity calculations and crustal stripping corrections the authors used the EGM2008 model and elevation, ice plus sediment data from CRUST2.0, respectively.

The GEMMA model is a combination of the CRUST2.0 seismic model with gravity observations from the GOCE satellite mission. The GEMMA model was reduced to a two-layer model by removing the effects of topography, bathymetry and densities, and can be seen as "an update of the CRUST2.0 Moho model" with a 0.5º x 0.5º resolution. For details on the inversion problem go to Reguzzoni et al. (2013).

The 2º x 2º Delft Moho model (DMM-1) is built on combining gravity disturbances from the EIGEN-6C2 model (see Förste et al., 2013) together with the two seismic models: CRUST1.0 and Meier07 by Meier et al. (2007).

Model	Coverage	Method	Resolution	Reference
GMCT	Global	Seismic data compilation	2º	Soler et al. (1982)
M84C	Global	Seismic waveform inversion	8º	Woodhouse and Dziewonski (1984)
CM91	Global	Seismic data compilation	2º	Cadek and Martinec (1991)
3SMAC	Global	3D seismological model	2º	Nataf and Ricard (1996)
CRUST5.1	Global	Statistical inference based on seismic studies	5º	Mooney et al. (1998)
CRUST2.0	Global	Statistical inference based on seismic studies	2º	Bassin et al. (2000)
CUB2	Global	Surface wave inversion	2º	Schapiro and Ritzwoller (2002)
MDM	Global	Surface wave inversion	2º	Meier et al. (2007)
Pasyanos07	Continental	Surface wave analysis	1º	Pasyanos and Nyblade (2007)
SSLIP	Global	SS waveform stacks	10º	Rychert and Shearer (2010)
Tedla2011	Continental	Gravity, 3-D Euler deconvolution	0.225º	Tedla et al. (2011)
Tugume13	Continental	Gravity, Parker–Oldenburg iterative inversion	0.25º	Tugume_et al. (2013)
GEMMA	Global	Combined gravity and seismic model	0.5º	Reguzzoni et al. (2013)
VMM	Global	Isostatic model	1º	Bagherbandi and Sjöberg (2012)
CRUST1.0	Global	Statistical inference based on seismic studies	1º	Laske et al. (2013)
DMM1	Global	Combined gravity and seismic model	2º	Hamayun (2014)
LITHO1.0	Global	Surface wave analysis	1º	Pasyanos et al. (2014)

Table 5.1. Overview of previous global and continental crustal models, the applied method and their resolution.

The observed gravity disturbances were corrected for contributions due to elevation, ice, sediments and crustal heterogeneities exploiting the ETOPO1, CRUST1.0 and Meier07 models. The residual density signal is considered to result from the difference between the actual density and the reference crustal density of 2670 kg/m^3. As the method (stand-alone inversion of gravimetric data) is known not to necessarily produce realistic results, the CRUST1.0 and Meier07 models were used as a priori information on Moho depth by applying the Variance Components Estimation (VCE) procedure. The computed crustal thickness results were then further refined during a comparison with the European Moho model by Grad et al. (2009). For more details on the modelling procedure and related inherent uncertainties the reader is referred to Hamayun (2014).

New continental-scale Moho estimates beneath Africa, based on gravity modelling, were presented by Tedla et al. (2011) and Tugume et al. (2013). Both studies provide gravity-derived crustal thickness maps, calibrated against seismic Moho estimates and show little variations in crustal thickness between terrains of Archean and Proterozoic age.

Tedla et al. (2011) performed a gravity Euler deconvolution to estimate the Moho depth at a resolution of 0.25º, but the application of this method and its validity to the African continent has been questioned (Reid et al., 2012; van der Meijde and Nyblade, 2014). The technique is using the spectral content of the gravity field to detect subsurface interfaces and it is especially problematic along continent boundaries or regions with strongly thinned crust (van der Meijde et al., 2015). Besides, the thinnest crust in Tedla2011 is around 33.25 km indicating a cut-off in the Euler solutions at this depth (Tugume et al., 2013). In addition, Tedla et al. (2011) did not consider seismic data to benchmark their crustal model in order to reduce the trade-offs.

The model of Tugume et al. (2013) is based on a 3D Parker-Oldenburg iterative inversion (Oldenburg, 1974; Parker, 1973) of EIGEN-6C gravity data using sediment corrected Bouguer anomalies to obtain a simple two-layer model with the Moho as the only subsurface interface. The final model was chosen comparing the calculated Moho map with seismic point estimates and the misfit between the input and modelled gravity anomalies caused by the computed Moho

topography.

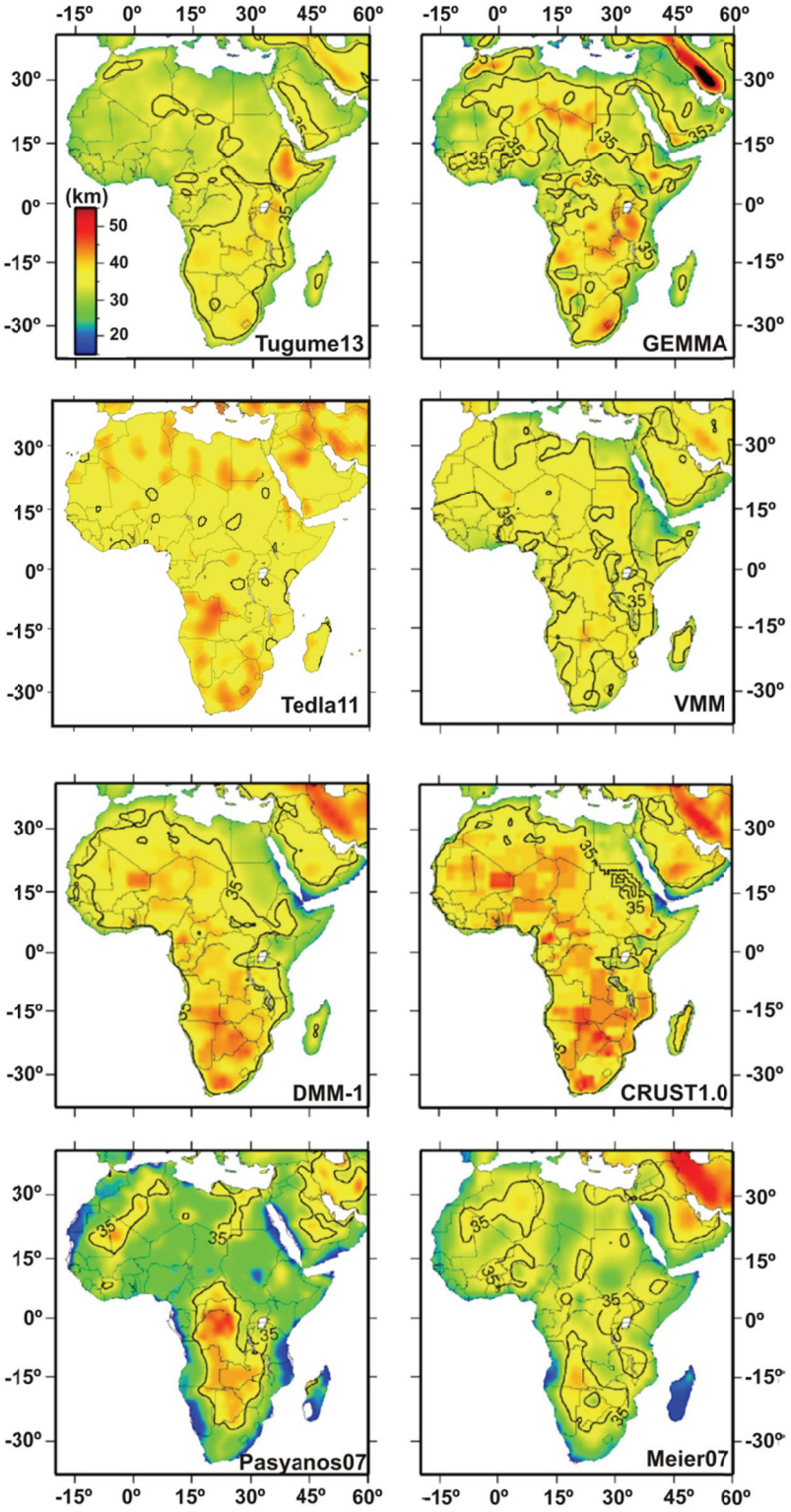

Figure 5.1. Juxtaposition of existing crustal models for Africa as described in the text. The gravity based models are Tugume13, GEMMA, Tedla11, VMM, and DMM-1. Seismological models are CRUST1.0, Pasyanos07 and Meier07. Thick black lines denote the 35 km contour line. Note the relatively smooth Moho variations in the gravity based models compared to the seismological models. Similarities in DMM-1 and CRUST1.0 result from the incorporation of CRUST1.0 into the DMM-1 model.The figure was taken and modified from van der Meijde et al. (2015).

The estimated model's average uncertainties are around ±3 km for the whole continent. The crustal model of Tugume et al. (2013) shows overall thinner crust than the Tedla et al. (2011) model for eastern, southern, and central Africa, with differences of more than 6 km for portions of western and northern Africa. Among all models Tugume2013 is the only one, which predicts thickest crust in Africa beneath the Ethiopian Plateau. A common feature of the above referenced models is the no incorporation of the lithospheric mantle in their calculations.

Interestingly, a comparison between the existing crustal models for Africa shows remarkable variations in regions were no seismic data are available, especially between global and continental models. The following Figure 5.1 compares the previously explained models to highlight these structural contrasts.

A feature common to all models is the relatively thick crust (35 to 45 km) beneath the cratons of Western and Southern Africa. The majority of them (except Tugume13 and Meier07) also predict thicker crust of around 35 km beneath the Congo basin, though a pronounced regional thickening related with the basin is only observed in the two seismological models CRUST1.0 and Pasyanos07. In contrast, Tugume13 and Meier07 rather promote crustal thinning beneath the centre of the basin, which leads to maximum thickness differences among the models of more than 20 km for the Congo Craton. Furthermore, the models contradict Moho geometry especially in the regions of Northern and Western Africa. Seismic models such as Pasyanos07 and Meier07 show significant variations in the crustal structure, whereas the gravity based models VMM, Tugume2013 and DMM-1rather promote a homogeneous and more constant Moho geometry. Nevertheless, strong differences in crustal thickness variations inside and around the WAC, as well as in the Saharan Metacraton occur between all models. In summary, a comparison of the crustal models shows an overall agreement in crustal structure for Southern Africa, though significant differences in absolute thickness values exist (>15 km). However, the predicted variations in Moho geometry for the data-poor regions to the north of the equator are very dissimilar and of opposite sign, as in the case of the Mesozoic rifts.

Therefore, if one wants to correlate the continent's surface tectonics with its crustal structure at depth, choosing an adequate Moho model is not

straightforward. Recently, van der Meijde et al. (2015) pointed out that the model's differences may rise up to 28 km in Moho depth, and that gravity based models show actually less variation among them than seismic models and between gravity based and seismic models, as visible in Figure 5.1. Furthermore, as there is almost no control on the quality of the resulting structure in off-data regions, the authors warn that the impact of these differences for geodynamic interpretation might be significant.

5.2 Lithospheric models

Revealing the deeper structure of the lithosphere is even more complicated, as the lithosphere-asthenosphere boundary does not correspond to a sharp change in temperature or composition. Locally, the chemo-physical state and minimum thickness of the African lithosphere is known from thermo-barometric studies of kimberlitic xenoliths (e.g., in South Africa; Jones, 1988; Griffin et al., 1999; Rudnick and Nyblade, 1999; Artemieva and Mooney, 2001; Deen et al., 2006), whereas the lateral and vertical seismic structure of the upper mantle is imaged by a number of global and regional surface-wave tomography models (e.g., Ritsema and van der Heijst, 2000; Debayle et al., 2001; Sebai et al., 2006; Pasyanos and Nyblade, 2007; Lebedev and van der Hilst, 2008; Priestley et al., 2008; Fishwick, 2010). A dominant feature of the African upper mantle in these models is the contrast between the fast velocities related with Archean cratonic regions and slower velocities (5 - 10%) beneath younger tectonic units (see Fig. 5.2 lower right panel). The velocity structure from surface-wave tomography has been frequently used to investigate variations in lithospheric thickness (seismic models). Another way is to constrain the base of the conductive thermal boundary layer from surface heat flow data (thermal models). The majority of existing LAB models for Africa, which will be introduced in the following, is based on either of those techniques. A list of available global and continental models of lithospheric thickness in Africa and the respective approach is given in Table 5.2.

5.2.1 Thermal models

The thermal thickness of the lithosphere can be estimated by the use of thermal models, which result in reasonable agreement with geophysical observations on heat flow data, xenolith derived pressure-temperature estimates and also with the actual knowledge of crustal parameters (e.g., thickness, radiogenic heat production, density, seismic velocity). As previously mentioned, these models assume that the LAB coincides with the base of the conductive thermal boundary layer, which is usually defined as the intersection of a geotherm with an isotherm (e.g., T_m = 1300 ºC).

First global estimates of lithosphere thickness based on regional geotherms calculated from global heat flow data compilations were presented by Pollack and Chapman (1977) and Artemieva and Mooney (2001). Other than Artemieva and Mooney (2001), Pollack and Chapman (1977) used the depth at which the continental geotherms reach ~0.85 of the melting temperature to define the base of the lithosphere and calculated thermal thickness from a degree-12, spherical harmonic representation of the global surface heat flow field. Their model predicts >300 km thick lithospheric root beneath cratonic West Africa, similar to the estimations of ~350 km by Artemieva and Mooney (2001). The latter presented a LAB map at a resolution of 5º x 5º, which shows two typical thicknesses for Archean (200 - 220 km) and early Proterozoic lithosphere (300 - 350 km). The South African cratons show comparably thin roots (~220 km) and a thick root (>300 km) is found beneath West Africa.

Later Artemieva (2006) and Hamza and Vieira (2012) presented thermal thickness models with higher resolution of 1º x 1º and 2º x 2º, respectively. These models are based on updated global databases of heat flow measurements and crustal structure, which was incorporated from the global models CRUST5.1 and CRUST2.0. For her thermal model for the continental lithosphere TC1 Artemieva (2006) applied a statistical age relationship of continental geotherms based on a new compilation of tectono-thermal ages of lithospheric terranes to fill the gap of no or low quality heat flow data (e.g., in most of North Africa). The strong correlation between the tectonic age and thermal regime demonstrates that the depth to the LAB linearly decreases with age from Mesoarchean to present.

Similar to the previous model by Artemieva and Mooney (2001), the TC1 model shows thinner lithosphere (~200 km) in early Archean cratons of Southern Africa (e.g., the Kaapvaal Craton) than in the late Archean cratons of Tanzania and West Africa (250 - 350 km) (see Fig. 5.2). Hamza and Vieira (2012) also find relatively thick lithosphere (>200 km) beneath Precambrian regions in Africa, with thinner lithospheric roots (~200 km) beneath the Kaapvaal Craton and thicker roots (250 – 300 km) in the area of the Congo Basin and the West African Craton.

5.2.2. Seismic models

Converting the upper mantle velocity structure from surface-wave tomographic models into its vertical temperature distribution has become a favoured technique in seismology to image the base of the thermal lithosphere. Surface-waves propagate predominantly within the crust and upper mantle and due to the good path coverage and lateral resolution, tomographic studies have proven a useful tool to provide estimates of lithospheric thickness in regions without seismic stations, in case that an optimal distribution of seismic sources is given.

A number of authors (e.g., Priestley and Tilmann, 2009; Fishwick and Bastow, 2011; Priestley and McKenzie, 2013) used a method that was first applied by Priestley and McKenzie (2006) to obtain depth to the LAB from seismic velocities. The method combines pressure and temperature estimates from mantle xenoliths with shear-wave velocities from 3D surface-wave tomography to develop an empirical relationship between velocity, temperature and pressure, which is used to convert variations in shear-wave velocities as a function of depth to lithosphere thickness. After the obtained vertical temperature profiles were fitted to individual geotherms, the base of the lithosphere was defined by the intersection of the extrapolated conductive geotherms with the isentropic temperature profile of the mantle at a potential temperature of 1315 ºC. The lithosphere thickness models PT09, FB2011 and PMK2013 were produced applying this strategy and are shown in Figure 5.2 below.

The PMK2013 model is basically an updated version of the PK06 model

with a higher horizontal resolution, as an order of magnitude more seismograms were used (Priestley and McKenzie, 2013). To give an example of the upper mantle velocity structure beneath Africa a map showing shear-wave speeds at 200 km depth from the global tomographic study of Lebedev and van der Hilst (2008) was added to Figure 5.2 (lower right panel).

A comparison of the PT09, FB2011and PMK2013 models shows that the results from surface-wave tomography are in overall agreement. The observed lateral variations in lithospheric thickness related with the big African cratons are similar, with thick lithosphere (180 - 240 km) underlying the cratons and thinner lithosphere (<140 km) beneath Eastern and Northern Africa. These estimates and the lateral trend in LAB geometry are also in good agreement with the thermal TC1-model by Artemieva (2006). Main differences are observed in the continental model FB2011 compared to the global PT09 and PMK2013 models.

The lithospheric structure appears to be better resolved and more heterogeneous in the FB2011 model. Also FB2011 predicts a homogeneous and thinner lithospheric root (150 to 160 km) beneath the Tanzania Craton, whereas the PT09 model and PMK2013 show a much thicker lithosphere (~250 km) and a sharp decrease at the centre and the northern edge of the craton, respectively.

Further information on the LAB geometry beneath Africa can be extracted from a number of global models, which provide large-scale estimates of lithospheric thickness based on different seismic techniques and lithosphere properties. In some cases, the resolution of these models is too coarse to provide sufficient information for wavelengths smaller than 500 km (e.g., the model of Rychert and Shearer, 2009) and/or they show broad agreement with the previously introduced models. Therefore, I decided to only summarize, but not to display these models within the following section. To explore further details on the methods and particular features of the mentioned LAB models the reader is referred to the publications of the respective authors

Plomerova et al. (2002) presented a 10º x 10º global model of the LAB mapping changes in the upper mantle anisotropy. In this model depth to the LAB is associated with changes in anisotropy (mantle fabric) and the base of the

lithosphere is defined as the boundary between the fossil ("frozen-in") seismic anisotropy and the anisotropy due to present-day asthenospheric mantle flow.

Model	Coverage	Method	Resolution	Reference
PC77	Global	Thermal thickness from heat flow	12º x 12º	Pollack and Chapman (1977)
AM01	Global	Thermal thickness from heat flow	5ºx5º	Artemieva and Mooney (2001)
PLOM02	Global	Seismic anisotropy	10º x 10º	Plomerová et al. (2002)
TC1	Global	Thermal thickness from heat flow	1º x 1º	Artemieva (2006)
CLB06	Global	S-wave tomography	1.25º x 1.25º	Conrad and Lithgow-Bertelloni (2006)
PK06	Global	Thermal thickness from seismic velocity structure	3.5º x 3.5º	Priestley and McKenzie (2006)
PT09	Continental	Thermal thickness from seismic velocity structure	n.d.	Priestley and Tilmann (2009)
RS09	Global	*Ps* imaging	5º x 5º	Rychert and Shearer (2009)
Pasyanos10	Eurasia/Africa	Long-period surface wave dispersion	1º x 1º	Pasyanos (2010)
FB2011	Continental	Thermal thickness from seismic velocity structure	3º x 3º	Fishwick and Bastow (2011)
HV12	Global	Thermal thickness from heat flow	2º x 2º	Hamza and Vieira (2012)
PMK13	Global	Thermal thickness from seismic velocity structure	2.5º x 2.5º	Priestley and McKenzie (2013)
LITHO1.0	Global	Long-period surface wave dispersion	1º x 1º	Pasyanos et al. (2014)

Table 5.2. Summary of existing lithospheric thickness estimates for Africa from global and continental models. Information on the underlying approach and spatial resolution is also given.

To detect this boundary, the authors used the depth-dependence of azimuthal and relative polarization anisotropy of surface waves.

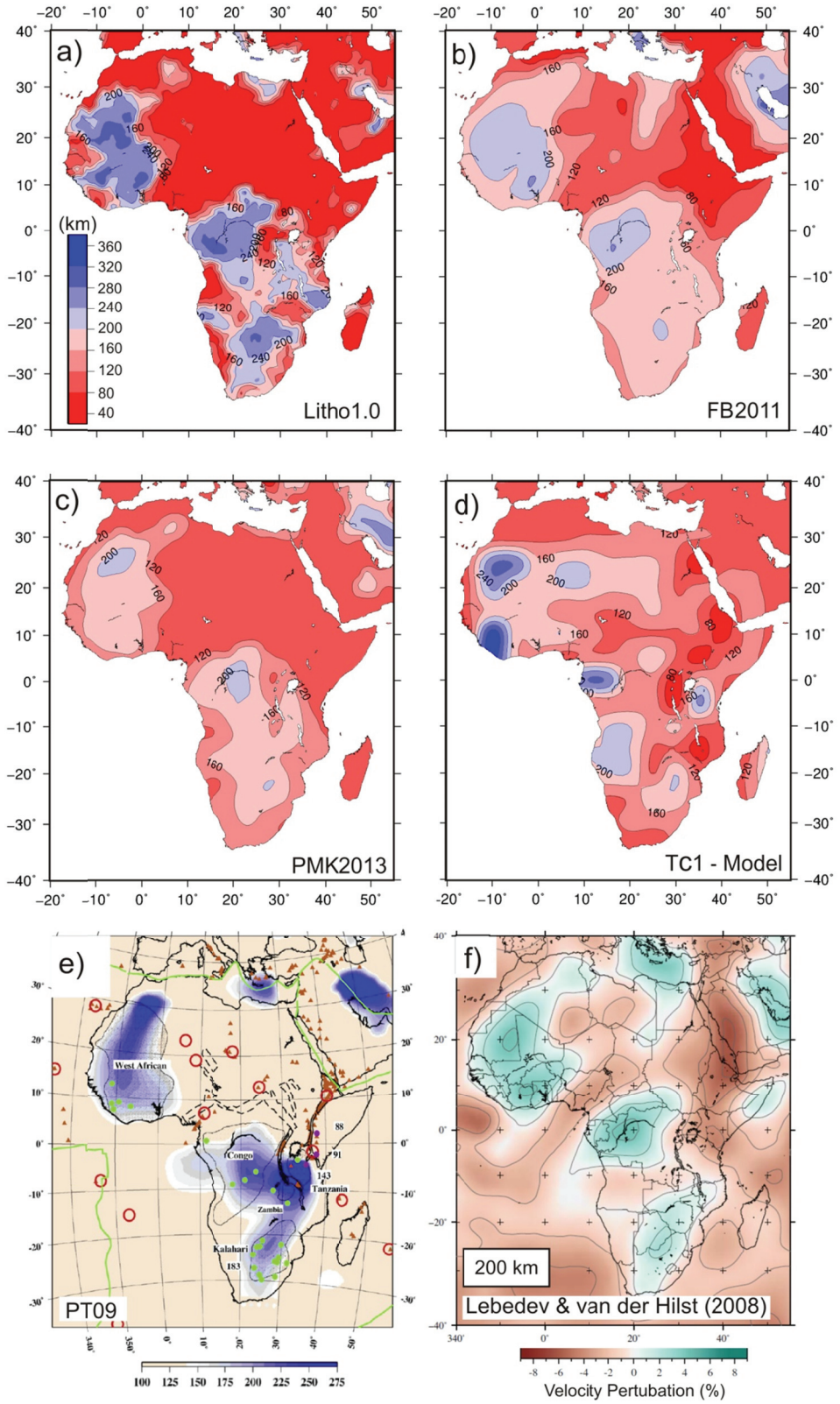

Figure 5.2. Overview of existing thermal and seismic models of lithospheric thickness. The upper four panels (a-d) are displayed with black contour lines every 40 km starting from 120 km and share the same colorscale. a) LITHO1.0 model, b) FB2011 model, c) PMK2013 model and d) the thermal model TC1. The lower panels show e) the PT09 model derived from surface wave tomography and f) a shear-wave speed map at 200 km depth beneath Africa from the global tomographic study of Lebedev and van der Hilst (2008).

Their model shows very thick lithospheric roots beneath West and south-eastern Africa and very thin lithosphere along the Mediterranean and South Atlantic margins, as well as in the Afar region. Anyhow, due to the low resolution the model only allows to image large-scale features, such as the thick lithospheric root beneath the WAC, but it is not sufficient to resolve the regional trend of variations in LAB topography beneath individual tectonic domains.

In S-wave tomography models, the base of the lithosphere can also be defined as the bottom of the region with faster than average seismic velocities (+1.5% to +2%), compared to global seismic reference models, which is overlying a low velocity zone. During the course of a study aimed to quantify lateral variations in upper mantle anisotropy, Conrad and Lithgow-Bertelloni (2006) produced a map providing global depth to the LAB. For continental regions the authors used the method of Gung et al. (2003) who applied the maximum depth for which the velocity anomalies from the S20RTSb seismic tomography model (Ritsema et al., 2004) are greater than +2% to calculate the thickness of the lithosphere. For Africa their model predicts thick lithospheric roots beneath the cratons of West (>260 km), Central (>230 km) and Southern Africa (>200 km), but constantly thin lithosphere (<110 km) for the rest of the continent.

Due to the thin lithosphere in off-craton regions the expected changes in LAB geometry across cratonic boundaries would result in a strong decrease in lithospheric thickness over short distances of up to -150 km in the case of the WAC. In general, the resolution of the model is very smooth and unable to resolve small-scale tectonic features.

Recently, Pasyanos et al. (2014) released the 1º x 1º LITHO1.0 model (Fig. 5.2), which consists of a series of geophysically identified layers (e.g., sediments, crust, lithosphere and asthenosphere) and provides key parameters of the lithosphere and uppermost mantle (e.g., densities, velocities and thicknesses). The authors used long-period surface wave data to model the LAB depth following a method that was previously applied by Pasyanos et al. (2010) to construct a lithospheric thickness model for Eurasia and Africa (Pasyanos10) (see Table 5.2). In both models the LAB is mapped determining the seismic lithospheric thickness, which is defined as the thickness of the high-velocity mantle layer overlying a

lower velocity layer (asthenosphere) that is required to fit the surface wave data. In general, lithospheric thickness estimates of LITHO1.0 are similar in location and depth for the big African cratons (WAC, Kaapvaal and Congo) compared to the previously mentioned LAB models (see Fig.5.2), but it shows only minor variations over broad regions in Northern Africa.

In contrast, the Pasyanos10 model is able to recover small-scale features in these regions, such as disrupted lithosphere beneath the Saharan Metacraton. Furthermore, the model predicts thickest lithosphere in the West African Craton, a pronounced lithospheric root beneath the Congo Craton and lithospheric thinning in Eastern Africa related with the Nubian Shield

A comparison of the existing lithosphere thickness models illustrates that most models show a similar trend in lateral thickness variations related with the large African cratons, but the observed differences in absolute LAB depth are significant and may be more than 80 km in areas with sparse seismic coverage (e.g., Northern Africa) and up to more than 60 km even beneath regions that have been studied extensively with seismic investigations (e.g., southern Africa).

Chapter 6. Results

Chapter 6. Results

In this section I will first demonstrate how the optimal lithospheric reference column for the African continent was chosen and how the incorporation of sediments and lateral changes in density distribution influence the crustal and lithospheric structure and also the accuracy of the resulting crustal models. Subsequently, the final model parameter setup will be presented and the obtained crustal model will be compared with data from seismic experiments focusing on seismically well sampled regions (Morocco, Cameroon, East Africa and Southern Africa) to evaluate the quality of the model and the trend in concordance with the regional crustal structure. In a second step the obtained crustal and lithospheric thickness maps for Africa will be presented. Though the objective is to provide insights into the continent-scale structure of the lithosphere beneath Africa I will not only describe the general long-wavelength features of the *crustal model*, but also the observed regional trend for tectonic regions that have been previously intensively investigated. The calculated crustal and lithospheric thickness values were projected on 10 arc-min grids in order to resolve features that are within the resolution of the input EGM-2008 geoid data (spherical harmonics developed until degree and order 2159, Pavlis et al., 2012).

6.1 The lithospheric reference column

Deriving the crust and lithospheric mantle thicknesses from elevation and geoid anomaly data depends on the choice of an appropriate reference column to which refer their variations and then, on the N_0 value. Determining the reference column for the African continent is not straightforward since it depends not only on the actual crust and lithospheric mantle thickness values (h_c and h_m, respectively) in a given location, but also on the crust and mantle depth-density distribution ($\rho_c(z)$ *and* $\rho_m(z)$, respectively. h_c can be derived from seismic experiments and h_m can be calculated from elevation data considering local isostasy and knowing $\rho_c(z)$ and $\rho_m(z)$. With the thermal approach it is assumed $\rho_m(z) = \rho_a (1 + \alpha[T_a - T_m (z)])$ and that the main unknowns are $\rho_c(z)$ and the thermal parameters, which can

actually show noticeable variations and uncertainties. Therefore, rather than choosing a reference column for a given location of Africa, I have selected the column that best fits the available crustal thickness data that are coming from seismic experiments for the whole continent.

Figure 6.1 shows the fit, in percentage, between the calculated and measured crustal thickness within the uncertainty range of 4 - 5 km, depending on the type of seismic experiment. The calculated crustal thickness depends on the selected reference column and therefore on the considered average crustal density and the integration constant N_0 in the geoid equation (as in Chapter 3.2). Fig. 6.1a) shows the fit obtained after considering all the compiled seismic data and illustrates that the fit increases for crustal densities lower than 2810 kg/m^3, leading to fit percentages ranging from 58 and 64%. It shows that the low crustal densities (~2750 kg/m^3) are required to match crustal thickness data in the Ethiopian Plateau and the MER, a region overlying the Afar plume and characterized by high elevation (E > 2000 m), positive geoid anomalies (N ~5 m), and moderate crustal thickness. However, the sublithospheric processes beneath the Afar region causes magmatism, transient thermal perturbations, and non-isostatic (dynamic) contribution to elevation. Therefore, the Afar plume region (i.e., Afar Depression, Ethiopian Plateau, MER and Kenya Dome) was excluded from the evaluation procedure to avoid bias related with this anomalous region. In addition, I excluded results from a RF study by Wölbern et al. (2010) in the Rwenzori Mountain region. The Rwenzori Mountains are located amidst a rift valley in the western branch of the EARS and show high altitudes of >5000 m, high seismic activity (Koehn et al. 2008), and evidence of removal of the lower crust (Wölbern et al. 2010). The series of tests was then repeated, comparing the results with the thermally stable parts of the continent, attaining a reasonable range of density values (2820 to 2780 kg/m^3) for a number of reference columns that agree well with seismic observations and show an increased fitting from 74 to 76% (Fig. 6.1b). The effects of crustal density heterogeneities and/or mantle contributions to elevation in the Afar area will be further examined in the Discussion chapter.

In summary, the best fitting reference column for the African continent was chosen,

which agrees with 61% of all Moho estimates and with 76.3% of the data, when the Afar plume region is excluded.

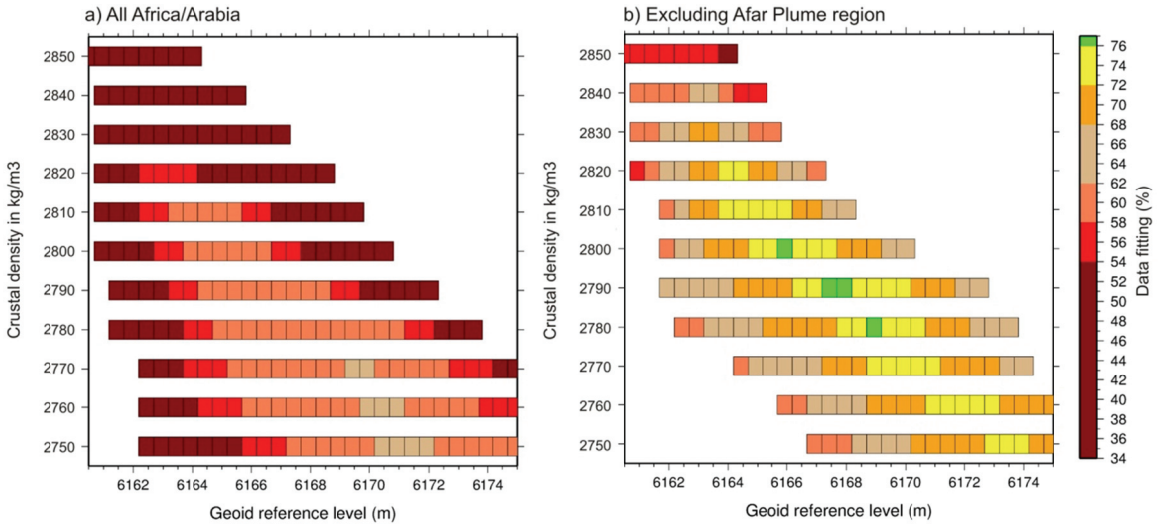

Figure 6.1. Degree of fitting (in %) between calculated and observed crustal thickness for different reference columns determined by the average crustal density and geoid reference level values: a) Considering all available seismic data in Africa; b) Considering all available seismic data in Africa excluding the Afar plume region. Misfits are calculated considering uncertainties in seismic estimates of ±4 km for DSS and ±5 km for RF experiments.

This column, with elevation at sea level, has an average crustal density of ρ_c = 2790 kg/m^3, a crustal thickness of Z_c = 32.16 km and a total lithospheric thickness of Z_L = 153.1 km, resulting in a value of N_0 = 6168 m. I emphasize that different pairs of ρ_c and N_0 values might fit the measured crustal thickness data (especially within threshold limits) data equally well in terms of fit percentage, but additional seismic constraints on the resulting lithospheric thickness from tomography studies (e.g., Ritsema and van Heijst, 2000; Sebai et al., 2006; Fishwick and Bastow, 2011; Priestley and McKenzie, 2013; see sections 5.2.2) were used for discrimination.

The average crustal density of 2790 kg/m^3 determined here agrees well with recent gravity field analysis associated with the refined CRUST1.0 model by Tenzer et al. (2015), who found the same average density value for a global average continental crust, including continental shelves and consisting of igneous, sedimentary, and metamorphic rocks.

6.2 Influence of lateral density variations

6.2.1 Sediment thickness

To account for lateral changes in crustal density related with the presence of sedimentary basins sediment thickness information from an updated 1ºx1º global sediment thickness map from Laske and Masters (1997) was used following the scheme of equations, as explained in Chapter 3.2. The thickness of African sedimentary layers varies from less than 2 km, for most of the continent, to 3 - 4 km in Northern Africa, up to 7 km in the centre of the Taoudeni and Congo basins, and to more than 10 km in the Kalahari Basin (Fig. 4.4).

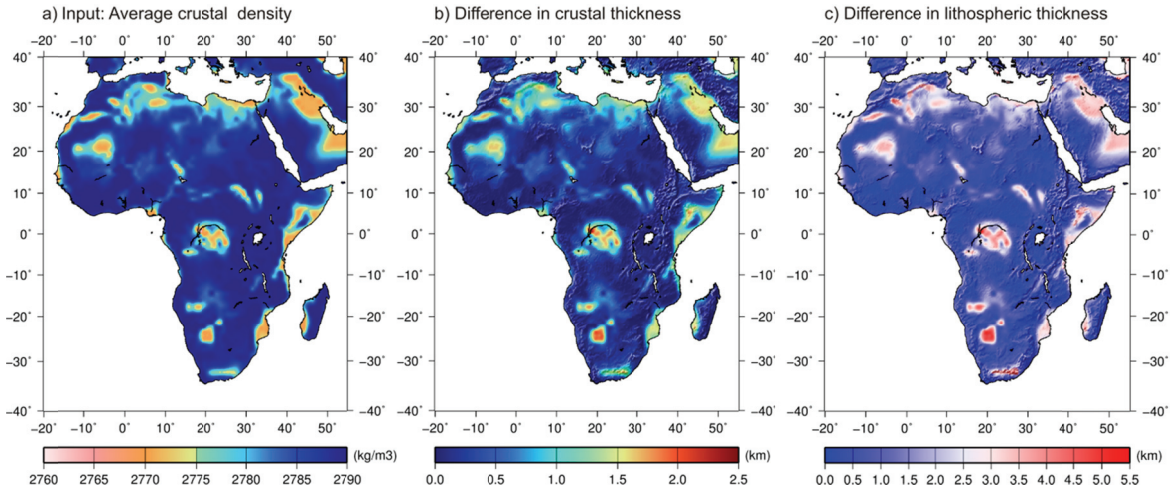

Figure 6.2. The effect of sediments in Africa on a) lateral changes in crustal density and the resulting crustal (b) and lithospheric (c) thickness. Panels b) and c) display the residual thickness maps showing the differences between a model using a constant average density distribution and a model including lateral density variations. Maximum deviations from the reference model (constant densities) are of course found in thick sediment basins, were the effect on the crustal density structure is strongest.

The sediment model from Laske and Masters (1997) is included in CRUST1.0, where the upper crustal sedimentary layer is divided into “soft” and “hard” sediments, which in Africa reach a maximum thickness of about 2 km and 14 km, respectively. In CRUST1.0 “soft” sediments vary in density between 1700 and 2300 kg/m3, whereas “hard” sediments vary from 2300 to 2600 kg/m^3. Considering the strong contribution of thick sediment piles (>2 km, see Fig. 4.4), a surface density for sediments of 2500 kg/m^3 was chosen to be a suitable average value. The observed differences in the resulting density distribution, as well as in the crustal and lithospheric structures, when using a lower sediment density of

2400 kg/m^3 were negligible. Therefore, incorporating the sediment thickness data and a density of 2500 kg/m^3 for uncompressed sediments at the surface of the model, results in an average crustal density distribution that varies laterally from 2760 to 2790 kg/m^3 across the continent (Fig. 6.2a), where maximum deviations of ~30 kg/m^3 with respect to a constant average density distribution occur in regions with more than 5 km of sediment accumulation. Consequently, the resulting maximum differences in thickness for the crust and the lithosphere are related with the thick sedimentary basins and are around 2.5 km and 5.5 km, respectively (see Fig. 6.2 a/b).

However, neither the final crustal nor lithospheric thickness maps show significant variations (an observation also made by Tugume et al., 2013) nor a better fit with seismic data when the sediment layers are incorporated.

Furthermore, a comparison of the crustal model with seismic Moho estimates did not show a better fitting with seismic data. Incorporating changes in crustal density due to variations in sediment thickness helped to understand the effects on the resulting lithospheric structure within the applied approach, but in regions with poor seismic coverage, where the type of sediment cover is undefined, as well as thickness and age (e.g., in Central Africa), much more detailed information is needed.

6.1.2 Crustal density

Another way to evaluate lateral variations in crustal density is to use the CRUST1.0 global dataset (Laske et al., 2013). This dataset includes estimated density values for sediments and consolidated crystalline crust on a grid with a resolution of 1º x 1º (for more details on CRUST1.0 go to subchapter 4.3.2 and 5.1). Densities within African cratons are between 2770 and 2810 kg/m^3 (see Fig. 4.5) and therefore in good agreement with the average constant crustal density value used in the reference column. Furthermore, CRUST1.0 provides densities at the base of the crust with values varying from 2840 to 3040 kg/m^3. Therefore, knowing the average and bottom crustal densities, the 2D lateral density structure

from CRUST1.0 is incorporated into the analysis using:

$$\rho'_0 = 2 * \rho_{cs} - \rho_M$$

(as explained in the Methodology chapter 3.2) to adjust the density at the surface of the model. The resulting changes in the average crustal density relative to the initial value of 2790 kg/m^3 range from -290 to +120 kg/m^3 with maximum negative and positive differences restricted to the northeastern African margins and the northern portion of the EARS, respectively. Nevertheless, for the majority of the continent, the changes in density range from -60 to +55 kg/m^3.

The calculated differences using a heterogeneous density structure in crustal and lithospheric thickness with respect to the constant density model are shown in Figure 6.3 below. A comparison shows that significant thickness differences are observed for both crust and lithosphere although differences are acceptable for most parts of the continent with ±5 km and ±10 km for the Moho and the LAB.

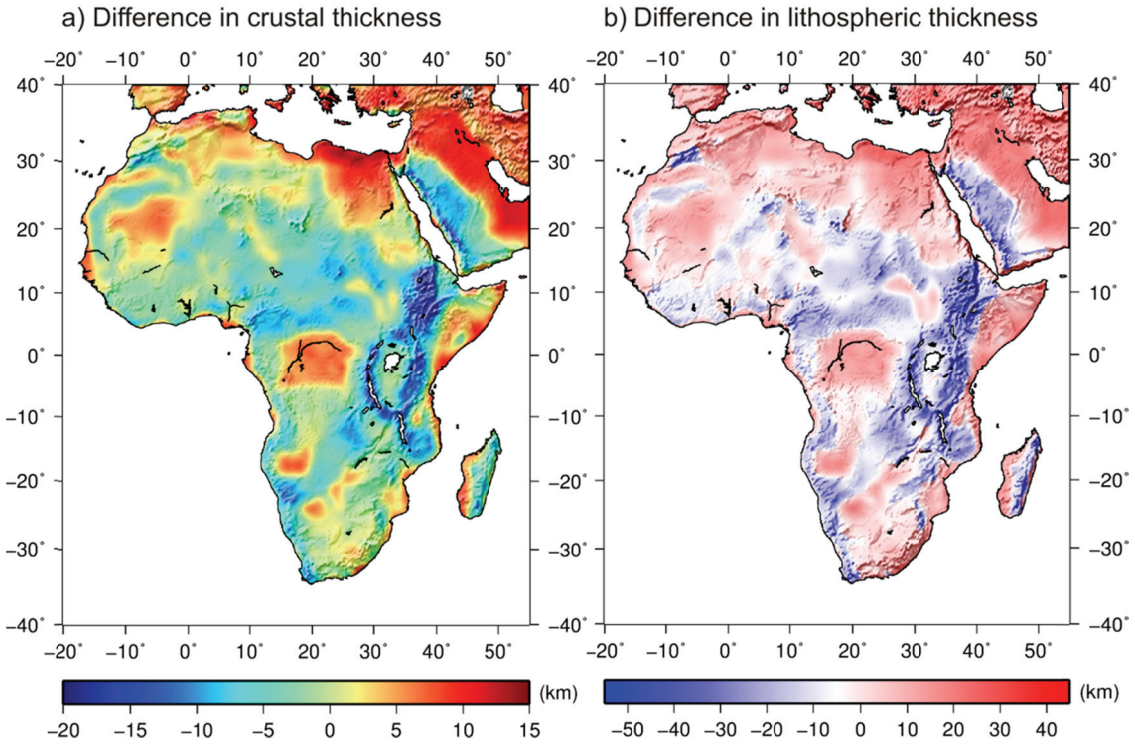

Figure 6.3. The effect of input densities from CRUST1.0 on a) the resulting crustal and (b) lithospheric thickness estimates. The panels display the residual thickness maps showing the differences between a model using a constant average density distribution and a model including lateral density variations. Crust and lithosphere show strong differences in the rifts of East Africa (+20 km/+50 km), the big African basins (-8 km) and the north-eastern Mediterranean margin (-10 to -15 km).

Strongest changes are not distributed arbitrarily but coincide clearly with regional tectonic features.

For the big sedimentary basins in Western and Central Africa crust and lithosphere are significantly thinner, with strongest thinning observed around the north-eastern margin, the region where CRUST1.0 predicts very low crustal density values. The crust and the lithosphere are about 15 km and 20 km thinner for this region. In East Africa high densities from CRUST1.0 along the Cenozoic rifts lead to a strong increase in crustal and lithospheric thickness of >15 km and >50 km, respectively. This is a critical observation, considering that extensional forces in East Africa currently cause crustal and lithospheric thinning. Rift related processes such as magmatic intrusions and mafic underplating are adding high density material to the crustal column and in this sense the higher density values along the rift provided by CRUST1.0 are reasonable. Anyhow, the uncertainties of the CRUST1.0 density data are unknown, and the strong thickening of crust and lithosphere appears to be a rather unrealistic feature for an active rift setting.

A comparison of the heterogeneous density model with the seismic estimates of crustal thickness shows that the incorporation of lateral density changes from CRUST1.0 could improve the calculated Moho depth only in a very few locations in Southern Africa. Overall, the obtained fit using all the seismic observations decreases to ~41% for the whole continent and the fit obtained when the Afar region is excluded decreases to ~54.75%. Hence, it was not possible to improve the lateral constant density model. Therefore, including information from global model CRUST1.0 could be helpful where knowledge of sediment thickness and crustal density structure is well known, but might introduce additional uncertainties, where this knowledge is absent.

6.3 The final model parameter setup

As demonstrated above, applying the method by Fullea et al. (2007) using a simple constant average density distribution in the crust, with ρ_c = 2790 kg/m^3,

resulted in a first order estimate of crustal thickness, which shows a fairly well agreement (~76%) with existing seismic observations of crustal thickness in Africa, when excluding the Afar plume region. However, additional information from CRUST1.0 was used to account for 2D lateral variations in the crustal density distribution. Neither the incorporation of sediment thickness nor the average crustal density data resulted in an improvement of the model in terms of fitting the seismic data. To the contrary, the resulting crustal maps using densities from CRUST1.0 showed strong misfits across various regions in Africa. As the only way to measure the quality of the model is the comparison with point constraints I chose the "simple" constant average density model based on the "best fitting" lithospheric reference column to extrapolate crustal thickness into regions where knowledge on crustal structure is zero. The complete setup of the parameters used in the modelling approach is given in Table 6.1 below.

Parameter	Symbol	Value
Upper crustal density	ρc_Top	2630 kg/m^3
Lower crustal density	ρc_Bottom	2950 kg/m^3
Lithospheric mantle density	$\rho m\ (T)$	3200*[1-3.2*10^{-5} (T-1350 ºC)]
Asthenosphere density	ρa	3200 kg/m^3
Sea water density	ρw	1030 kg/m^3
Compensation level depth	*Zmax*	300 km
Moho depth of the reference column	*ZC_Ref*	32.16 km
LAB depth of the reference column	*ZL_Ref*	153.1 km
Linear coefficient of thermal expansion	*a*	3.2 10^{-5} K^{-1}
Crustal surface heat production	*H*S	0.5 µW/m^3
Crustal thermal conductivity	*kC*	2.5 Wm^{-1}K^{-1}
Mantle thermal conductivity	*k*M	3.2 Wm^{-1}K^{-1}
Surface temperature	*T*S	0 ºC.
Temperature at the LAB	*Ta*	1350 ºC

Table 6.1. Model input parameter setup

Table 6.2 compares the compiled crustal thickness values from seismic experiments with those obtained from the modelling and other previously published global and continental models, distinguishing the cases of using the complete dataset and excluding the Afar region. The maximum difference between seismic data and all models are 13 - 19 km. regardless of whether the Afar area is considered or not, indicating that these differences are not related with this particular region. In contrast, the minimum differences range between -17 and -23 km for the whole continent of Africa and between -9 to -16 km when the Afar region is excluded, indicating that modelled crustal thickness exceeds that observed in the Afar area independent of the model. The final crustal model has a root mean square error (RMSE) of 6.4 km relative to the seismic estimates, showing the best minimum RMSE (4.3 km) and a maximum fit (76.3%) when the Afar plume region is excluded (last column in Table 6.2).

Models	Max (km)	Min (km)	RMSE (km)	Fitting (%)
	All data/Excl. Afar	All data/Excl. Afar	All data/Excl. Afar	All data/Excl. Afar
This work	16.3/16.3	-23.0/-13.9	6.4/4.3	61.0/76.3
CRUST1.0[(1)]	18.5/18.5	-17.0/-15.7	5.3/5.0	69.9/74.5
Tedla[(2)]	12.7/12.7	-19.0/-16.4	6.4/5.9	57.9/59.3
Tugume[(3)]	18.9/18.9	-17.4/-11.3	6.1/5.3	56.6/64.0

Table 6.2. Statistical comparison of crustal thickness estimates from seismic experiments with published models for all Africa and excluding the Afar region. Columns denote maximum and minimum differences, root mean square error (RMSE) and degree of fitting (in %) considering uncertainties in seismic estimates of ±4 km for deep seismic sounding experiments and ±5 km for receiver function analysis and fitting with the seismic Moho compilation applying the aforementioned fitting criteria. References: (1) Laske et al. (2013); (2) Tedla et al. (2011); (3) Tugume et al. (2013).

6.4 Model evaluation: Comparison with seismic Moho estimates

Crustal thickness results across Africa are in overall good agreement with those from seismic investigations. At regional scale, good fit is observed in Morocco, Tunisia, and the Arabian-Nubian Shield, along the CVL, and in the Tanzania, Zimbabwe and Kaapvaal cratons (Fig. 6.4a). It is worth noting that the predicted crustal thickness values largely exceed the observations in the region affected by

the Afar plume in the EARS, with deviations of >10 km (Fig. 6.4b).

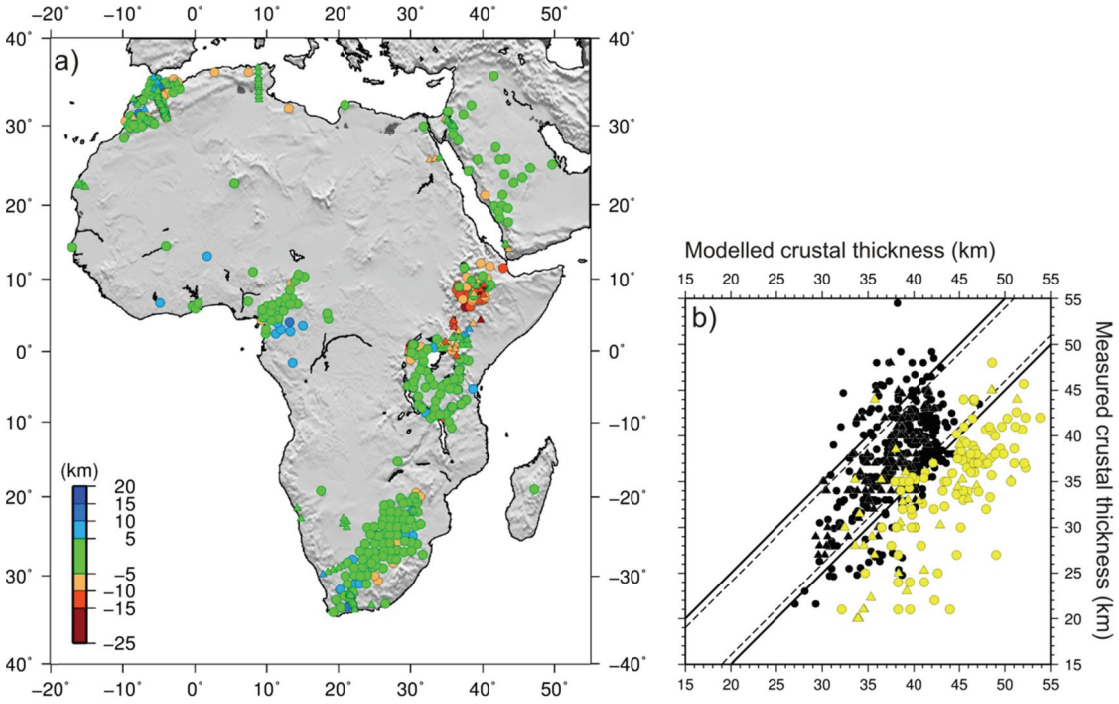

Figure 6.4. a) Difference between observed and calculated crustal thickness at each seismic station (see colour scale). Triangles denote Deep Seismic Sounding experiments and circles denote Receiver Function experiments. b) Scatter plot showing observed versus calculated crustal thickness. Black continuous (±5 km) and dashed (±4 km) lines denote uncertainties related with seismic experiments. Coloured symbols: Yellow refers to the Afar plume region, and black refers to the rest of Africa/Arabia.

The degree of fit between modelled and observed crustal thickness was previously summarized in Table 6.2, where the results show increased fit with seismic estimates (from 61 to 76.3%), when the Afar plume region is excluded. The excess crustal thickness predicted in this region is due to the fact that the hypotheses of the applied approach are not strictly valid. That is, the given assumptions do not apply to portions of lithospheric mantle affected by the Afar plume, which causes magmatism, dynamic uplift, and transient thermal regime (see Discussion).

Nevertheless, higher than expected thickness differences are also observed for stations located outside the Afar plume region. In East Africa misfits occur locally in narrow tectonic structures related with the Western and Eastern Rift valleys and, particularly, in the Turkana depression, where larger extension in the northern Kenya Rift causes stronger thinning (up to ~21 km, Gajewski et al., 1994). In west and southern Africa misfits exceeding by few km the seismic

uncertainties (4 - 5 km) are observed in the WAC as well as in the Namaqua-Natal Mobile Belt and northern Kaapvaal, respectively. Some of these misfits coincide with areas where shear wave velocity profiles indicate either unclear Moho signals or multiple Moho detections (e.g., in the Kaapvaal Craton, Kgaswane et al., 2009), thus suggesting that the uncertainties associated with seismic estimates can exceed 5 km in these cases. Therefore, the calculations could be within the range of measured values and do not allow for firm conclusions on the validity of the modelling assumptions.

In Northern Africa, comparison with seismic data in the Rif (northern Morocco) is somewhat ambiguous. Misfits of >5 km occur along the north-south direction of the wide-angle seismic profile by Gil et al. (2014) located in the external zone of the Rif, where crustal thickening is observed related with slab pull under the Gibraltar Arc. However, the results are in good agreement with RF estimates from Mancilla et al. (2012) in the same area. In contrast, in the region affected by crustal thinning beneath north-eastern Morocco, the model shows misfits >5 km with RF (Mancilla et al., 2012), but good agreement with the estimates from DSS (Gil et al., 2014). Thus, the model's differences of >5 km compared with seismic estimates in the Rif cannot be ascertained as they are well within the range of values coming from two independent experiments. Furthermore, it should be mentioned that these discrepancies are related with the complex Neogene tectonic evolution of the Iberia-Africa plate boundary, where several deep-seated processes, such as mantle delamination, slab retreating, and lateral slab tear, can interact (e.g., Spakman and Wortel, 2004; Faccenna et al., 2004; Vergés and Fernandez, 2012; Bezada et al., 2013; Mériaux et al., 2015; Miller et al., 2015; Mancilla et al., 2015).

Figure 6.5 summarizes the degree of fit (in percent) between the modelled and observed crustal thicknesses for the whole continent, the whole continent excluding the Afar plume region, and for the different regions in which data can be grouped. A positive/negative mean mismatch indicates under/over calculated crustal thickness, respectively. In the Afar plume region, calculated values are clearly overestimated due to the influence of the mantle plume (see Discussion), an effect that is also partly affecting the East African Plateau region, especially in

the rifts surrounding the Tanzania Craton. In the other regions, calculated values reproduce the observations well, with mean mismatches between -0.52 and +0.15 km.

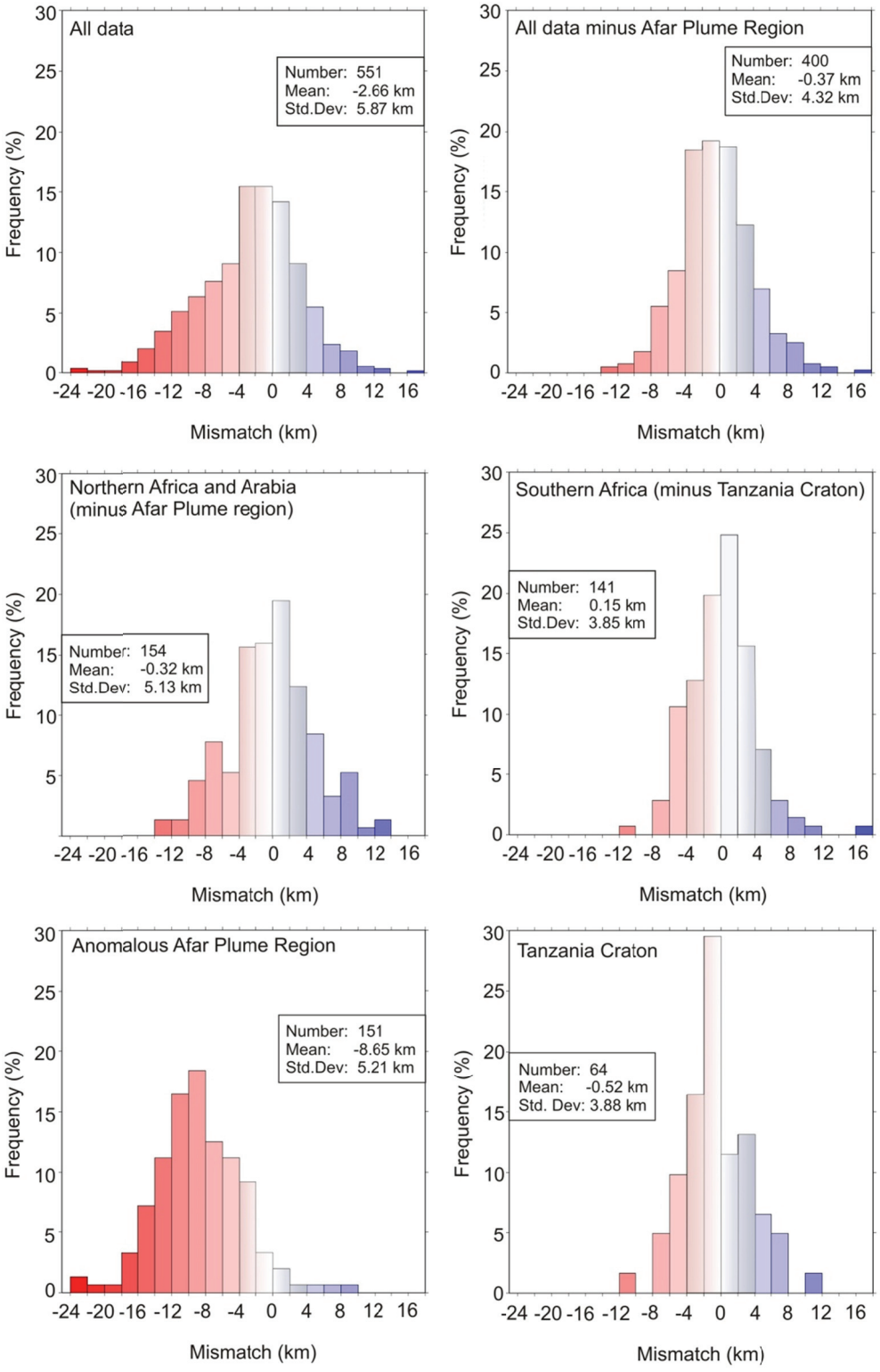

Figure 6.5. Histograms showing the mismatch between observed and calculated crustal thickness for whole Africa and the different regions where seismic data are available. A positive/negative mean mismatch indicates average under/over calculated crustal thickness, respectively.

Note that excluding the Afar plume region results in a much better fit, with a mean mismatch of -0.37 km and a standard deviation of 4.32 km.

6.5 The crustal thicknesses map

Figure 6.6 shows the calculated crustal thickness map for the African continent. The circled area in the northern EARS denotes the region affected by the Afar mantle plume where the hypotheses of the method are not completely fulfilled. Modelled crustal thickness varies from minimum values of 28 - 30 km along the Atlantic coastal zone, particularly in northern Africa, to maximum values of ~48 km in southern Africa, particularly beneath the Tanzania and Kaapvaal cratons. Significant variations in Moho geometry appear to be sensitive to the large-scale tectonic framework of the continent, but also occur within the boundaries of distinct tectonic regions (e.g., Saharan Metacraton, WAC, Congo Craton, Rif-Tell-Atlas Alpine System; Fig. 6.6 right panel). Overall, thick crust (>37 km) is associated with Archean cratons and shields and with Proterozoic belts. Crustal thicknesses higher than 40 km are observed within the southern African cratons, Phanerozoic mountain belts, and single dome structures related with hotspots in northern Africa. The crustal model depicts a bimodal distribution, with a clear north-south division, and distinct crustal structure and thicker cratonic crust in southern Africa (38 - 44 km) compared to the northern half of the continent (33 - 39 km).

6.5.1 Northern Africa

General structure

In northern Africa, maximum crustal thickness values (42 km) correspond to the WAC and to the northern part of the WAMZ. A noticeable crustal thinning towards the western and southern margins of the WAC is imaged, with values of 32 - 36 km in the Reguibat and Man-Leo shields (Fig. 3.1). The most striking feature is the conspicuous NNE-SSW oriented crustal thinning from 34 to 28 km separating the western and eastern regions of Northern Africa. This thinning cuts the Sahara

Metacraton and is located between the Murzuq and Al Kufrah cratons connecting apparently the CVL, the Tibesti hotspot and the Haruj volcanic field (Fig. 6.6). The results show that, the Chad Craton is affected by crustal thinning, with Moho depths of ~32 - 34 km. Towards the east (i.e., the Al Kufrah Craton and Arabian-Nubian Shield), crustal thickness increases to 35 - 39 km.

Regional trend

Thickest crust in Northern Africa is related with the NW-SE trending Atlas mountain chain (~39 km) with local maxima in the High Atlas (42 km). Compared with Moho estimates from active seismic experiments in Morocco (Wigger et al., 1992; Ayarza et al., 2014; Gil et al., 2014) the model is in good agreement with the crustal structure across the Atlas Mountains. Within the ±4 km threshold, modelled Moho depth agrees with all data points along the RIFSIS profile crossing the Middle Atlas (Gil et al., 2014) and the SIMA profile (Ayarza et al., 2014) and reflects very well the observed Moho depth variations observed by Ayarza et al. (2014) from ~35 km south of the High Atlas to ~41 km in the root zone and ~31 km towards the north of it. In the NW Moroccan platform modelled crustal thickness of ~31 km is thinner compared with Moho depths of ~35 km published by Contrucci et al. (2004). Anyhow, Tadili et al. (1986) showed that crustal thickness varies from 25 km along the Atlantic coast to 40 km in the central High Atlas, which argues for a possibly thinner crust (<35 km) along the Moroccan margin.

In the western part of the High and Middle Atlas Mountains modelled crustal thickness is between 34 and 42 km and correlates very well with similar Moho depths from refraction data by Makris et al. (1983), but is too thick (>38 km) to the very SW of the High Atlas. Compared with Moho depth estimates from RF studies in Morocco, presented by Mancilla et al. (2012), the model is in ±5 km agreement with 15 of the 25 locations showing crustal thickness from 32 to 36 km in the Rif Cordillera and the Moroccan Meseta. In the northern Rif the model shows thinner crust than imaged by (Mancilla et al., 2012 and Gil et al., 2014) with crustal thickness from 35 to 39 km, decreasing eastwards to 30 km at the Mediterranean margin. General agreement is better in the eastern part of the Rif and modelled minimum crustal thickness of 35 km in the region leads to

discrepancies of >5 km, where Mancilla et al. (2012) found crust thinner than 27 km.

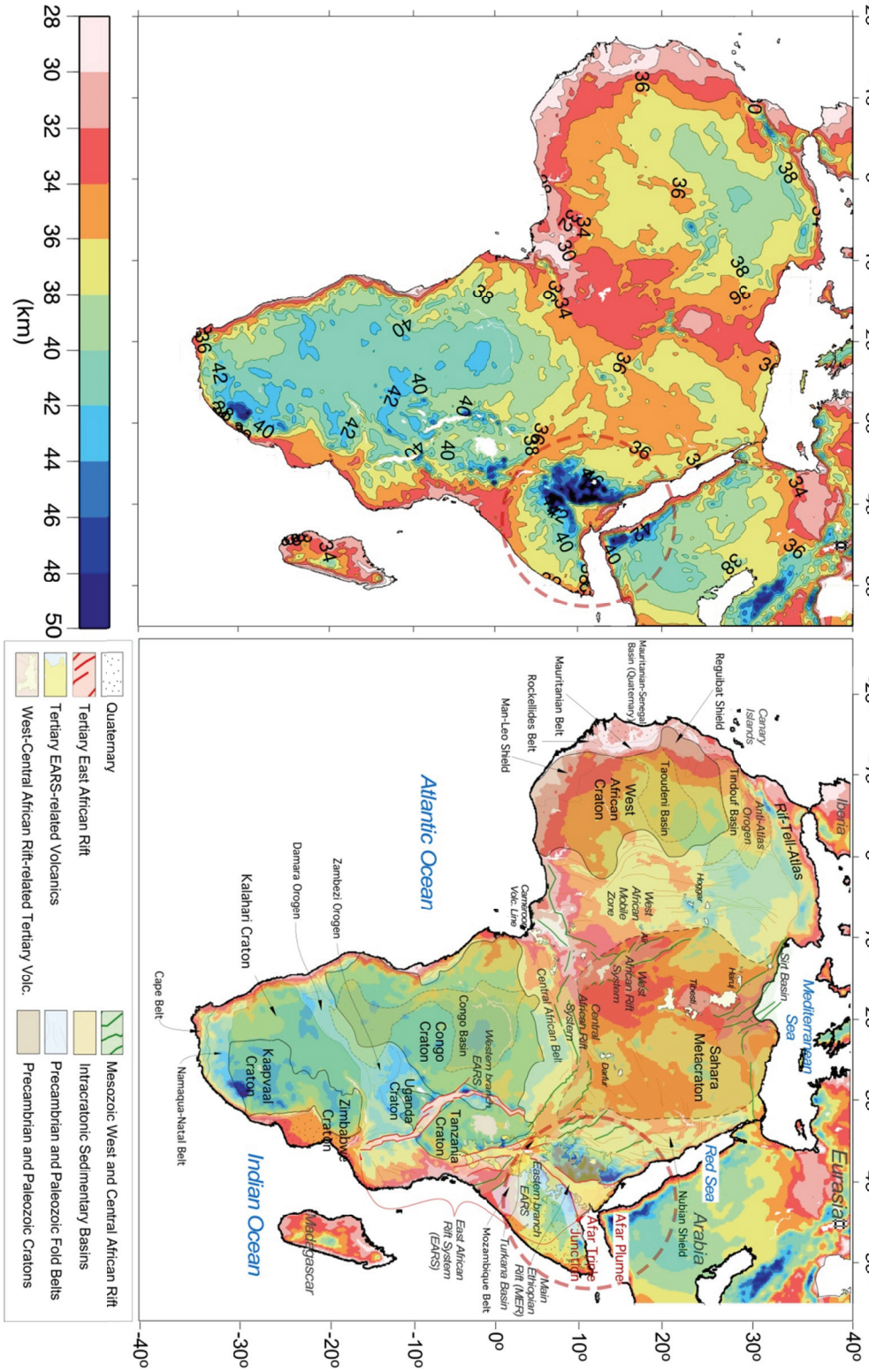

Figure 6.6. Left panel: Calculated crustal thickness map with isolines every 2 km. Right panel: calculated crustal thickness map superimposed on the structural map with the main tectonic units. The encircled area denotes the Afar plume region where crustal thickness is overcalculated because the assumptions of the approach are not fulfilled.

Beneath the northern Tindouf Basin the crust is 33 to 34 km thick and deepens to ~37 km below the Paleoproterozoic reworked portion of the eastern Reguibat Shield. Minor crustal thinning (<3 km) is observed south of the Taoudeni Basin's boundary along the contact with the eastern portion of the Man Leo Shield, where Paleoproterozoic reworking affected the Archean crust during the Eburnian Orogeny. The Archean crustal portions of the northern Reguibat and the southern Man Leo Shield are underlain by moderate thick crust of ~32 km. To the west of the craton flattening of the crust-mantle boundary occurs, where thin crust ~30 km is observed beneath the N-S running Neoproterozoic Maurentanide Belt.

In the West African Mobile Zone crustal thickness is ~38 km beneath Algeria, ~34 km in the Benin-Nigerian Block and shows thicker crust (39 - 42 km) in Central and South Algeria related with the Tuareg Shield and the Hoggar Dome. Locally thicker crust of ~39 km is observed to the southeast of the Tuareg Shield beneath the Aïr Massif in Niger. Along the eastern boundary of the northern and southern segment of the WAMZ an abrupt decrease in crustal thickness from ~36 km to ~32 km marks the contact with the Sahara Metacraton.

Beneath the vast Sahara Metacraton crustal thickness is highly variable with thinnest crust (31-34 km) in its western portion, thickest crust (~37 km) in the centre and intermediate crust (~35 km) in the eastern part. Large-scale crustal thinning is well pronounced from north to south in the western part of the metacraton, where crustal thickness beneath Lybia and Chad is ~32 km. The overall N-S crustal thinning is interrupted by exceptionally thicker crust ~37 km between the Tuareg Shield and the Tibesti Massif, related with the proposed Murzuq Craton (Fezaa et al., 2010) and the Tibesti itself (~40 km). Similarly, the results show thicker crust ~37 km in the central and north-eastern areas of the Sahara Metacraton, which coincide very well with the proposed Al Kufrah Craton (Le Heron and Howard, 2012). Equally thick crust of ~37 km is observed beneath the uplifted Darfur area in the south central part of the metacraton. For the possible remnants of the former pre-Neoproterozoic Sahara craton outlined by Ligeois et al. (2013); Murzuq, Al Kufrah and Chad cratons the model shows reasonably thick crust ~ 37 km for the former two, whereas the proposed Chad Craton seems to be underlain by thin crust of ~32 km. The E-W running

Oubanguides Belt, which separates the Sahara Metacraton from the Congo Craton shows increased crustal thickness of 37 to 39 km.

Beneath Cameroon a marked crustal structure shows thicker crust related with the Cameroon Volcanic Line. Crustal thickness along the CVL varies from 31 to 42 km and is significantly thicker than in the Benue Trough (~30 km) to the north. Modelled crustal thickness beneath Cameroon along the CVL is in very good agreement with Moho estimates of 28 to 40.5 km by Tokam et al. (2010).

6.5.2 Southern Africa

General structure

In southern Africa, the model depicts a generally more homogeneous crustal structure. Regional crustal thickness values are about 40 - 42 km, thinning very abruptly towards the western and southern margins and more gently towards the eastern margin. In the Congo Craton crustal thickness is between 36 and 42 km, whereas to the east, beneath the Uganda and Tanzania cratons, it shows typical values for cratonic crust of 38 to 43 km and agrees well with seismic Moho estimates in the region. The big Proterozoic intracontinental Congo basin, located in the centre of the Congo Craton is marked by increased crustal thickness ~43 km. Maximum crustal thickness values exceeding 46 km are found in the Kaapvaal Craton. East of the Tanzania Craton and along the eastern branch of the EARS, crustal thickness ranges between 30 and 34 km.

Regional trend

Crustal thickness beneath the Congo Craton varies from 36 to 43 km, where increased crustal thickness (>42 km) is found in the Congo Basin area and the south-western Angolan Shield. The northern Bomu-Kibalian and eastern Kasai Shields also show slightly thicker crust (~41 km), whereas crustal thickness in the western Gabon-Kamerun Shield is around 37 km. Unfortunately, there is only very few data in the Congo Craton. Tokam et al. (2010) showed that crustal thickness beneath the north-western edge of the Congo Craton is between 43 and 48 km.

The model does not predict such thick crust for this region, but shows clearly lower thickness values of around 37 km. Nevertheless, for the northern boundary of the craton the results (~39 km) are in good agreement with thickness values of 40 - 43 km reported by Sandvol et al. (1998) and Hansen et al. (2009).

To the east of the Congo Craton the model shows continuously thick crust (~39 km) underlying the Tanzania Craton. Locally, only minor variations in crustal structure occur across the craton resulting in thickness values of 37 to 41 km. This observation is in very good agreement with seismic RF studies by Last et al. (1997), who found that crustal thickness for the Tanzania Craton lies in the range of 37 to 42 km. Local maxima of >44 km are found to the west and are related with the surrounding Proterozoic Rwenzori, Kibaran and Ubendian belts. The Ugandan Craton to the north shows thinner crust with values between 35 and 37 km.

Crustal thickness in the Zimbabwe Craton is between 36 and 41 km and increases slightly southwards to >42 km in the Limpopo Belt. Though slightly thicker, these values appear in good agreement compared with Moho depths from receiver functions of 34 - 37 km (Nguuri et al., 2001) and 36 to 39 km (Gore et al., 2009) for undisturbed parts of the Zimbabwe Craton (not affected during Pan-African Orogeny). Furthermore, both Nguuri et al. (2001) and Gore et al. (2009) show crustal thickening up to ~45 km beneath the Limpopo Belt, a feature also visible in the model but only for the very northern part of the mountain belt, where the model shows increased crustal thickness (>42 km). In contrast, the southern portion of the Limpopo Belt is underlain by thinner crust increasing from 36 km in the east to 39 km in the west. Crustal thinning beneath the Limpopo Belt was also observed by Stuart and Zengeni (1987), who used mine tremors as sources to image a step in Moho depth of 6 km beneath the belt and crustal thicknesses of ~44 km in the Zimbabwe Craton and ~34 km in the adjacent Limpopo Belt.

Modelled crustal thickness (38 - 44 km) agrees well with most seismic estimates across southern Africa, where measured Moho depth is between 35 and 50 km in the Kaapvaal and Zimbabwe cratons (e.g., James et al., 2003; Kwadiba et al., 2003; Nair et al., 2006; Niu and James, 2002; Youssof et al., 2013). Yet, the model is not able to predict the extreme short-wavelength variability in

Moho depth beneath the various tectonic blocks in southernmost Africa, such as those observed by Youssof et al. (2013). Overall, the model shows thicker crust (>43 km) in the eastern Kaapvaal portions and a general better match with seismic data for the Northern and Central Terranes of the Witwatersrand Block. For the north-eastern section of the craton Moho depths are up to 45 km (Nair et al., 2006; Stankiewicz et al., 2013), although several authors reported values higher than 50 km (Stankiewicz et al., 2002; James et al., 2001, 2003; Kwadiba et al., 2003; Wright et al., 2003). The model does not depict such thick crust in the northern Kaapvaal. Instead, the results show crustal thickness up to 41 km in the Northern Terrane (Pietersburg Terrane) and up to 45 km in the Central Terrane, which agrees very well with 40 - 44 km thick crust from RF studies by Nair et al. (2006). Crustal thickness of 41 - 44 km beneath the Bushveld Complex is in good agreement with Moho estimates from 38.5 km to 46 km presented by Kgaswane et al. (2012). For the southern portion of the Kaapvaal the model shows crustal thickness of 40 to 43 km, which is rather thick compared with Moho depths of 35 to 39 km from RF studies in the region (Nguuri et al., 2001; Niu and James, 2002; Stankiewicz et al., 2002; Stankiewicz et al., 2013). In the western Kimberley Block crustal thickness does not show significant variations and is on average 40 - 42 km. Flat Moho topography in the Western Block was previously reported by James et al. (2003) and later by de Wit and Tinker (2004), who showed minor undulations in Moho depth from 38 to 40 km along a deep seismic refraction profile. Nevertheless, in the very south-western section of the Kimberley Block crustal thickness is 39-43 km, which coincides very well with observed variations in Moho depth of 37-43 km, presented by Stankiewicz et al. (2002).

Crustal thickness in the surrounding belts is ~41 km in the Okwa/Magondi Belt, 38-42 km in the Kheis Belt, 37 - 50 km in NNB and 37 - 42 km in the CFB. Reported values from the SASE project (Nguuri et al., 2001; Stankiewicz et al., 2002; Niu and James, 2002; James et al., 2003; Kwadiba et al., 2003; Wright et al., 2003; Webb et al., 2004; and Nair et al., 2006) for these provinces are 40-45 km, 40 km, 40-50 km and 26-45 km, respectively, showing that modelled results are very well within the range of seismically determined Moho depth. A remarkable feature to the southeast of the Kaapvaal in the border with the eastern Namaqua-Natal belt is the very thick crust beneath Lesotho with up to 50 km.

Assessing the validity of the model in this region is difficult, as Lesotho is not covered by the SASE network and no seismic data are available. Nevertheless, the ≥10 km increase in crustal thickness across the Archean-Proterozoic boundary between the Kaapvaal craton and the Namaqua-Natal belt due to magmatic underplating and/or orogenic thickening has been previously described (Durrheim and Mooney, 1994; Schmitz and Bowring., 2004; Sommer et al., 2013) and was seismically imaged (Nair et al., 2006; Youssuff et al., 2013) at the south-western margin of the Kaapvaal Craton. Hence, up to 50 km thick Proterozoic crust in the Western Namaqua-Natal belt might be a larger lithospheric feature that further extends into the Eastern Namaqualand beneath the Lesotho Plateau.

6.6 The lithospheric thickness map

The resulting lithospheric thickness or LAB-depth map (Fig. 6.7) shows a large spatial variability with values ranging from 90 - 230 km. Overall, the distribution of thick lithosphere correlates well with the tectonic boundaries of the big African cratons and with geoid minima (Fig. 4.3b). Thin lithospheres is observed along the coastal regions of the Atlantic Margin, the central part of northern Africa, and the eastern branch of the EARS, coinciding with geoid maxima (Fig. 4.3b). In the region affected by the Afar mantle plume (circled area in Fig. 6.7, right panel), results are not reliable due to the above mentioned limitations. Unlike for the crust, the LAB depth map does not show a bimodal distribution between northern and southern Africa but instead, lithospheric thickening and thinning appears to be associated with cratons and mobile belts and with Mesozoic and Cenozoic extension, respectively (Fig. 6.7). In the WAC the lithosphere thickness varies from 110 km beneath the Man Leo Shield to the south to ~200 km beneath the northern part of the craton. Thick lithosphere in northwest Africa is not limited to the WAC but extends to the northeast into the northern segment of the WAMZ, with values exceeding 200 km. Beneath the Taoudeni Basin, the lithosphere thickens from 140 to >200 km following a SW-NE trend. A similar pattern with thick lithosphere extending far into the Sirt Basin is also indicated by positive S-wave anomalies between 150 and 200 km in global (Lebedev and van der Hilst, 2008) and continental surface-wave models (Ritsema and van Heijst, 2000).

Modelled lithosphere beneath the WAC is on average 165 km thick, with values up to 200 km, which is in good agreement with surface wave tomography estimates by Sebai et al. (2006).

6.6.1 Northern Africa

In the WAC depth to the LAB varies from 120 to >200 km. Thick lithosphere in the northern part of the craton beneath the Taoudeni Basin area is between 160 and 170 km. In the Archean portions of the craton modelled lithosphere is comparably thin beneath the Man Leo (120 - 140 km) and Reguibat Shields (120 - 160 km). The model shows that lithosphere is thicker towards the north eastern edge (>180 km) and that distribution of thick lithosphere in northwest Africa is not limited to the WAC, but exceeds the boundaries to the northeast into the northern segment of the WAMZ. Similar extension of thick lithosphere far into the Algerian platform is known from global and continental surface-wave models (Ritsema and van Heijst, 2000; Lebedev and van der Hilst, 2008). Calculated thickness beneath the WAC is on average between 160 km and 190 km, which is in good agreement with Sebai et al. (2006), who observe a significant change in azimuthal anisotropy amplitude and direction at around 180 km depth. For the Neoproterozoic belts to the west of the craton (Mauritanides and Rockellides) the model predicts lithospheric thinning with a change in LAB depth across the craton's boundary from 160 to less than 140 km. For the complex Pan-African suture to the east, the WAMZ, the model shows strong variations in lithospheric thickness from more than 200 km in the north to less than 140 km in the south. Thinnest lithosphere (140 - 120 km) in the WAMZ is found beneath the strongly deformed Tuareg Shield, which includes the Hoggar Domain and in the Benin-Nigeria Shield to the south.

In the Sahara Metacraton thick lithosphere (>160 km) is limited to its north-eastern portion, coincident with the Al Kufrah Craton with maximum thickness of 190 km (Fig. 6.7). These values are consistent with continent-scale seismic studies, imaging fast velocities down to 150 (Ritsema and van Heijst, 2000) and 180 km depth (Sebai et al., 2006) beneath this region.

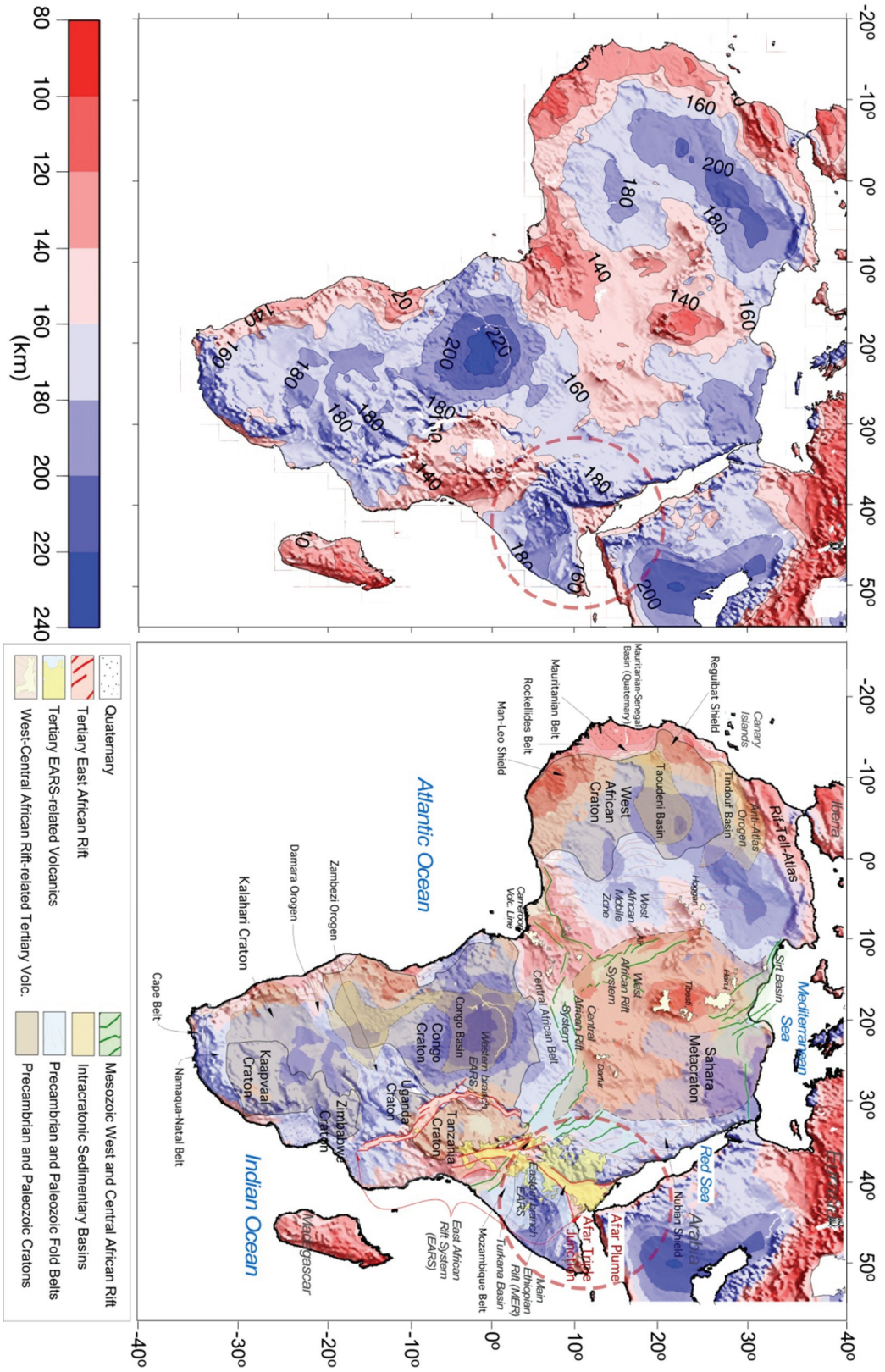

Figure 6.7. Left panel: Calculated lithospheric thickness map with isolines every 20 km. Right panel: calculated lithospheric thickness map superimposed on the structural map with the main tectonic units. Isolines every 20 km. The encircled area denotes the Afar plume region where lithospheric thickness is overcalculated because the assumptions of the approach are not fulfilled.

In the southern portion of the Metacraton, including the Chad Craton, the lithosphere thickens from 130 km in the west to 160 km in the east. S-wave tomography shows a similar trend, with increasing velocity perturbations between 100 and 175 km depth oriented in a west-east direction (Begg et al., 2009). Overall, the western half of the Saharan Metacraton shows a relatively thin lithosphere (110 - 130 km) coinciding with the Tibesti hotspot and the Haruj volcanic province. Due to the absence of regional seismic data in the Sahara region it is very difficult to compare the lithospheric thickness results for the Saharan Metacraton. Nonetheless, thicker lithosphere to the northeast appears to be reasonable, as continent-scale seismic studies image fast velocities between 150 km (Ritsema and van Heijst, 2000) and 180 km (Sebai et al., 2006) beneath this region.

6.6.2 Southern Africa

Thickest lithosphere (170 to 220 km) in Africa was modelled in the Congo craton with maximum thickness of 230 km beneath the centre of the Congo Basin. Increased lithosphere thickness beneath the Congo Craton is in good agreement with previous seismic models proposing a maximum lithospheric thickness of 230 km beneath the centre of the Congo Basin (e.g., Pasyanos and Nyblade, 2007; Pasyanos, 2010; Fishwick, 2010). The fact that thickest lithosphere in Africa is related with the Congo Craton, especially to the Congo Basin area, is a common feature in seismic tomography models, suggesting a deep cratonic root down to depths of 200 - 250 km (Ritsema and van Heijst, 2000; Sebai et al., 2006; Priestley et al., 2008; Begg et al., 2009). To the south thick lithosphere (~190 km) extends beneath the Archean Kasai Shield and to the south-southeast towards the Kalahari Craton and the Damara and Zambezi belts, with values of 170 - 190 km. In contrast, in the north-eastern Bomu-Kibalian Shield and the western Gabon-Camerun Shield the model shows thinner lithosphere beneath the Archean Shields at the edges of the Congo craton with ~165 km and ~150 km, respectively. Whereas no significant variations in lithospheric thickness are visible across the southern border of the craton, the separation of the West African from the Congo Craton is very well pronounced and marked by a broad region of thin lithosphere

(~120 km) with minimum values of ~110 km beneath the Central African Belt.

For the cratons to the east of the Congo the model shows thinner lithosphere with constant thickness. Depth to the LAB beneath the Uganda Craton is between 160 and 180 km and between 140 and 160 km beneath the Tanzania Craton. The results are in good agreement with findings from tomography as discussed later within the next chapter. Thinnest lithosphere in the region (<120 km) is found beneath the Paleoproterozoic Usagaran Belt to the east of the Tanzania Craton, which is to the eastern branch of the EARS.

Thick lithosphere of 170 - 190 km in the very southern portion of the continent is observed beneath the Zimbabwe and Kaapvaal cratons and the Mesoproterozoic Namaqua-Natal Belt. On average, the Kaapvaal Craton lithosphere is ~170 km thick, which appears to be rather thin compared with LAB depths inferred from body-wave studies, which show high velocity roots down to 200 km (Ritsema and van Heijst, 2000), if not 300 km (James et al., 2001; Fouch et al., 2004). Surface-wave and receiver function studies also indicate very thick lithosphere, down to ~300 km (Chevrot and Zhao, 2007; Wittlinger and Farra, 2007). In contrast, a number of seismic studies argue for a thinner lithosphere beneath the southern and central Kaapvaal Craton, as they image a fast mantle lid down to 160 - 180 ± 20 km (Li and Burke, 2006; Priestley, 1999, 2006, 2008), and display a distinct low-velocity zone beneath 150 km (Savage and Silver, 2008; Wang et al., 2008; Vinnik et al., 2009), as well as a change in anisotropy (Freybourger et al., 2001) and LAB conversions at ~155 km depth (Hansen et al., 2009). Chemical tomography from Begg et al. (2009) shows the base of depleted lithosphere varying from ~150 to 200 km depth, whereas LAB-depth estimates of 150 to 170 km are inferred from heat flow and geothermobarometry on kimberlitic xenoliths (Jones, 1988; Rudnick and Nyblade, 1999; Artemieva and Mooney, 2001; Deen et al., 2006; Priestley et al., 2006). Therefore, the results agree well with minimum lithosphere thickness estimates in the Kaapvaal Craton and thus appear to be fairly reasonable. Moreover, we observe a slightly thinner lithosphere (~150 km) along the western boundary of the Kaapvaal Craton towards the north-western Namaqua-Natal Belt, which is also indicated by low-velocity anomalies at 150 km depth in the regional P- and S-wave models of Fouch et al. (2004).

6.7 Lithospheric cross sections

To better illustrate the relationship between tectonic features (e.g., volcanic regions, basins and plateaus) and the modelled lithospheric structure, two >7000 km long transcontinental profiles were selected and are portrayed in Figure 6.8).

The figure shows the two lithospheric profiles crossing the African continent in both a north-south and northeast-southwest orientation, revealing surprisingly small undulations in Moho depth despite the great diversity of surface features.

As visible in profile A - A`, for the southern continent the Moho topography remains remarkably flat beneath regions changing from lowered to uplifted topography. Anyhow, though not clearly pronounced, slight crustal thickening (<5 km) is visible in both transects beneath the cratonic regions in comparison with surrounding off-craton areas. In contrast changes in the LAB topography are much more pronounced. These profiles display evidence for different deformation styles between the crust and lithospheric mantle. Although the regional patterns of crust and lithospheric thickness look similar, major differences are delineated in the Atlas region (Northeast-Morocco), where the crust is relatively thick compared to the lithospheric mantle (e.g., Zeyen et al., 2005; Teixell et al., 2005; Fullea et al., 2007). Similar deviations are seen near the CVL and the Tibesti and Haruj volcanic fields, where the crust is relatively thin compared to the lithospheric mantle. The intracratonic basins (e.g., Congo Basin and Taoudeni Basin) display remarkable lithospheric mantle thickening. Despite the fact that the dominant contribution to the geoid is generally related with topography, Figure 6.8 shows large departures in the regional trends of elevation and geoid along both profiles, especially in the central Africa region. The smooth Moho geometry results in a LAB depth that mimics the geoid variations, such that the higher the geoid, the shallower the LAB.

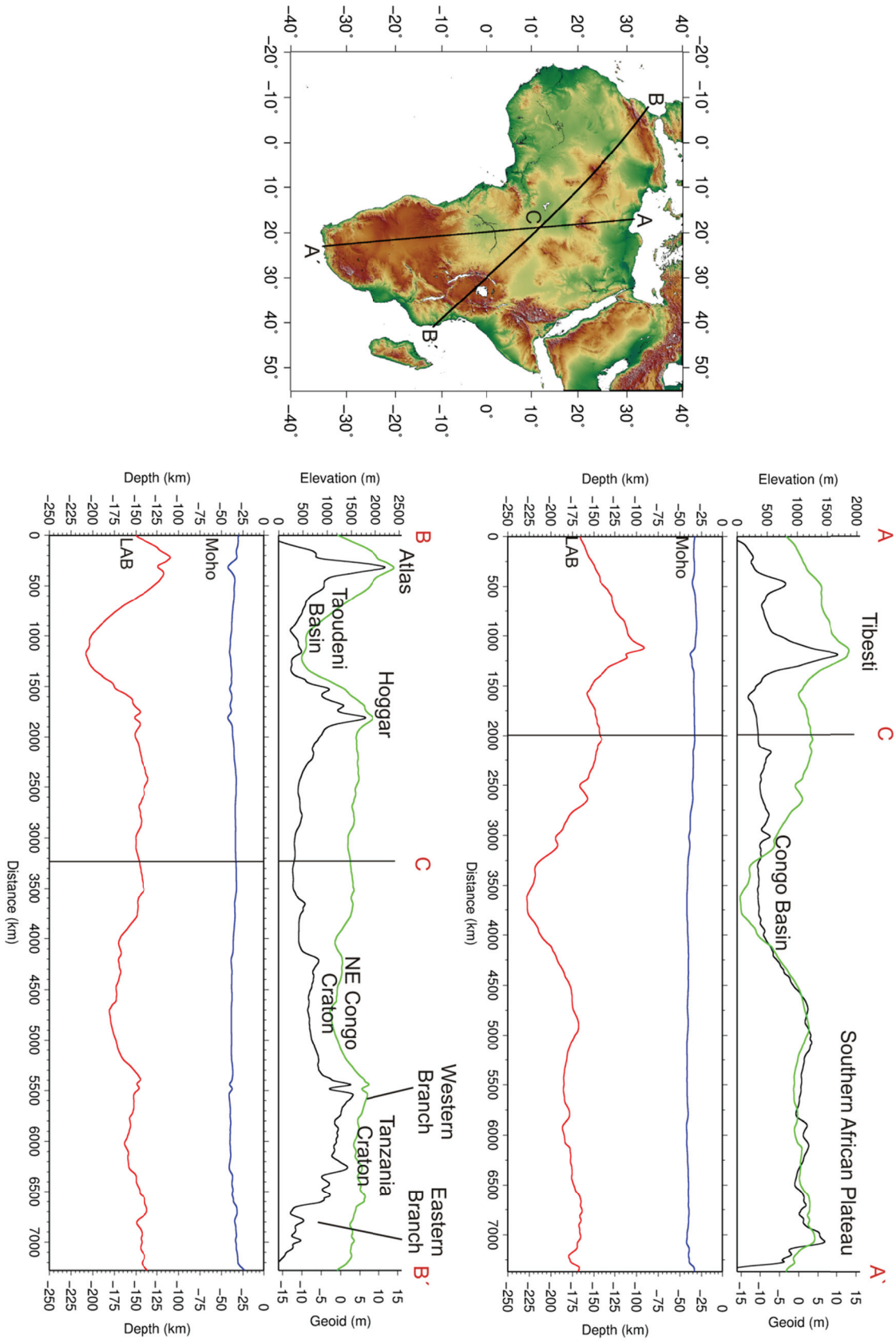

Figure 6.8. Lithospheric cross-sections across the Africa continent showing the observed elevation and geoid height anomaly (upper panels), and the calculated crustal (blue line) and lithospheric (red line) thickness (lower panels). Different thickness ratios of crust and lithosphere mantle characterize the Tibesti and Hoggar hotspots and the Atlas Mountains, the Congo and Taoudeni intracratonic basins, and the cratonic domains of Congo, Tanzania and southern African Plateau.

Chapter 7. Discussion

Chapter 7. Discussion

The presented crustal and lithospheric thickness model is based on a set of assumptions that, in some places are not partially or totally fulfilled. Apart from the simplifications required by the applied method, concerning the crust and lithospheric mantle densities, the model assumes local isostasy and a steady-state thermal regime. For wavelengths more than 100 kilometres, depending on the effective elastic thickness and vertical load distribution, local isostasy is an acceptable approximation (e.g., McKenzie and Bowin 1976; England and Molnar 1997), and thermal equilibrium is particularly fulfilled in old tectonothermal provinces. Hence, lithosphere thermal equilibrium is valid across most of the study area. In regions affected by transient temperature conditions due to lithosphere thinning or thickening, steady-state thermal modelling tends to overestimate or underestimate the actual lithospheric thickness, respectively, and to minimize the LAB depth variations. Therefore, the results of the presented model should be interpreted as the physical conditions needed to produce the required density distribution rather than as the actual thermal boundaries (for more details see Fullea et al., 2007; Robert et al., 2015).

In addition to the above mentioned assumptions and limitations, there is the contribution to topography associated with the transmission to the Earth's surface of viscous vertical stresses produced by sublithospheric mantle convection, the so-called dynamic topography. In that case, the assumption of isostasy, either local (Airy) or regional (flexure), is not accomplished. The dynamic topography signature of the African continent has been the subject of a vigorous debate over the last decade. The fundamental observation, inspired by the seminal work of Burke (1996), is that a surge of intraplate volcanism and of uplift and subsidence shaped the African continental topography during the last 30 Ma. Since then, a number of studies have tried to quantify the contribution of vertical motion on the African topography and whether this may be related with mantle dynamics. For example, several studies proposed that large-scale, deep-mantle dynamics under the African plate are dominated by the influence of a superplume located under

southern Africa (Hager et al., 1985; Silver et al., 1988; Lithgow-Bertelloni and Silver, 1998; Behn et al., 2004, Gurnis et al., 2000; Conrad and Gurnis, 2003; Forte et al., 2010; Moucha and Forte, 2011).

To ascertain the amplitude of dynamic topography is a complicated task and, in general, it has been done with two different approaches. The first uses a direct conversion from free air gravity to an estimated topographic effect resulting from dynamic forces on the base of the plate using a 50 mGal/km conversion, assuming a mantle density of 3300 kg/m^3 (Craig et al., 2011). This approach shows localized dome-shaped positive features distributed over the entire continent, particularly associated with the EARS (about 500 m), between the Ethiopian and Kenya dome, and also with the Southern African dome (up to 700 m), as well as Hoggar and Tibesti and in the Atlas. Negative anomalies are well marked in the Congo basin (up to 500 m) and in the Saharan Basin. The second approach uses large-scale tomography to deduce mantle flow and to compare with residual topography (Le Stunff and Ricard, 1995; Hager et al., 1985; Forte 2007). More recently, joint inversion approaches have been carried out between global seismic and surface geodynamic datasets, including geoid, gravity, and topography anomalies as well as surface plate motions (Simmons et al., 2009; Forte et al., 2010). The latter approach shows small dynamic topography in South Africa, a remarkable positive anomaly around the Ethiopian-Yemen dome, and negative anomalies associated with downwelling in the Egypt and Congo basins. Moucha and Forte (2011) investigated the origin of the Congo Basin negative anomaly, concluding that it may be related with both a dense anomaly in the deep lithosphere (Buiter et al., 2012) and the convective drawdown driven by surrounding deep mantle upwellings. Different results in terms of amplitude of dynamic topography obtained by different methodologies (e.g., Craig et al., 2011 vs. Forte et al., 2010) recently raised scepticism on the role mantle dynamics have on surface topography (Molnar et al., 2015).

It is worth noting that the only region where the difference between calculated and measured crustal thickness clearly exceeds the accepted uncertainties (4 - 5 km) is the Afar plume region, therefore substantiating the contribution of dynamic topography (section 6.4). This does not imply that in the

rest of regions the assumptions of the model are strictly fulfilled, but that the encountered differences, even exceeding the uncertainty range, can be explained by variations in the average crustal density related with sedimentation, magmatic intrusions, and/or underplating (section 6.5).

In this section I evaluate the significance of the obtained results for Africa in terms of: 1) previous global and continental-scale models of crustal and lithospheric thickness; 2) contributions from processes modifying the average crustal density; and 3) contributions of dynamic topography in the Afar plume region.

Within 1), the comparison with previous models, the WAC was chosen to provide an ideal large-scale tectonic unit to compare the results obtained from this study with a number of CMB and LAB models along a transect crossing the WAC. In their recent publication, Jessel et al. (2016) examined the architecture of the WAC and compiled a wide range of existing geophysical data, including seismic tomographic inversions, receiver functions and CMB and LAB depth estimates. It was therefore convenient to project the obtained results for this region onto a profile crossing the WAC as presented by Jessel et al. (2016).

7.1 Comparison with crustal models

As mentioned previously, several crustal models are available for Africa, based on different methods and input data (Table 7.1). Instead of an extensive comparison, I decided to compare the obtained crustal thickness map with the global-scale CRUST1.0 model, as it is the most widely used among the modelling community, and two gravity-derived continental-scale models, namely Tedla2011 and Tugume2013. Figure 7.1 shows the differences between these models and results from this work plotted as subtracted grids. A Bouguer anomaly map from Pérez-Gussinyé et al. (2009) is added to provide additional qualitative information on lateral density variations within the crust and on CMB topography. Table 7.1 summarizes the differences between the above referenced models and the presented crustal model. The model with the minimum difference is Tugume2013,

with a RMSE of 4 km. Note that although the RMSE varies between 4.04 and 4.95 km for all the models, the minimum and maximum variations range from +16.7 to -26.8 km, indicating that, at some regions, differences can be pronounced.

Models	Max(km)	Min(km)	RMSE(km)
CRUST1.0[(1)] *minus* this work	16.1	-26.5	4.95
Tedla2011[(2)] *minus* this work	16.7	-15.8	4.45
Tugume2013[(3)] *minus* this work	10.5	-16.5	4.04
CRUST1.0[(1)] *minus* Tugume2013[(3)]	15.92	-18.89	5.99
CRUST1.0[(1)] *minus* Tedla2011[(2)]	11.55	-26.81	5.27
Tugume[(3)] *minus* Tedla[(2)]	5.72	-23.25	6.64

Table 7.1. Statistical comparison among referred crustal models and this work. The grid size in each comparison was adapted to the model with lower resolution. Columns denote maximum and minimum differences and root mean square error (RMSE). References: (1) Laske et al. (2013); (2) Tedla et al. (2011); (3) Tugume et al. (2013).

A comparison with CRUST1.0 shows that modelled results lie within ±2 to ±4 km for most areas of the continent and that largest differences (>6 km) are concentrated in five regions (Fig. 7.1a). Predicted crust is significantly thicker in the Mediterranean margin, the EARS and in the Kaapvaal Craton. However, crust is thinner than in CRUST1.0 towards the west and south of the WAC and particularly, along the West African Rift extending from the CVL to the Tibesti hotspot and the Haruj volcanic field.

The largest differences related with the EARS region are due to the limitations of the underlying approach. However, overestimation of crustal thickness relative to CRUST1.0 is not restricted to the Afar plume region, but it extends further north along the Red Sea margin, and to the south along the branches of the Eastern and Western rift valleys. These differences are most likely related with the fact that the current thermal transient effects and regional mantle conditions depart from the assumption of thermal steady-state and isostatic equilibrium.

Large differences (>8 km) are also observed along the Mediterranean margin and it is difficult to identify the cause as the model well fits the few

available seismic data at the eastern Mediterranean coast (Fig. 6.1). The thicker crust might be related with the different input densities used, as in CRUST1.0 the crustal type for northern Libya and Egypt is defined as 'extended crust' with very low average crustal density (<2700 kg/m^3).

In the southernmost African cratons, modelled crust is, on average, 4 - 6 km thicker than that of CRUST1.0, but not in the surrounding Proterozoic belts.

The most outstanding differences however, are along the western and southern edges of the WAC and along the Cameroon-Haruj lineament, where CRUST1.0 suggests crustal thickening and where the model predicts crustal thinning (Fig. 7.1a). Similar results are obtained in a comparison with the Tedla2011 model, but not with other gravity-based (e.g., Bagherbandi et al., 2013; Tugume et al., 2013) and seismological crustal models (Meier et al., 2007; Pasyanos and Nyblade, 2007). Moho estimates from RF (Kosarian, 2006) and DSS (Klingelhoefer et al., 2009) show crustal thicknesses of 26 to 28 km in the West African margin that along with a long-wavelength, north-south orientated Bouguer anomaly around 0 mGal give support to the obtained results (Fig. 7d).

Similarly, the results question the crustal thickening suggested by CRUST1.0 along the Cameroon-Haruj lineament, which largely coincides with the Mesozoic West and Central African Rift System (WCARS). Unfortunately, there are no seismic constraints on the crustal structure in these regions, but the relative Bouguer anomaly high (~10 to -30 mGal) in Nigeria and Niger (Fig. 7.1d), together with spectral studies of gravity data indicates a reduction in crustal thickness beneath the western portions of the Saharan Metacraton (Okereke, 1984; Fairhead, 1986; Fairhead and Okereke, 1987; Fairhead and Green, 1989). Moreover, Fairhead (1986) pointed out that in contrast to other rifts, the evolution of the WCARS is primarily characterized by subsidence and that the amount of extension is at least 4 times greater than in the western and central Kenya rifts. Therefore, it is reasonable to argue that the observed crustal thinning in this work beneath the Mesozoic rift systems is a likely feature.

Overall the model is in good agreement with Tedla2011, but differences in crustal thickness show an apparent undulating pattern (Fig. 7.1c). Along the

Mauritanian Belt, the Nigerian margin and the northern portion of the Saharan Metacraton, these differences are similar to those previously discussed with CRUST1.0.

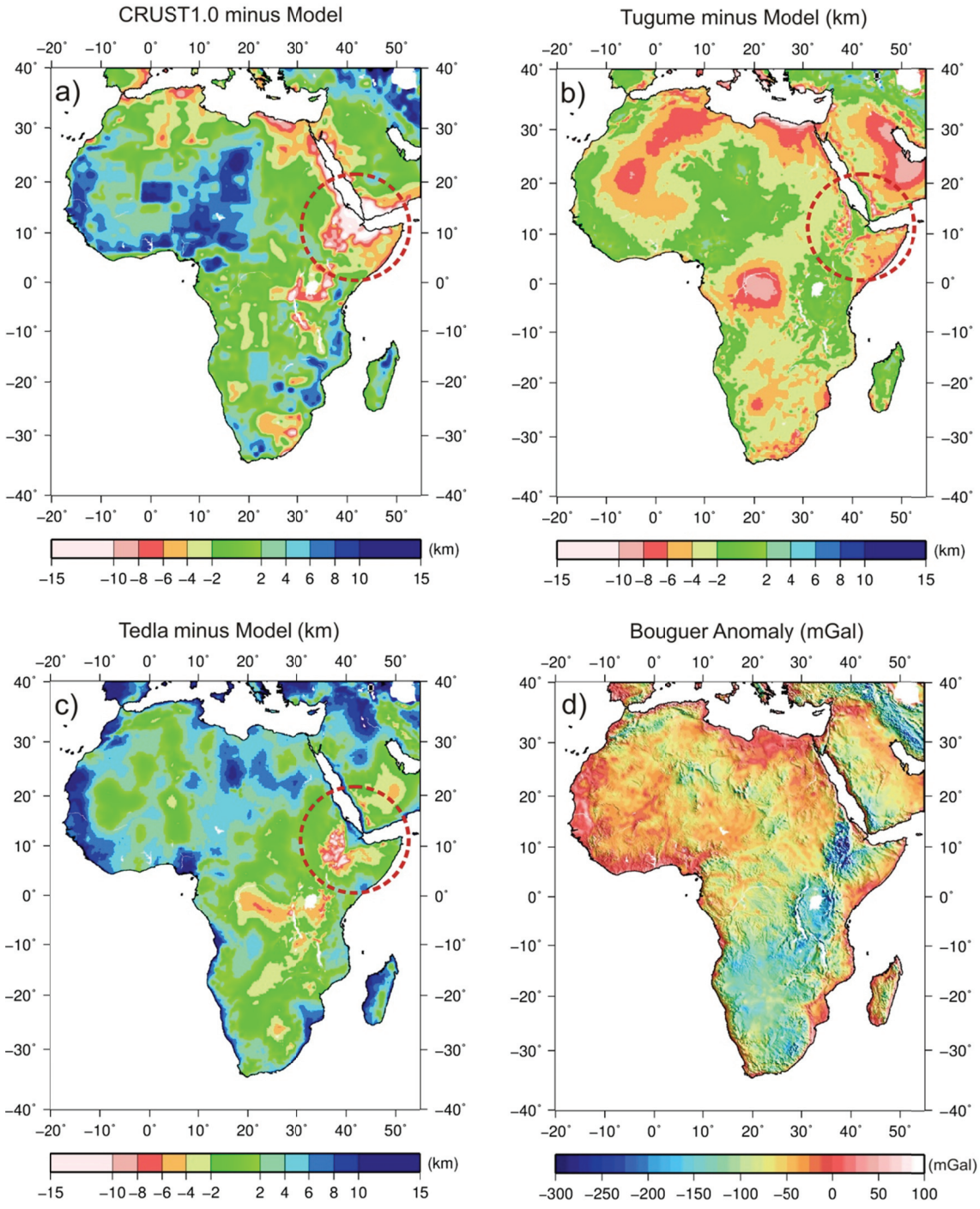

Figure 7.1. Comparison between global and continental crustal models and the model presented in this work. Differences are plotted as subtracted grids with respect to crustall thickness calculated in this study: a) CRUST1.0 (Laske et al., 2013) minus this study; b) Tugume2013 (Tugume et al., 2013) minus this study; c) Tedla2011 (Tedla et al., 2011) minus this study d) Bouguer anomaly map (Pérez-Gussinyé et al., 2009).

Likewise, for the Ethiopian Plateau, the Tanzania Craton and the centre of the Congo Craton the model shows a thicker crust. Tedla et al. (2011) performed a gravity Euler deconvolution to estimate the Moho depth at a resolution of 0.25º, but the application of this method and its validity to the African continent has been questioned (Reid et al., 2012; van der Meijde and Nyblade, 2014). The technique is using the spectral content of the gravity field to detect subsurface interfaces, and it is especially problematic along continental boundaries or in regions with significantly thinned crust (van der Meijde et al., 2015). Additionally, the thinnest crust in the Tedla2011 model is around 33 km, indicating a cut-off in the Euler solutions at this depth (Tugume et al., 2013). Tedla et al. (2011) did not considered seismic estimates of Moho depth to benchmark their crustal model in order to reduce the trade-offs between their modelled results and the measured crustal thickness in Africa.

The comparison with the Tugume2013 model shows that the obtained crustal thickness in this work is overall higher, with differences ranging from 0 - 4 km for most of the African continent (Fig. 7.1b). The model of Tugume et al. (2013) is based on a 3D Parker-Oldenburg iterative inversion (Oldenburg, 1974; Parker, 1973) of EIGEN-6C gravity data and predicts a relatively flat and thin crust (28 - 34 km) for north, west and central Africa and a thicker crust (36 - 40 km) in southern Africa. Major differences with this work (below -4 km) are observed along a southwest-northeast oriented corridor, running from the central regions of the WAC to the northeast regions of the Atlas Mountains, along the northernmost regions of the Sahara Metacraton, the northern coastal zones of the Nubian Shield, and the Congo Basin.

Locally, thinner crust is also seen in southern Africa and in east Africa (e.g., in the flanks of the Ethiopian Plateau). In the Afar Depression and in the central and southern regions of the EARS, the Tugume2013 model shows similar mismatches than in this study, relative to the seismic estimates and the CRUST1.0 and Tedla2011 models.

In a recent review of global and continental crustal models, van der Meijde et al. (2015) showed that all models have thick crust in the west of northern Africa, indicating that crustal thickness is rather underestimated in Tugume2013 (see

also Fig. 5.1). In addition, the spatial extent of negative differences with the results of this work (Fig. 7.1b) mimics the distribution of thick sediments (>4 km) inferred from the global sediment model (Laske and Masters, 1997), which was used by Tugume et al. (2013) to correct the input gravity signal for sedimentary basins. Hence, the resulting effect of the correction on Moho topography proposed by Tugume et al., (2013) might not be valid for terranes that underwent intracratonic basin formation, especially in those areas where detailed information on sediment thickness and basin structure is missing, and its geodynamic evolution is debatable, as for example in the Congo Basin (e.g., Hartley and Allen, 1994; Downey and Gurnis, 2009; Crosby et al., 2010).

7.1.2 Crustal thickness in the WAC

Figure 7.2 compares the three models and results from this work together with a number of continental and global crustal models along a NW-SE profile across the West African Craton and adjacent areas as presented in Jessel et al. (2016). Huge differences are visible in both crustal thickness and the amplitude of lateral thickness oscillations, especially for the southern part of the profile. Despite their lower resolution, the global models (3SMAC, VMM, CRUST1.0, GEMMA and LITHO1.0) show more significant short wavelength variations in crustal thickness compared to the continental models (Pasyanos07, Tugume2013, Tedla2011) and this study. Along the profile thickness estimates for cratonic crust beneath the WAC range between 27 km and 47 km, with the LITHO1.0 model predicting a significantly thicker crust than the other models. Overall, results from this work and the gravity based models (Tugume2013, Tedla2011, GEMMA, and VMM) show smoother Moho-geometries with minor thickness variations. Anyhow, among them the VMM is the only model that shows crustal thinning beneath the southern part of the profile, with a negative kink approximately across the boundary of the Taoudeni Basin. A similar feature is also observed in Pasyanos07 which shows thinned crust of around 26 km beneath this region.

Anyhow, the regional crustal thinning in VMM and Pasynaos07 is not visible in the rest of the models.

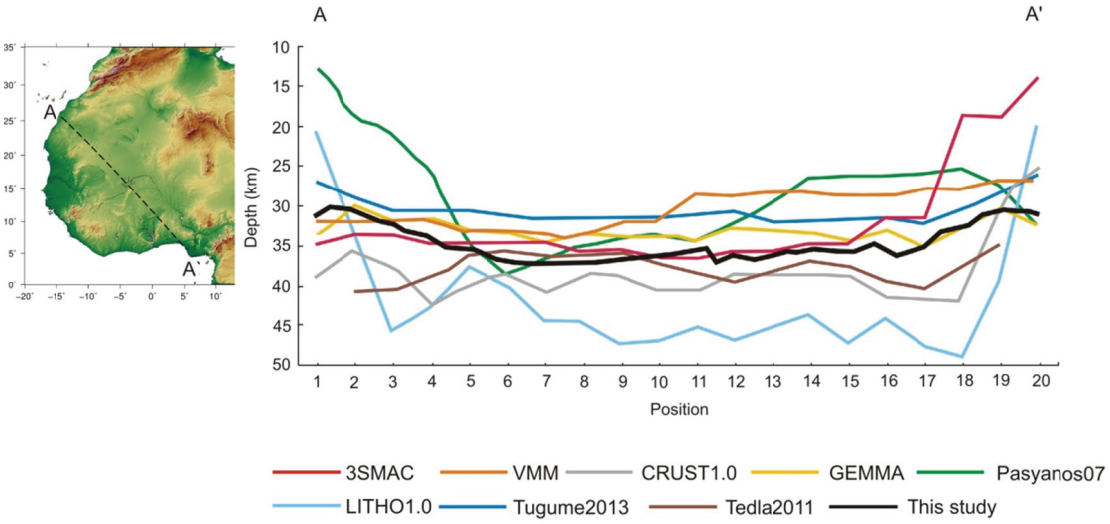

Figure 7.2. Comparison of crustal thickness models along a profile crossing the WAC. Profile location is given in the map to the left. Global models are 3SMAC (Nataf and Ricard, 1996), VMM (Bagherbandi and Sjöberg, 2012), CRUST1.0 (Laske et al., 2013), GEMMA (Reguzzoni et al., 2013) and LITHO1.0 (Pasyanos et al., 2014). Continental models are Pasyanos07 (Pasyanos and Nyblade, 2007), Tugume2013 (Tugume et al., 2013), Tedla2011 (Tedla et al., 2011) and this work. Note the difference in short wavelength variations between global and continental models. The figure was modified after Jessel et al. (2016).

Hence, biggest differences (> 23 km) among the crustal models regarding the regional thickness trend occur between the VMM and Pasyanos07 model and the other models, including this work. For the very south of the profile the 3SMAC model shows a rapid decrease in thickness from 30 to 20 km, which is not supported by the proposed structure of the other models. Generally, crustal thickness calculations from this study are well between minimum and maximum proposed values and show an overall similar pattern in Moho geometry as observed in the Tedla2011, Tugume2013, GEMMA and partly the 3SMAC.

7.2 Comparison with lithospheric models

In this section I compare the obtained lithospheric thickness map for Africa with available continental (Fishwick and Bastow, 2011) and global (Priestley and McKenzie, 2013; Pasyanos et al., 2014) estimates from surface-wave tomography and a global thermal model (Artemieva, 2006). Hereafter, these models will be named FB2011, PMK2013, LITHO1.0, and TC1, respectively (Fig. 7.3). Comparing estimates of lithospheric thickness is a complex task, since as discussed in Chapter 3; the nature of this boundary is elusive and debatable in

terms of its properties (Artemieva, 2009; Eaton et al., 2009; Artemieva, 2011). Especially beneath cratons, its rheological characteristics might change over a thick transition zone, ranging from 20 km in presence of fluids to 50 km in dry conditions (Eaton et al., 2009). Usually, seismic LAB models account for the velocity-depth distribution of different seismic waves, mainly P-, S-, and surface-waves and therefore, cannot be directly related with the thickness of the thermal lithosphere. However, since there is a strong rheological change between the conductive lithosphere and the underlying convective upper mantle, the velocity-depth sections reflect lateral variations in lithospheric thickness rather than the precise LAB depth. Therefore, I present a relative comparison between the results of this study and the different models focusing on regional changes in the lateral LAB geometry beneath Africa.

Depth to the LAB in the above mentioned models was obtained by the use of different data and methods (for details see Chapter 5.2). Whereas the TC1 model presents thickness of the thermal lithosphere based on global heat flow data, the FB2011, PMK2013 and LITHO1.0 models were constructed converting regional velocity variations into temperature estimates and further into lithospheric thickness. Special caution interpreting these models is recommended, as velocity anomalies of non-thermal origin may account for up to +3% of Vs amplitude caused by variations in chemical composition and/or to the presence of melts/fluids (e.g., Artemieva, 2009; Afonso et al., 2010). Furthermore, differences between the presented results and the FB2011, PMK2013 and LITHO1.0 models may be related with their spatial resolution and vertical uncertainties. Usually, the horizontal resolution of these models allow features on the order of 200 - 250 km to be recovered, with a vertical resolution of 25 - 50 km (Fishwick and Bastow, 2011; Priestley and McKenzie, 2013).

Interestingly, a comparison between this work and the seismic PMK2013 and FB2011 models shows that the overall distribution pattern of thick lithosphere is very similar, especially beneath the cratons (Fig. 7.3). The PMK2013 and FB2011 models (Fig. 7.3 b and c) exhibit a thick lithosphere (>160 km) beneath western, central and southernmost Africa and thinner lithosphere (<140 km) beneath the Atlas region, the CVL, the WCARS, the Saharan Metacraton and

along the Atlantic margins.

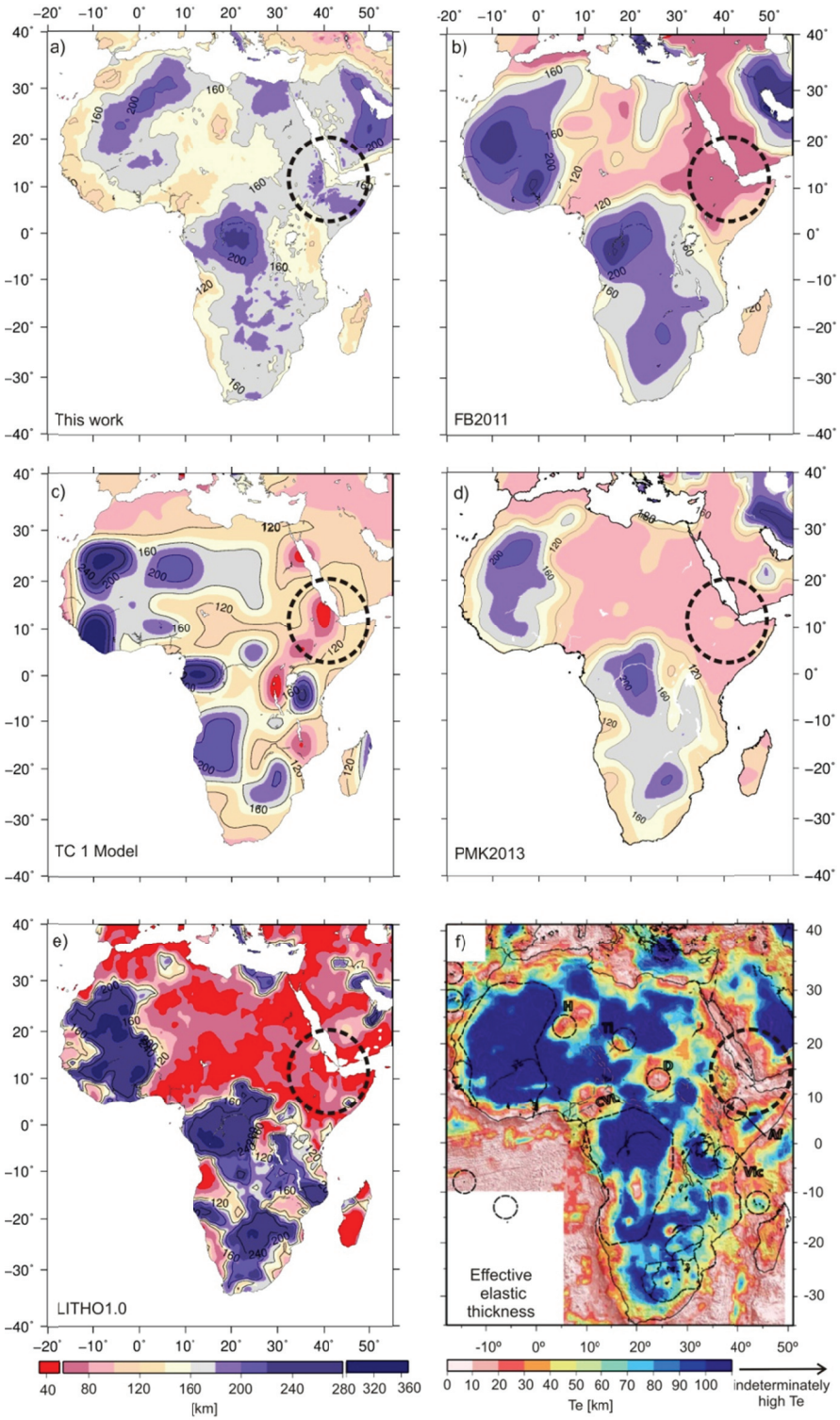

Figure 7.3. Comparison of LAB maps for Africa. a) this work; b) global PMK2013 model (Priestley and McKenzie, 2013); c) continental FB2011 model (Fishwick and Bastow, 2011); d) global TC1 model (Artemieva, 2006) and e) the LITHO1.0 model (Pasyanos et al., 2014). Note that the colour scale has been adapted to facilitate the comparison with the FB2011 model. Dark blue and red spots in the TC1 and LITHO1.0 models depict out of range values compared to the PMK2013 and FB2011 models and this study and show were lithospheric thickness thicker or thinner, respectively. f) Shows the map of effective elastic thickness of Africa from Perez-Gussinyé et al. (2009).

In the WAC, results from this study show a thick lithospheric root beneath the Tauodeni Basin, which agrees very well with the observations in the FB2011 and PMK2013. Both models (also the LITHO1.0 model) display another common feature; the extension of thick lithosphere towards the northeast, across the boundaries of the WAC, paralleling the Atlas Mountains. As this thickening is also expressed in the presented crustal model (see Fig. 6.3) both thick crust and lithosphere might be a realistic feature in this region. Compared to FB2011, the lithospheric thinning along the western boundary of the WAC is more pronounced in this study and the PMK2013 and TC1 models, where they show thinner lithosphere beneath the Neoproterozoic Mauritanian Belt relative to the WAC.

Large variations in lithospheric thickness are visible beneath the Saharan Metacraton in this study and the continental FB2011 model, but not in the global PMK2013 (Fig. 7.3). Indeed, the PMK2013 model shows almost no variations in lithospheric structure beneath north-eastern Africa, which might be related with the parameterization used to estimate the LAB-depth and/or the limited vertical resolution of the model (see Priestley and McKenzie, 2013 for details). The observed lateral thickness variations in this study and in FB2011 are of similar amplitude (~80 km) and seem to be related with the remnants of the pre-Neoproterozoic Saharan craton (i.e., the Kufrah Craton), the Mesozoic rifts and the Cenozoic volcanic provinces.

The TC1 model shows a completely different LAB geometry beneath the Saharan Metacraton with thickest lithosphere (> 160 km) in the region coinciding with the Tibesti hotspot and the Haruj Volcanic province, where all the other models, including this work, suggest thinner lithosphere (<80 - 120 km) compared with the surrounding.

Overall the lithospheric structure in the PMK2013 and LITHO1.0 models is fairly similar. Both propose strongly thinned metacratonized lithosphere without significant lateral variations and lithospheric thickening to the NE as visible in all models, with exception of TC1. Among all models, LITHO1.0 shows the thinnest lithosphere beneath the Saharan Metacraton with values lower than 60 km, which should be treated with caution, because despite the fact that the region was affected by metacratonization it is still underlain by huge portions of Precambrian

continental lithosphere (e.g., Black and Ligeois, 1993; Fezza et al., 2010).

Furthermore, all models (except the TC1 model) show a north-northeast and an east-northeast trend in lithospheric thinning along the WCARS extending from the CVL towards the Haruj volcanic province and the Darfur hotspot, respectively, which coincides with crustal thinning in the region (see this work, Tugume et al., 2013; Meier et al., 2007; Pasyanos and Nyblade, 2007). According to Fairhead (1988), the over 8000 km long WCARS has a consistent geological and geophysical expression, that is best explained by lithospheric extension accomplished by ductile flow of the lower crust and upper lithospheric mantle as quantified by McKenzie (1978) and by Jarvis and McKenzie (1980). Though absolute lithosphere thickness in this study is around 40 km thicker in the WCARS compared to the FB2011 and PMK2013 models, due to the differences between thermal and seismic LAB definitions and the vertical resolution, the impact of the tectonic processes caused by large-scale Mesozoic extension on the lithospheric structure are well expressed in the obtained results in both the crustal (Fig. 6.3) and lithospheric thickness maps (Fig. 6.4).

The presented LAB map is also in good agreement with lithospheric thickness variations across the Congo Craton seen in FB2011, PMK2013 and LITHO1.0 and also with lithosphere thickness estimates of ~210 km from kimberlitic garnet xenocrysts (Batumike et al., 2009). A thick cratonic root beneath the Congo Craton is visible in all models, but its lateral and vertical extend varies with differences in maximum thickness of ~100 km. With the exception of PMK2013, all models show extension of the thick root beneath the western part of the craton, but the distribution pattern of thick lithosphere in the TC1 model, where maximum root thickness is located in the western part solely, is very dissimilar. For the centre of the Congo Craton differences in lithospheric thickness between TC1 and other models amount to more than 120 km, this exceeds three times the minimum thickness proposed by TC1. A decrease in thickness to the south of the Congo Craton is visible in all models, but this thinning is more pronounced in the PMK2013 model.

The mobile belts surrounding the Tanzania Craton are affected by continental rifting, possibly associated with a mantle plume (Nyblade and

Robinson, 1994; Simiyu and Keller, 1997; Prodehl et al., 1997; McNutt, 1998; Ritsema et al., 1999; Weeraratne et al., 2003). In all models a region of thinned lithosphere, beneath the Western Branch of the EARS is visible separating the Congo and Tanzania cratons. Nevertheless, in this work and the FB2011 this is not as clearly expressed as in the other models (e.g., the TC1). Beneath the Tanzania Craton the modelled lithosphere in this work is slightly thinner than in other African cratons, but still shows a thick lithospheric keel of 140 to 160 km. This is also observed in the PMK2013 and FB2011models. In LITHO1.0 the lithospheric root is absent in the eastern portion of the craton. The TC1 and LITHO1.0 models propose a much thicker cratonic root beneath Tanzania down to >240 km. Generally, the results from this work also support the findings of a Rayleigh wave tomography study by Weeraratne et al. (2003), who found the LAB beneath the craton at a depth of 150 ±20 km, demonstrating the stability of the Archean lithosphere in the presence of a mantle upwelling. To the east of the Craton the modelled lithosphere beneath the Eastern branch of the EARS is thinner as observed in all models.

In Southernmost Africa obtained thickness estimates agree well with the thick lithosphere (>160 km) imaged in the FB2011, PMK2013 and TC1 models (Fig 7.3). Lithosphere in LITHO1.0 is 40-60 km thicker than in the other models. A relative local lithospheric thickening (>180 km) is visible in all models probably related with the collisional zone between the Kaapvaal and Zimbabwe cratons. Anyhow, predicted lithosphere thickness beneath the Kaapvaal is lower compared to other African cratons, which is also visible in any of the other models. Thinner lithosphere relative to the big African cratons is also consistent with seismic estimates of 180 ±20 km (Li and Burke, 2006) and 170 - 200 km (Priestley et al., 2008; Priestley and Tilmann, 2009) and probably reflects originally rigid cratonic lithosphere that was affected by thermal weakening and metasomatic modification at its base during the Mesozoic, as suggested by Griffin et al. (2003) and Kobussen et al. (2008).

In summary, a comparison of the presented lithospheric thickness map with seismic tomography models shows great similarity in distribution of thick lithosphere and depth to the LAB in the African cratons. Biggest differences with

all models occur in the Afar plume region, where the applied approach is not valid, and in general with the heat flow based TC1 model, which shows a somewhat distinct pattern in LAB geometry. In the recently published LITHO1.0 model the lithosphere is significantly thinner in off-craton and thicker in cratonic regions than in any of the other models. In Northern Africa the modelled lithospheric structure reveals i) thick lithosphere related with the WAC and across its boundaries to the northeast, ii) significant lateral variations in the Saharan Metacraton related with Archean remnants of cratonic lithosphere and iii) lithospheric thinning along the WCARS. These large-scale features agree very well with the PMK2013 and FB2011 models. Also for southern Africa the obtained results coincide surprisingly well with the PMK2013 and FB2011 models, considering the different datasets used in the modelling processes. Despite the differing methodologies, the obtained lithosphere thickness map for Africa predicts similar features as imaged in previous LAB studies.

The overall coincidence, except for the Afar region, with the above referred tomography models can be extended to the effective elastic thickness (*Te*) model by Perez-Gussinyé et al. (2009), who calculated the thickness of the elastic lithosphere from topography and Bouguer anomaly data. The wavelength band over which topography and Bouguer anomaly are correlated (Bouguer coherence) provides information on the elastic properties of the lithosphere. Although maximum values are limited to 110 km near the saturation level the authors found features comparable to tomography studies and this work with maximum *Te* values related with cratonic domains and minimum values to the Afar plume region and the West and Central African Rifts Systems (see Fig 7.3f).

7.2.1 Lithosphere thickness in the WAC

As with the crustal model in the previous section the modelled lithospheric structure is compared with global and continental models along a profile across the West African Craton and adjacent areas (Fig. 7.4). The figure shows that results from this work do not propose such a thick lithosphere beneath the WAC as LITHO1.0, FB2011, and Pasyanos10, but in the area of the Taoudeni Basin the

estimated thickness values coincide very well with LAB depth estimations of ~180 km coming from seismic PMK2013 and thermal TC1 models. Despite the differences in absolute values the lateral LAB geometry agrees very well with most of the models.

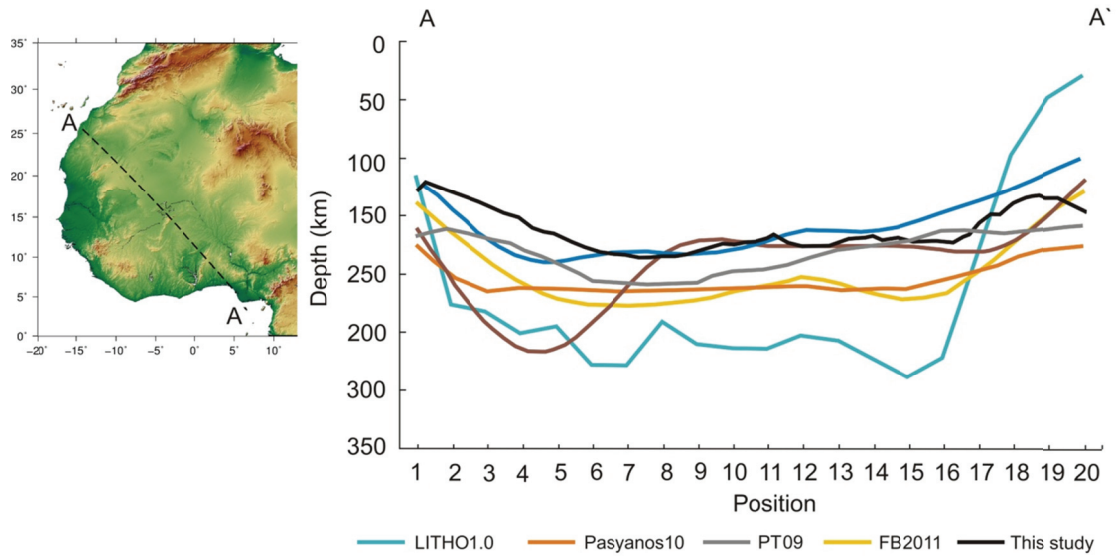

Figure 7.4. Comparison of lithospheric thickness models along a profile crossing the WAC. Profile location is given in the map to the left. Global models are LITHO1.0 (Pasyanos et al., 2014), PMK2013 (Priestley and McKenzie, 2013) and TC1 (Artemieva, 2006). Continental models are Pasyanos10 (Pasyanos, 2010), PT09 (Priestley and Tilmann, 2009), FB2011 (Fishwick and Bastow, 2011) and this work. The figure was modified after Jessel et al. (2016).

The apparent lithospheric trend reflected in tomography models and this work displays thickening away from the margin towards the Taoudeni Basin, where most models show maximum thickness, followed by a slight thinning across the southern basin boundary, which reverts to an increase in lithospheric thickness towards the south of the profile in the area of the Neoproterozoic Volta Basin. Strongest coincidence in terms of lateral thickness variations is observed between the obtained results and the continental PT09 and FB2011 models.

In contrast, both TC1 and LITHO1.0 propose very thick lithosphere beneath the northern part of the WAC, in the Archean Reguibat Inlier, and the Pasyanos10 model predicts a very smooth geometry without significant variations in LAB depth. Anyhow, overall, the lithosphere models show higher consistency along the profile than the crustal models (see Fig. 7.2) and the majority of models feature thickening beneath the Proterozoic intracratonic Taoudeni basin.

7.3 Crustal density and Moho depth

Using a linear, depth-dependent crustal density with a homogeneous average value throughout the continent results in a good fit with the available seismic data, but it does not necessarily satisfy the differences in crustal thickness for distinct tectonic domains. Local differences, exceeding ±5 km between modelled and seismic estimates of Moho depth, can be attributed to deviations from the model's input average density distribution. For instance, in the northwest Congo Craton, calculated crustal thickness values are ~8 km thinner compared with receiver function studies by Tokam et al. (2010), who observe a significantly thick crust (~45 km). These authors also imaged a 23 km thick, high velocity lower crustal layer, which is more than 10 km thicker than beneath the Tanzania, Kaapvaal, and Zimbabwe cratons. The associated effect of the thick mafic layer can be related with an increase of 60 to 80 kg/m^3 on the bulk density of the crustal column. Increasing the average crustal density to 2870 kg/m^3 in the Congo Craton would result in a modelled crustal thickness of ~45 km, in agreement with the seismic estimates.

Likewise, changing the input crustal density within bounds of ±40 kg/m^3 enabled to associate misfits in Southernmost Africa with variations in the local density structure. These variations can be related with magmatic events, which might have added high density rocks to the crust (i.e., in the Namaqua-Natal Belt and Bushveld Igneous Complex), and/or to sediment accumulations that might have lowered the bulk crustal density (i.e, in the Witwatersrand Basin). The related maximum variations in crustal thickness were about ±4.2 km and resulted in a complete fit of modelled crustal thickness compared to seismic estimates from the SASE experiment. In summary, it is possible to fit the estimated crustal thickness from seismic experiments by locally changing the average crustal density within reasonable bounds. However, the applied methodology to calculate the crustal thickness for the whole Africa continent, where data is not available, has the tradeoff of assuming a homogeneous crustal density value because possible lateral density variations are unconstrained.

7.4 Uncompensated topography in the Afar plume region

The Afar plume region, including the surrounding plateaus, exhibits rough topography, comprising a >1000 km wide domal uplift intersected by the ~80 km wide MER valley with highly uplifted rift flanks (>2000 m). The MER is surrounded by the elevated Ethiopian and Somalian plateaus (~1500 m) as well as a low relief (<500 m) zone to the north, in the Afar Depression. The model shows overcalculated crustal thicknesses in this region, locally exceeding 15 km compared to available seismic observations (e.g., Maguire et al., 1994; Prodehl et al., 1997; Dugda et al., 2005; Wölbern et al, 2010, Fig. 6.4). On average, the modelled crust is ~10 km thicker than estimates from RF studies by Dugda et al. (2005), showing thicknesses between 35 - 40 km in the Ethiopian Plateau, 30 - 35 km in the MER and about 25 km in the Afar Depression. Upper mantle seismic tomography (Bastow et al., 2005; Benoit et al., 2006; Bastow et al., 2008) beneath the seismically and volcanically active MER shows a broad thermal upwelling or mantle plume from 75 km depth down to 400 km (Nyblade et al., 2000; Benoit et al., 2003; Nolet et al., 2003), which drives extension between the Nubian and Somalian plates. After plume impingement at ~30 Ma a rapid lithospheric thinning occurred (Dugda et al., 2007; Gani et al., 2007) and broad Oligocene flood basalt volcanism affected the region, such that the thermally modified Pan-African lithosphere underlies huge portions of the Ethiopian Plateau and Afar Depression (Keranen et al., 2009). The Cenozoic interaction of mantle magmas with the crust (i.e., volcanism, dike intrusions and underplating) would increase the average crustal density and the calculated crustal thickness in the plateau, resulting in a larger misfit. Clearly, the modelling approach cannot conciliate the observed geoid and elevation with the measured crustal thickness in this region. As the thermal perturbation associated with the Afar plume might involve a dynamic component to the uplift in the plateau (e.g., Ebinger et al., 1989; Moucha and Forte, 2011), the overcalculated crustal thickness in the model could be explained by an offset in the input elevation data between the non-isostatic (dynamic) and the isostatic topography components.

In order to test if the model misfits in the Afar region can be explained by dynamic topography induced by sub-lithospheric buoyancy forces (e.g., Cazenave

et al., 1989; Hager and Richards, 1989; Ricard et al., 1993), I tested the effect of the non-isostatic (dynamic) component of elevation on the calculated crustal thickness using a simplified setup. Firstl, I assume a single plume, as suggested by various authors (Manighetti et al., 1997; Ebinger and Sleep, 1998; George et al., 1998; Gurnis et al., 2000; King and Ritsema, 2000; Davis and Slack, 2002), with a radius of r=1000 km, which is consistent with tomographic (Ritsema et al., 1999; Zhao, 2001; Ni et al., 2002) and mantle He isotope studies (Franz et al., 1999; Pik et al., 2006). The plume is centred at 42ºE, 11ºN near the Lake Aheb in Afar, as indicated by structural, magnetic, and geochemical data (Schilling, 1973; Rooney et al., 2011). Secondly, I plot the observed crustal thickness from RF analysis by Dugda et al. (2005) and the EAGLE DSS survey by Maguire et al. (2006) against the calculated values (Fig. 7.5). This plot shows that, on average, the modelled crustal thickness exceeds the measured values by 9.81 km (y-intercept value in the regression line in Fig. 7.5).

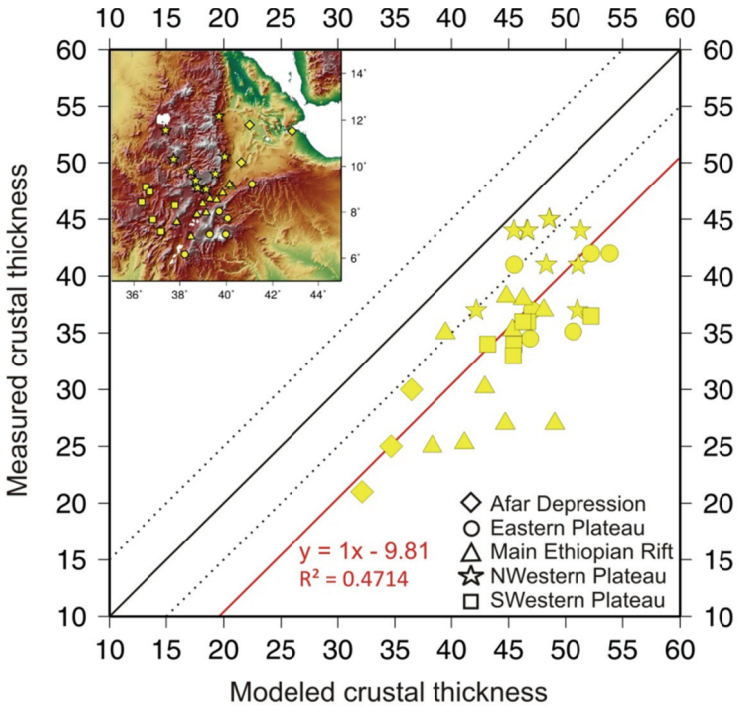

Figure 7.5. Scatterplot of observed (Dugda et al., 2005; Maguire et al., 2006) versus calculated crustal thickness in the Ethiopian Plateau and Afar depression (see inset for location). Solid black line denotes perfect agreement between observed and calculated values and dashed lines denote the associated uncertainties (±5 km). Red solid line corresponds to the regression line parallel to the 1:1 line, showing a shift of -9.81 km. Symbols refer to the station location in the Ethiopian Plateau as displayed in the inset. Stars = NW Plateau, squares = SW Plateau, tringles = Main Ethiopian Rift Valley, diamonds = Turkana Depression and circles = E Plateau.

The isostatic contribution to elevation due to crustal thickness variations is

$$\delta\varepsilon = \frac{(\rho_m - \rho_c)}{\rho_\epsilon}\delta h_c$$

where ρ_m, ρ_c and ρ_ε are the densities of the mantle (3300 kg/m^3), crust (2790 kg/m^3), and topography (2670 kg/m^3), respectively and δ_ε and δh_c are the variations of elevation and crustal thickness, respectively. Therefore, with the above considered densities, the topography associated with a change of 9.81 km in crustal thickness is 1874 m, which is the average residual topography relative to the model in the Afar region. Finally, I have assumed that the dynamic contribution (ε_r) to topography is close to the inferred residual topography, and that it is a function of the radial distance *d* from the plume centre, such that ε_r = 1800 m for 0 ≤ *d* ≤ 500 km and decreases linearly to zero, being ε_r = 2 x 1800 (1 – d/r) for 1000 ≥ *d* > 500 km. The so estimated dynamic contribution is then subtracted from the filtered ETOPO1 elevation corresponding to the location of each considered seismic station (Dugda et al., 2005; Maguire et al., 2006) and is used as the input data to recalculate the crustal thickness with the applied method.

Figure 7.6 shows the observed versus crustal thicknesses for a combination of appropriate corrected elevations (-1600 to 1200 m), determined as described above, and for the corresponding geoid anomalies (2 - 7 m) in the Afar plume region, using a range of average crustal densities from 2790 to 2850 kg/m^3. After topography correction, the majority of the data fall inside the area of possible thickness solutions when the uncertainties associated with seismic experiments is also considered. It is worth noting that as shown in Fig. 7.6, an increase in the average crustal density, probably related with magmatic processes, is required to fit about 71% of the observed crustal thickness values. The resulting lithospheric thickness after corrections is reduced by ~60 km on average, thus also better fitting the tomography estimates.

Gravity, admittance, and river profile modelling (Roberts and White, 2010; Jones et al., 2012) suggest a maximum surface uplift of modern African swells from 800 to 2000 m. However, smaller peak amplitudes of dynamic topography (~700 m) are predicted in the EARS from mantle flow calculations based on

subduction history (Lithgow-Bertelloni and Silver, 1998), and are estimated to be between 400 and 1200 m, based on mantle convection modelled backwards in time (Moucha and Forte, 2011).

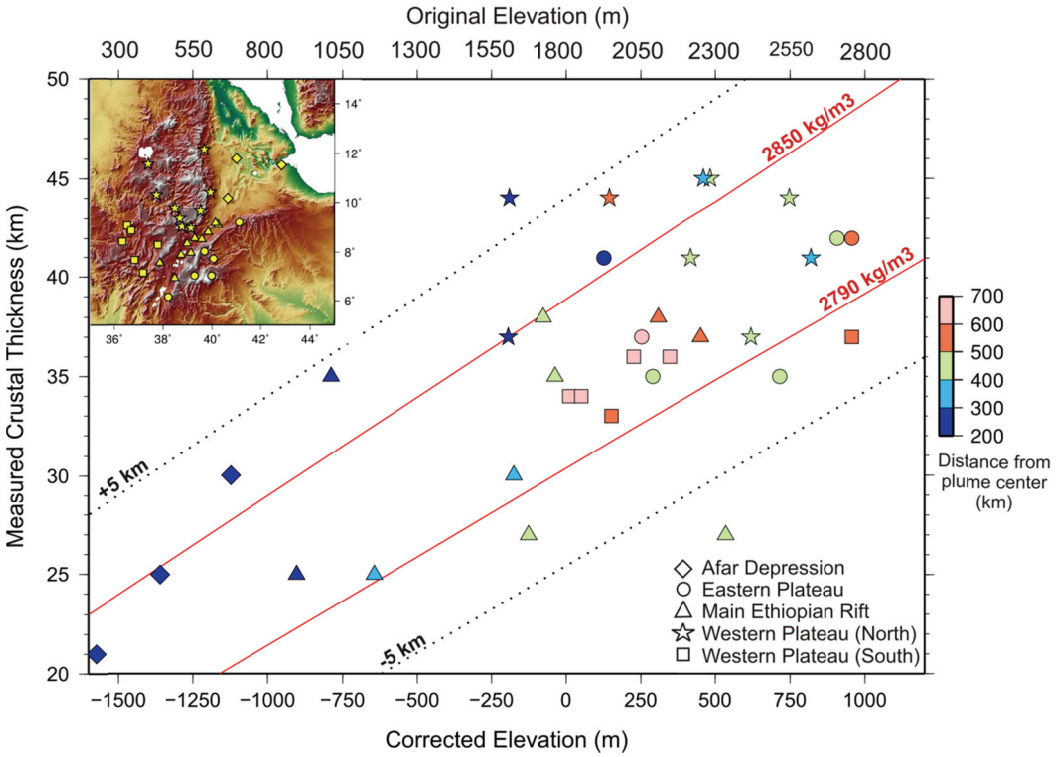

Figure 7.6. Crustal thickness from seismic experiments (Dugda et al., 2005; Maguire et al., 2006) plotted against corrected elevation by non-isostatic contribution to topography. Symbols denote the location of stations (see inset), and colors denote the distance to the center of the Afar plume. Topography correction is of 1800 m for distances ≤500 km to the center of the plume and decreases linearly until vanishing at 1000 km distance. Red lines denote the range of average crustal densities considered in calculations and dashed lines denote the associated uncertainties (±5 km).

The positive signal in the Ethiopian dome has also been well established by regional investigations that show amplitudes up to 1000 - 1500 m (Faccenna et al., 2013). On the other hand, Molnar et al. (2015) propose that mantle flow calculations tend to overestimate dynamic topography and therefore, the estimated non-isostatic topography of 1800 m must be considered as an upper bound.

8. Summary, conclusions and future recommendations

8. Summary, conclusions and future recommendations

The main objective of this thesis is to apply a straightforward top to bottom approach in order to present new crustal and lithospheric thickness maps for Africa, which provide new insights into the vast regions of the continent where knowledge of the lithosphere's structure is absent and existing models are predicting contradicting results. In the following, I will briefly summarize the work presented in this thesis and present the main conclusions reached from this study. Last but not least an outlook to future work is given.

8.1 Summary

A new map of crust and lithosphere thickness for continental Africa is presented based on joint modelling of elevation and geoid data combined with thermal analysis under the assumptions of local isostasy and thermal steady-state condition. The obtained results are constrained by a new comprehensive compilation of seismic Moho-depth data consisting of 551 data points covering about 20% of Africa, and by published tomography models relative to LAB-depth resulting in a more confident image of the present-day lithospheric structure of Africa.

The incorporation of sediment thickness and lateral density variations do not modify noticeably the obtained results and consequently were not considered in the final model. Combining elevation, geoid, and thermal analysis allowed me to calculate the crustal thickness with confidence relative to the seismic observed values, with the exception of the Afar plume region, and therefore to extrapolate results to those areas with no seismic constraints (80% of Africa).

The calculated crustal thickness shows significant differences with previous gravity-based continental models and seismic global models. The obtained crustal thickness map correlates better with geological structure and tectonic provinces as well as with gravity anomalies, and shows a higher spatial resolution.

The LAB-depth map shows large spatial variability, with deeper LAB related to cratonic domains and shallower LAB related to Mesozoic and Cenozoic rifting domains, in agreement with tomography models. The main novelty is that in the Africa continent I integrate in a unique model both crustal and lithospheric mantle thickness variations. Though crustal and lithosphere thickness maps show similar regional patterns, major differences are found in the Atlas Mountains, the West African Rift System, and the intracratonic basins.

8.2 Main conclusions

From the presented work, I can draw the following concluding remarks:

- The applied methodology is improved by defining a reference column at sea level to calculate the optimal average crustal density and geoid level, resulting in ρ_c = 2790 kg/m^3, N_0 = 6168 m, and a fitting of 76% compared to available seismic observations, when the Afar plume region is excluded. The reference column has a crustal thickness of Z_c = 32.16 km and a total lithospheric thickness of Z_L = 153 km.

- Incorporation of sediment thickness and crustal density data from CRUST1.0 into the calculations leads to significant misfits between the resulting crustal model and the seismic data. Thus, the consider crustal model with an average constant density distribution proves to provide a good first-order crustal thickness map, which is in much better agreement with the seismic Moho estimates in Africa.

- The calculated crustal thickness values across Africa have a RMSE of 6.5 km and a fit of 60.8% relative to the whole compiled seismic dataset, showing the best minimum RMSE (4.3 km) and a maximum fit (76.3%) compared to other global and continental models, after excluding the Afar plume region.

- The crustal model depicts a bimodal distribution, with a clear north-south division and with distinct crustal structure and thicker cratonic crust in southern Africa (38 - 44 km) compared to northern Africa (33 - 39 km). The

most striking feature is the crustal thinning (28 - 34 km) along the Mesozoic West African Rift separating the western and eastern regions of northern Africa. Overall, the thick crust (37 - 48 km) is related to Archean cratons and shields as well as Proterozoic belts, whereas thin crust (28 - 30 km) is found along the Atlantic coastal zone and regions affected by Mesozoic and Cenozoic extension.

- The calculated lithospheric thickness shows a large spatial variability ranging from 90 to 230 km. Though the regional patterns of crustal and lithospheric thickness share similarities, major differences are delineated in the Atlas region (Northeast-Morocco), where the crust is relatively thick compared to the lithospheric mantle; along the Mesozoic West African Rift, where the crust is relatively thin compared to the lithospheric mantle; and beneath the intracratonic basins (e.g., Congo Basin and Taoudeni Basin), where the maximum LAB depths exceed 200 km. The different deformations patterns indicate strong strain partitioning most probably due to intra-lithospheric decoupling along the CMB.

- Strongest variations within craton boundaries in both crustal (28 - 38km) and lithospheric (110 - 190km) thickness are found beneath the vast Saharan Metacraton, where the results very well reflect the disturbed nature of the metacratonized mantle lithosphere. Thick crust and a strong lithospheric root beneath the proposed Kufrah Craton suggest the survival of pre-Neoproterozic cratonic remnants and that huge portions in the eastern Metacraton escaped regional lithospheric delamination during Neoproterozoic remobilization.

- Comparing the crustal model with other existing models shows differences along the western and southern edges of the WAC, and along the West African Rift, where the modelled results predict large-scale crustal thinning instead of relative thickening. The lithospheric model shows an overall similar pattern to that seen in tomography models, especially in Archean and Proterozoic regions.

- Density variations of ±60 kg/m^3 relative to the initial value of 2790 kg/m^3

resulted in minor crustal thickness changes of ±2 km for most parts of the continent and up to ±5 km in the MER, and the Taoudeni, Congo and Kalahari basins allowing for a better fit with seismic data. The related differences in LAB depth were ±5 km with maximum changes in the aforementioned regions of ±15 km.

- The sublithospheric mantle flow associated with the Afar plume may involve a dynamic component to the topography in that region. The calculated crustal thickness in the model, that on average exceeds 9.8 km compared to seismic observations, can be corrected by applying a reduction in the elevation of ~1800 m at seismic stations located within a radius of 500 km from the centre of the plume. After corrections, the resulting LAB depth is reduced by ~60 km.

8.3 Future recommendations

The presented results demonstrate the efficiency of the applied methodology in successfully modelling first-order features of the lithosphere. However, the model`s inherent assumptions and numerical simplifications (assumed crustal and lithospheric density distribution and rock parameters) may cause significant deviations from the actual lithospheric structure.

Further methodological improvements have been made since the work of Fullea et al. (2007), including 1D, 2D and 3D approaches (Fullea et al., 2009; Afonso et al., 2013; Fullea et al., 2014). All of them include a self-consistent petrological-geophysical approach to better constraint the upper mantle down to 400 km depth, allowing to incorporate additional observables such as body and surface seismic waves, magnetotelluric results and mineral composition.

Therefore, future works and intended improvements should consider the following recommendations:

- Application of the newly developed 1D approach to consider lateral chemical variations within the lithospheric mantle which can result in

significant density variations at depth and laterally, related to enrichment/depletion mantle processes. This would result in an improvement of the LAB topography and a better comparison with tomography models.

- Application of 2D petrological/geophysical approaches will allow to better constrain the crustal and the lithospheric mantle structure along selected transects crossing different tectonic provinces where confident geological and geophysical data are available.

- A combined forward/inversion 3D approach for the whole continent would result in the most confident crust/lithospheric structure considering the available methodologies, which allows incorporating the maximum number of constraints.

- A common feature of these methodologies is that they assume steady-state thermal regime and isostasy, either local or regional. These implies that thermal transient effects related to recent tectonics or departures from isostasy (dynamic topography) related to sublithospheric mantle convection are not considered. Accounting for these effects requires the development/application of full geodynamic models and more importantly a new set of geophysical and geological observations of the whole continent.

Abbreviations

CMB - Crust-Mantle Boundary

CVL - Cameroon Volcanic Line

DSS - Deep Seismic Sounding

EAGLE - Ethiopia-Afar Geoscientific Lithospheric Experiment

EARS - East African Rift System

GOCE - Gravity field and steady-state Ocean Circulation Explorer

GRACE - Gravity Recovery and Climate Experiment

KRISP - Kenya Rift International Seismic Project

LAB - Lithosphere-Asthenosphere Boundary

MAMBA - Geophysical Measurements Across the continental Margin of Namibia

MER - Main Ethiopian Rift

Moho - Mohorovic Discontinuity

RF - Receiver Function

RMSE - Root Mean Square Error

SASE - South Africa Seismic Experiment

SIMA - Seismic Imaging of the Moroccan Atlas

WAC - West African Craton

WAMZ - West African Mobile Zone

WCARS - West and the Central African Rift System

List of Figures and Tables

Supplementary material

The supplementary material is stored on the CD, in the back of the book.

The Cd contains the following files:

- PDF version of this thesis
- The seismic data compilation: DSS and RF (lon/lat/Moho/ref)
- The crustal thickness model (lon/lat/Z_C)
- The lithospheric thickness model (lon/lat/Z_L)

References

Abdelsalam, M., J. P. Liégeois, and R. J. Stern (2002), The Saharan metacraton, J. Afr. Earth Sci., 34, 119-136.

Abdelsalam, M. G., S. S. Gao, and J. P. Liégeois (2011), Upper mantle structure of the Saharan Metacraton, J. Afr. Earth Sci., 60, 328-336.

Achauer, U., P. K. Maguire, J. Mechie, W. V. Green, and the KRISP Working Group (1992), Some remarks on the structure and geodynamics of the Kenya rift, Tectonophysics, 213, 257-268.

Afonso, J. C., G. Ranalli, and M. Fernàndez (2005), Thermal expansivity and elastic properties of the lithospheric mantle: results from mineral physics of composites, Phys. Earth Planet. Int., 149, 279-306.

Afonso, J. C., J. Fullea, Y. Yang, J. A. D. Connolly, and A. G. Jones (2013), 3D multi-observable probabilistic inversion for the compositional and thermal structure of the lithosphere and upper mantle II: General methodology and resolution analysis, J. Geophys. Res., 118, 16501676, doi:10.1002/jgrb.50123.

Airy, G. B. (1855), On the computation of the effect of the attraction of the mountain masses as disturbing the apperent astronomical latitude of stations in geodetic surveys, Philo. Trans. R. Soc., 145, 101.

Al-Damegh, K., E. Sandvol, and M. Barazangi (2005), Crustal structure of the Arabian plate: new constraints from the analysis of teleseismic receiver functions, Earth Planet. Sci. Lett., 231, 177-196.

Amante, C., and B. W. Eakins (2009), ETOPO1 1 Arc-Minute Global Relief Model: Procedures, Data Sources and Analysis, NOAA Technical Memorandum NESDIS NGDC-24, 19.

Artemieva, I. M., and W. D. Mooney (2001), Thermal thickness and evolution of Precambrian lithosphere: A global study, J. Geophys. Res., 106, 16,387-16,414.

Artemieva, I. M. (2006), Global 1°x1° thermal model TC1 for the continental

lithosphere: implications for lithosphere secular evolution, Tectonophysics, 416, 245-277.

Artemieva, I. M., (2011), The lithosphere: An interdisciplinary approach, Cambridge Univ. Press, Monograph, 794 pp., ISBN 9780521843966.

Artemjev, M. E., M. K. Kaban, V. A. Kucherinenko, G. V. Demyanov, and V. A. Taranov (1994), Subcrustal density inhomogeneities of Northern Eurasia as derived from the gravity data and isostatic models of the lithosphere, Tectonophysics, 240, 249-280.

Ashwal L. D., and K. Burke (1989), African lithospheric structure, volcanism, and topography, Earth Planet. Sci. Lett., 96, 8-14.

Ayarza, P., R. Carbonell, and A. Teixell (2014), Crustal thickness and velocity structure across the Moroccan Atlas from long offset wide-angle reflection seismic data: The SIMA experiment, Geochem. Geophys. Geosyst., 15, 1698-1717.

Bagherbandi, M., R. Tenzer, L. E. Sjöberg, and P. Novák (2013), Improved global crustal thickness modeling based on the VMM isostatic model and non-isostatic gravity correction, J. Geodyn., 66, 25-37.

Bailey, D. K. (1992), Episodic alkaline igneous activity across Africa: Implications for the causes of continental break-up, in Magmatism and the causes of continental break-up, ed. by Storey, B. C. et al., Geol. Soc. Spec. Publ., 68, 91-98.

Bassin, C., G. Laske, and G. Masters (2000), The current limits of resolution for surface wave tomography in North America, Eos Trans. AGU 81, F897.

Bastow, I. D., G. W. Stuart, J. M. Kendall, and C. J. Ebinger (2005), Upper-mantle seismic structure in a region of incipient continental breakup: northern Ethiopian rift, Geophys. J. Int., 162, 479-493.

Bastow, I. D., A. A Nyblade, G. W. Stuart, T. O. Rooney, and M. H. Benoit (2008), Upper mantle seismic structure beneath the ethiopian hotspot: rifting at the edge of the African low velocity anomaly, Geochem. Geophys. Geosyst., 9(12), Q122022.

Batumike J. M., W. L. Griffin, and S. Y. O'Reilly (2009), Lithospheric mantle

structure and the diamond potential of kimberlites in southern D. R. Congo, Lithos, 112, 166-176.

Bauer, K., S. Neben, B. Schreckenberger, R. Emmermann, K. Hinz, N. Fechner, K. Gohl, A. Schulze, R. B. Trumbull, and K. Weber (2000), Deep structure of the Namibia continental margin as derived from integrated geophysical studies, J. Geophys. Res., 105(B11), 25, 829-853, doi:10.1029/2000JB900227.

Begg, G., W. Griffin, L. Natapov, S. O'Reilly, S. Grand, C. O'Neill, J. Hronsky, Y. Djomani, C. Swain, T. Deen, and P. Bowden (2009), The lithospheric architecture of Africa: seismic tomography, mantle petrology, and tectonic evolution, Geosphere, 5, 23-50.

Behn M. D., C. P. Conrad, and P. Silver (2004), Detection of upper mantle flow associated with the African Superplume, Earth Planet. Sci. Lett., 224, 259-274.

Bell D., M. Grégoire, T. Grove, N. Chatterjee, R. Carlson, and P. Buseck (2005), Silica and volatile-element metasomatism of Archean mantle: a xenolith-scale example from the Kaapvaal Craton, Contrib. Mineral. Petr., 150(3), 251-367.

Benoit, M. H., A. A. Nyblade, J. C. VanDecar, and H. Gurrola (2003), Upper mantle P-wave velocity structure and transition zone thickness beneath the Arabian Shield, Geophys. Res. Lett., 30(10), 1531, doi:10.1029/2002GL016436.

Benoit, M. H., A. A. Nyblade, and J. C. Van Decar (2006), Upper mantle P wave speed variations beneath Ethiopia and the origin of the Afar Hotspot, Geology 34, 329-332.

Bezada, M. J., E. D. Humphreys, D. R. Toomey, M. Harnafi, J. M. Davila, and J. Gallart (2013), Evidence for slab rollback in westernmost Mediterranean from improved upper mantle imaging, Spain, Earth Planet. Sci. Lett., 368, 51-60.

Black, R., and M. Girod (1970), Late Palaeozoic to Recent igneous activity in the West Africa and its relationship to basement structure, in African Magmatism and Tectonics, ed by Clifford, T. N., and I. G. Gass, Oliver and Boyd, 185-210.

Black, R., and J. P. Liégeois (1993) Cratons, mobile belts, alkaline rocks and continental lithospheric mantle: the Pan-African testimony, J. Geol. Soc., 150, 89-

98.

Bodine, J. H., M. S. Steckler, and A. B. Watts, (1981), Observations of flexure and the rheology of the oceanic lithosphere, J. Geophys. Res., 86, doi: 10.1029/JB086iB05p03695.

Bowin, C. (1983), Depth of principal mass anomalies contributing to the Earth's geoidal undulations and gravity anomalies, Mar. Geodesy, 7, 61-100.

Boyd, F. R., and P. H. Nixon (1978), Ultramafic nodules from Kimberley Pipes, S. Afr. Geochim. Cosmochim. Acta, 42, 1367-82.

Braile L. W, B. Wang, C. R. Daudt, G. R. Keller, and J. P. Patel (1994), Modeling the 2-D seismic velocity structure across the Kenya rift, Tectonophysics, 236, 251-269.

Brown, C., and R. W. Girdler (1980), Interpretation of African gravity and its implication for the breakup of the continents, J. Geophys. Res., 85(B11), 6443-6455, doi:10.1029/JB085iB11p06443.

Buck, W. R. (1986), Small-scale convection induced by passive rifting: The cause for uplift of rift shoulders, Earth Planet. Sci. Lett., 77, 362-372.

Buiter, S. J. H., B. Steinberger, S. Medvedev, and J. Tetreault (2012), Could the mantle have caused subsidence of the Congo Basin?, Tectonophysics, 514-517, 62-80, doi:10.1016/j.tecto.2011.09.024.

Buness, H., P. Giese, C. Bobier, C. Eva, F. Merlanti, R. Pedone, and S. Mueller (1992), The EGT-85 seismic experiment in Tunisia - a reconnaissance of the deep structure, Tectonophysics, 207, 245-267.

Burke, K., and A. J. Whiteman (1973), Uplift, rifting and the break-up of Africa, in Implications of Continental Drift to the Earth, ed by Tarling, D. H. and S. K. Runcorn, Science, 2, 734-755.

Burke, K. (1996), The African plate, S. Afr. J. Geol., 99, 339-410.

Cadek, O., and Z. Martinec (1991), Spherical harmonic expansion of the Earth's crustal thickness up to degree and order 30, Stud. Geoph. Geod., 35, 151-165.

Camelbeeck, T., and M. D. Iranga (1996), Deep crustal earthquakes and active faults along the Rukwa trough, eastern Africa, Geophys. J. Int., 124, 612-630.

Carbonell R., A. Levander, and R. Kind (2013), The Mohorovičić discontinuity beneath the continental crust: an overview of seismic constraints, Tectonophysics, 609, 353-377.

Cavaroc, V. V., G. Padgett, D. G. Stephens, W. H. Kanes, Boudda-Ahmed, and I. D. Wollen (1976), Late Paleozoic of the Tindouf Basin-North Africa, J. Sediment. Petrol., 46, 77-88.

Cazenave, A., A. Souriau, and K. Dominh (1989), Global coupling of Earth surface topography with hotspots, geoid and mantle heterogeneities, Nature, 340, 54-57.

Chen, W. P., and P. Molnar, (1983), Focal depths of intracontinental and intraplate earthquakes and their tectonic implications for the thermal and mechanical properties of the lithosphere, J. Geophys. Res., 88, 4183-4214.

Chesler, R. (2012), The Geochemistry and Geochronology of Tanzanian Kimberlites, School of Earth Sciences, The University of Melbourne, Melbourne.

Chevrot, S., and L. Zhao (2007), Multiscale finite-frequency Rayleigh wave tomography of the Kaapvaal craton, Geophys. J. Int., 169, 201-215.
Chorowicz, J. (2005), The East African Rift System, J. Afr. Earth Sci., 43, 379-410.

Conrad, C. P., M. and Gurnis (2003), Seismic tomography, surface uplift, and the breakup of Gondwanaland: Integrating mantle convection backwards in time, Geochem. Geophys. Geosyst, 4(3), 1031.

Conrad, C. P., and C. Lithgow-Bertelloni (2006), Influence of continental roots and asthenosphere on plate-mantle coupling, Geophys. Res. Lett., 33, L05312.

Contrucci, I., F. Klingelhoefer, J. Perrot, R. Bartolome, M. A. Gutscher, M. Sahabi, J. Malod, and J. P. Rehault (2004), The crustal structure of the NW Moroccan continental margin from wide-angle and reflection seismic data, Geophys. J. Int., 159, 117-128.

Cooper, C. M., and M. S. Miller (2014), Craton formation: Internal structure

inherited from closing of the early oceans, Lithosphere, 6, 35-42.

Cornwell, D. G., P. K. H. Maguire, R. W. England, and G. W. Stuart (2010), Imaging detailed crustal structure and magmatic intrusion across the Ethiopian Rift using a dense linear broadband array, Geochem. Geophys. Geosyst.,11, Q0AB03.

Craig, T. J., J. A. Jackson, K. Priestley, and D. McKenzie (2011), Earthquake distribution patterns in Africa: their relationship to variations in lithospheric and geological structure, and their rheological implications, Geophys. J. Int., 185, 403-434, doi:10.1111/j.1365-246X.2011.04950.x.

Crosby, A. G., S. Fishwick, and N. White (2010), Structure and evolution of the intracratonic Congo Basin, Geochem. Geophys. Geosyst., 11, 6.

Davis, P. M., and P. D. Slack (2002), The uppermost mantle beneath the Kenya dome and relation to melting, rifting and uplift in East Africa, Geophys. Res. Lett., 29, 1117.

Debayle, E., J. J. Lévêque, and M. Cara (2001), Seismic evidence for a deeply rooted low-velocity anomaly in the upper mantle beneath the northeastern Afro/Arabian continent, Earth Plan. Sci. Lett., 193, 423-436.

Deen, T., W. L. Griffin, G. Begg, S. Y. O'Reilly, and L. M. Natapov (2006), Thermal and compositional structure of the subcontinental lithospheric mantle: Derivation from shear-wave seismic tomography, Geochem. Geophys. Geosyst., 7, Q07003, doi:10.1029/2005GC001120.

DESERT Group (2004), The crustal structure of the Dead Sea Transform, Geophys. J. Int., 156, 655-681.

deWit, M. J., C. Roering, R. J. Hart, R. A. Armstrong, C. E. J. deRonde, R. W. E. Green, M. Tredoux, E. Peberdy, and R. A. Hart (1992), Formation of an Archean continent, Nature, 357, 553-562.

Diaz, J., J. Gallart, and R. Carbonell (2016), Moho topography beneath the Iberian-Western Mediterranean region mapped from controlled-source and natural

seismicity surveys, manuscript submitted to Tectonophysics.

Di Leo, J. F., J. Wookey, J. M. Kendall, and N. D. Selby (2015), Probing the edge of the West African Craton: a first seismic glimpse from Niger, Geophys. Res. Lett. 42, 1694-1700.

Dopp S. (1964), Preliminary note on a refracted P phase in the Western Rift Valley of Africa, J. Geophys. Res., 69, 3027-3031.

Doucouré, C. M., and M. J. De Wit, (2003), Old inherited origin for the present near-bimodal topography of Africa, J. Afr. Earth Sci., 36, 371-388.

Downey, N. J., and M. Gurnis (2009), Instantaneous dynamics of the cratonic Congo basin, J. Geophys. Res., 114, 6401, doi:10.1029/2008JB006066.

Dugda, M. T., A. A. Nyblade, J. Julia, C. A. Langston, C. A. Ammon, and S. Simiyu (2005), Crustal structure in Ethiopia and Kenya from receiver function analysis: implications for rift development in eastern Africa, J. Geophys. Res., 110, B01303, doi:10.1029/2004JB003065.

Dugda, M. T., A. A. Nyblade, and J. Julià (2007), Thin Lithosphere Beneath Ethiopia and Djibouti Revealed by a Joint Inversion of Rayleigh Wave Group Velocties and Receiver Functions, J. Geophys. Res., 112, B08305, doi:10.1029/2006JB004918.

Durrheim, R. J., W. H. Barker, and R. W. E. Green (1992), Seismic studies in the Limpopo belt, Precambrian Res., 55, 187-200.

Durrheim, R. J., and W. D. Mooney (1994), Evolution of the Precambrian lithosphere; seismological and geochemical constraints, J. Geophys. Res. 99, 15359-15374.

Dutton, C. E. (1882), Review of Physics of the Earth's Crust, Am. J. Sci., 23, 283-290.

Eaton, D. W., F. Darbyshire, R. L. Evans, H. Grütter, A. G. Jones and X., Yuan (2009), The elusive lithosphere-asthenosphere boundary (LAB) beneath cratons, Lithos, 109, 1-22.

Ebinger, C. J., T. Bechtel, D. Forsyth, and C. Bowin (1989), Effective elastic plate thickness beneath the East African and Afar plateau, and isostatic compensation for the uplifts, J. Geophys. Res., 94, 2893-2901.

Ebinger, C. J., and N. H. Sleep (1998), Cenozoic magmatism throughout east Africa resulting from impact of a single plume, Nature, 395, 788-791.

El-Isa, Z., J. Mechie, C. Prodehl, J. Makris, and R. Rihm (1987), A crustal structure study of Jordan derived from seismic refraction data, Tectonophysics, 138, 235-253.

England, P., and P. Molnar (1997), Active deformation of Asia: From kinematics to dynamics, Science, 278, 647-650.

Faccenna, C., C. Piromallo, A. Crespo-Blan, L. Jolivet, and F. Rossetti (2004), Lateral slab deformation and the origin of the western Mediterranean arcs, Tectonics, 23, TC1012.

Faccenna, C., T. W. Becker, L. Jolivet, and M. Keskin (2013), Mantle convection in the Middle East: reconciling Afar upwelling, Arabia indentation and Aegean trench rollback, Earth Planet. Sci. Lett., 375, 254-269.

Fairhead, J. D., and C. V. Reeves (1977), Teleseismic delay times, Bouguer anomalies, and inferred thickness of the African lithosphere, Earth Planet. Sci. Lett., 36, 63-76.

Fairhead, J. D. (1986), Geophysical controls on sedimentation within the African rift systems, in Sedimentation in the African rifts, ed. by Frostick, L. et al., Geol. Soc. Spec. Publ., 25, 19-27.

Fairhead, J. D., and C. S. Okereke (1987), A regional gravity study of the West African rift system in Nigeria and Cameroon and its tectonic interpretation, Tectonophysics, 143, 141-159.

Fairhead, J. D. (1988), Mesozoic plate tectonic reconstructions of the Central-South Atlantic Ocean: the Role of the West and Central African Rift System, Tectonophysics, 155, 181-191.

Fairhead, J. D., and C. M. Green (1989), Controls on rifting in Africa and the regional tectonic model for the Nigeria and East Niger rift basins, in Rifting in Africa, ed. by Rosendahl, B. R., Afr. Earth Sci. Spec. Publ., 8, 231-249.

Fernàndez, M., I. Marzán, A. Correia, and E. Ramalho (1998), Heat flow, heat production and lithospheric thermal regime in the Iberian Peninsula, Tectonophysics, 291, 29-53.

Fezaa, N., J. P. Liégeois, N. Abdallah, E. H. Cherfouh, B. De Waele, O. Bruguier, and O. Ouabadi (2010), Late Ediacaran geological evolution (575-555 Ma) of the Djanet Terrane, Eastern Hoggar, Algeria, evidence for a Murzukian intracontinental episode, Precambrian Res., 180, 299-327.

Finnerty, A. A., and F. R. Boyd (1978), Pressure-dependent solubility of calcium in forsterite coexisting with diopside and enstatite, Carnegie Inst. Washington Yearb., 77, 713-717

Fishwick, S. (2010), Surface wave tomography: Imaging of the lithosphere-asthenosphere boundary beneath central and southern Africa?, Lithos, 120, 63-73.

Fishwick, S., and I. D. Bastow (2011), Towards a better understanding of African topography, a review of passive-source seismic studies of the African crust and upper mantle, in The Formation and Evolution of Africa: A Synopsis of 3.8 Ga of Earth History, ed. by Van Hinsbergen, D. J. J. et al., Geol. Soc. Spec. Publ., 357, 343-371.

Forte, A. M., J. X. Mitrovica, R. Moucha, N. A. Simmons, and S. P. Grand (2007), Descent of the ancient Farallon slab drives localized mantle flow below the New Madrid seismic zone, Geophys. Res. Lett., 34, L04308.

Forte, A. M., S. Quéré, R. Moucha, N. A. Simmons, S. P. Grand, J. X. Mitrovica, and D. B. Rowley (2010), Joint seismic-geodynamic-mineral physical modelling of African geodynamics: a reconciliation of deep-mantle convection with surface geophysical constraints, Earth Planet. Sci. Lett., 295, 329-34.

Fouch, M. J., D. E. James, J. C. van Decar, and S. van der Lee (2004), Mantle seismic structure beneath the Kaapvaal and Zimbabwe Cratons, S. Afr. J. Geol.,

107, 33-44, doi:10.2113/107.1-2.33.

Fowler, C. M. R. (2005), The solid Earth, Cambridge Univ. Press, 685p.

Franz, G., G. Steiner, F. Volker, D. Pudlo, and K. Hammerschmidt (1999), Plume-related alkaline magmatism in central Africa-the Meidob Hills (W Sudan), Chem. Geol., 157, 27-47.

Freybourger, M., J. B. Gaherty, and T. H. Jordan (2001), Structure of the Kaapvaal craton from surface waves, Geophys. Res. Lett., 28, 2489-2492.

Frizon de Lamotte, D., B. Saint Bezar, R. Bracene, and E. Mercier (2000), The two main steps of the Atlas building and Geodynamics of West Mediterranean, Tectonics, 19, 740-761.

Frizon de Lamotte, D., B. Fourdan, S. Leleu, F. Leparmentier, and P. Clarens (2015), Style of rifting and the stages of Pangea breakup, Tectonics, 34, 1009-1029.

Fullea, J., M. Fernàndez, H. Zeyen, and J. Vergés (2007), A rapid method to map the crustal and lithospheric thickness using elevation, geoid anomaly and thermal analysis. Application to the Gibraltar Arc System and adjacent zones, Tectonophysics, 430, 97-117.

Fullea, J., J. C. Afonso, J. A. D. Connolly, M. Fernàndez, D. García-Castellanos, and H. Zeyen (2009), LitMod3D: An interactive 3-D software to model the thermal, compositional, density, seismological, and rheological structure of the lithosphere and sublithospheric upper mantle, Geochem. Geophys. Geosyst., 10, Q08019, doi:10.1029/2009GC002391.

Fullea, J., M. R. Muller, A. G. Jones, and J. C. Afonso (2014), “The lithosphere-asthenosphere system beneath Ireland from integrated geophysical-petrological modelling II: 3D thermal and compositional structure”, Lithos, 189, 49-64, http://dx.doi.org/10.1016/j.lithos.2013.09.014

Furman, T., J. Bryce, J. Karson, and A. Iotti (2004), East African Rift System (EARS) plume structure: insights from Quaternary Mafic Lavas of Turkana, Kenya,

J. Petrol., 45, 1069-1088.

Gajewski, D., A. Schulte, D. Riaroh, and H, Thybo (1994), Deep seismic sounding in the Turkana depression, northern Kenya rift, in Crustal and Upper Mantle Structure of the Kenya Rift, ed. by Prodehl, C. et al., Tectonophysics, 236, 165-178.

Gani, N. D., M. R. Gani, and M. G. Abdelsalam (2007), Blue Nile incision on the Ethiopian Plateau: Pulsed plateau growth, Pliocene uplift, and hominin evolution, GSA Today, 17, 4-11.

Garcia-Castellanos, D., and A. Villaseñor (2011), Messinian salinity crisis regulated by competing tectonics and erosion at the Gibraltar Arc, Nature, 480, 359-363.

George, R., N. Rogers, and S. Kelley (1998), Earliest magmatism in Ethiopia: evidence for two mantle plumes in one flood basalt province, Geology, 26, 923-926.

Gil, A., J. Gallart, J. Diaz, R. Carbonell, M. Torne, A. Levander, and M. Harnafi (2014), Crustal structure beneath the Rif Cordillera, North Morocco, from the RIFSIS wide-angle reflection seismic experiment, Geochem. Geophys. Geosyst., 15, 4712-4733.

Globig, J., M. Fernandez, M. Torne, J. Vergés, A. Robert, and C. Faccenna (2016), New insights into the crust and lithospheric mantle structure of Africa from elevation, geoid and thermal analysis, manuscript submitted to J. Geophys. Res.

Gore, J., D. E James, and T. G. Zengeni (2009), Crustal structure of the Zimbabwe Craton and the Limpopo Belt of southern Africa: new constraints from seismic data and implications for its evolution, S. Afr. J. Geol., 112, 213-228.

Grad, M., T. Tiira, and ESC Moho Working Group (2009), The Moho depth of the European plate, Geophys. J. Int., 176, 279-292.

Grand, S. P., R. D. Van Der Hilst, and S. Widiyantroro (1997), Global seismic tomography: A snapshot of convection in the earth, GSA Today, 7, 1-7.

Green, R. W. E., and R. J. Durrheim (1990), A seismic refraction investigation of the Namaqualand Metamorphic Complex, South Africa, J. Geophys. Res., 95, doi:10.1029/89JB03582.

Griffin, W. L., and S. Y. O'Reilly (1987), Is the Moho the crust-mantle boundary?, Geology, 15, 241-244.

Griffin, W. L., S. Y. O'Reilly, and C. G. Ryan (1999), The composition and origin of subcontinental lithospheric mantle, in Mantle Petrology: Field observations and high-pressure experimentation: A tribute to Francis R. (Joe) Boyd, ed. by Fei, Y. et al., Geochem. Soc. Spec. Publ., 6, 13-45.

Gung, Y., M. Panning, and B. Romanowicz (2003), Global anisotropy and the thickness of continents, Nature, 422, 707-710.

Gurnis, M., J. X. Mitrovica, J. Ritsema, and H. J. van Heijst (2000), Constraining mantle density structure using geological evidence of surface uplift rates: The case of the African superplume, Geochem. Geophys. Geosyst., 1, 7.

Gvirtzman, Z., C. Faccenna, and T. W. Becker (2016), Isostasy, flexure, and dynamic topography, Tectonophysics, doi:10.1016/j.tecto.2016.05.041.
Hager, B. H., R. W. Clayton, M. A. Richards, R. P. Comer, and A. M.

Hager, B. H., Clayton, R. W., Mark R. A., Comer R. P., and A. M. Dziewonski (1985), Lower mantle heterogeneity, dynamic topography and the geoid, Nature, 313, 541-546.

Hager, B. H., and M. A. Richards (1989), Long-wavelength variations in Earth's geoid: physical models and dynamical implications, Phil. Trans. R. So. Lond. A, 328, 309-327.

Halliday, A. N., J. P. Davidson, P. Holden, C. Dewolf, D. C. Lee, and J. G. Fitton (1990), Trace-element fractionation in plumes and the origin of HIMU mantle beneath the Cameroon Line, Nature, 347, 523-528.

Hamayun (2014), Earth structure recovery from state-of-the art model of gravity field and additional geophysical information, PhD thesis, TU Delft.

Hamza, V. M., and F. P. Vieira (2012), Global distribution of the lithosphere-asthenosphere boundary: a new look, J. Geophys. Res. Solid Earth, 3(2), 199-212.

Hansen, S. E., A. A. Nyblade, J. Julia, P. H. G. M. Dirks, and R. J. Durrheim (2009), Upper-mantle low-velocity zone structure beneath the Kaapvaal craton from S-wave receiver functions, Geophys. J. Int., 178(2), 1021-1027.

Hansen, S., A. A. Nyblade, and M. Benoit (2012), Mantle structure beneath Africa and Arabia from adaptively parameterized P-wave tomography: Implications for the origin of Cenozoic Afro-Arabian tectonism, Earth Planet. Sci. Lett., 319-320, 23-34.

Hansen, S. E., and A. A. Nyblade (2013), The Deep Seismic Structure of the Ethiopia/Afar Hotspot and the African Superplume, Geol. J. Int., 194, 118-124.

Hartley, R. W., P. A. and Allen (1994), Interior cratonic basins of Africa: relation to continental break-up and role of mantle convection, Basin Res, 6, 95-113, doi:10.1111/j.1365-2117.1994.tb00078.x.

Haxby, W. F., and D. L. Turcotte (1978), On isostatic geoid anomalies, J. Geophys. Res., 83(B11), 5473-5478, doi:10.1029/JB083iB11p05473.

Hayford, J. F. (1909), The Figure of the Earth and Isostasy from Measurements in the United States, Publications of the U. S. Coast and Geodetic Survey.

Hayford, J. F., and W. Bowie (1912), The Effect of Topography and Isostatic Compensation upon the Intensity of Gravity, Publications of the U. S. Coast and Geodetic Survey.

Heiskanen, W. A., and F. A. Veneing Meinez (1958), The Earth and its gravity field, McGraw-Hill, New York.

Hilton, D. R., S. A. Halldórsson, P. H. Barry, T. P. Fischer, J. M. de Moor, C. J. Ramirez, F. Mangasini, and P. Scarsi (2011), Helium isotopes at Rungwe Volcanic Province, Tanzania, and the origin of East African Plateaux, Geophys. Res. Lett., 38, L21304.

Hirsch, K. K., K. Bauer, and M. Scheck-Wenderoth (2009), Deep structure of the

western South African passive margin Results of a combined approach of seismic, gravity and isostatic investigations, Tectonophysics, 470, 57-70.

Jaffal, M., F. Klingelhoefer, L. Matias, F. Teiseira, and M. Amrhar (2009), Crustal structure of the NW Moroccan margin from deep seismic data (SISMAR cruise), C. R. Geosci., 341, 495-503, doi:10.1016/j.crte.2009.04.003.

James, D. E., M. J. Fouch, J. C. VanDecar, S. van der Lee, and KAAPVAAL SEISMIC GROUP (2001), Tectospheric structure beneath southern Africa, Geophys. Res. Lett., 28, 2485-2488.

James, D. E., F. Niu, and J. Rokosky (2003), Crustal structure of the Kaapvaal Craton and its significance for early crustal evolution, Lithos, 71, 413-429.

Jarvis, G. T., and D. P. McKenzie (1980), Sedimentary basin formation with finite extension rates, Earth Planet. Sci. Lett., 48, 42-52.

Jaupart, C., and J. C. Mareschal (2007), Heat flow and thermal structure of the lithosphere, in Treatise on Geophysics, ed. by Schubert, G., Elsevier, 217-251.

Jelsma, H. A., and P. H. G. M. Dirks (2002), Neoarchean Tectonic Evolution of the Zimbabwe Craton, in The Early Earth: Physical, Chemical and Biological Development, ed. by Fowler, C. et al., Geol. Soc. Spec. Publ., 199, 183-211.

Jessell, M. W., G. C. Begg, and M. S. Miller (2016), The geophysical signatures of the West African Craton, Precambrian Res., 274, 3-24.

Jiménez-Munt, I., M. Fernàndez, E. Saura, J. Vergés, and D. Garcia-Castellanos (2012), 3D lithospheric structure and regional/residual Bouguer anomalies in the Arabia-Eurasia collision (Iran), Geophys. J. Int., 190(3), 1311-1324.

Jones, M. Q. W. (1988), Heat flow in the Witwatersrand Basin and environs and its significance for the South African shield geotherm and lithosphere thickness, J. Geophys. Res., 93, 3243-3260.

Jones, A. G. (1999), Imaging the continental upper mantle using electromagnetic methods, Lithos, 48, 57-80.

Jones, S. M., B. Lovell, and A. G. Crosby (2012), Comparison of modern and

geological observations of dynamic support from mantle convection, J. Geol. Soc. London, 169(6), 745-758.

Kaban, M. K., P. Schwintzer, and C. Reigber (2004), A new isostatic model of the lithosphere and gravity field, J. Geod., 78, 368-385.

Kadima, E., D. Delvaux, S. N. Sebagenzi, L. Tack, and S. M. Kabeya (2011), Structure and geological history of the Congo Basin: an integrated interpretation of gravity, magnetic and reflection seismic data, Basin Res., 23, 499–527, doi:10.1111/j.1365-2117.2011.00500.x.

Karato, S. I. (2012), On the origin of the asthenosphere, Earth Planet. Sci. Lett., 321, 95-103.

Karato, S. I., and P. Wu (1993), Rheology of the upper mantle: a synthesis, Science 260, 771-778.

Keranen, K. M., S. L. Klemperer, J. Julia, J. F. Lawrence, and A. A. Nyblade (2009), Low lower crustal velocity across Ethiopia: Is the Main Ethiopian Rift a narrow rift in a hot craton?, Geochem. Geophys. Geosyst., 10, Q0AB01, doi:10.1029/2008GC002293.

Kgaswane, E. M., A. A. Nyblade, J. Julia, P. H. G. M. Dirks, R. J. Durrheim, and M. E. Pasyanos (2009), Shear wave velocity structure of the lower crust in southern Africa: evidence for compositional heterogeneity within Archaean and Proterozoic terrains, J. Geophys. Res., 114, B12304.

Kgaswane, E. M., A. A. Nyblade, R. J. Durrheim, J. Julia, P. H. G. M. Dirks, and S. J. Webb (2012), Shear wave velocity structure of the Bushveld Complex, South Africa, Tectonophysics, 554, 83-104.

King, S. D., and D. L. Anderson (1995), An alternative mechanism to flood basalt formation, Earth Planet. Sci. Lett., 136, 269-279.

King, S. D., and J. Ritsema (2000), African hotspot volcanism: small-scale convection in the upper mantle beneath cratons, Science, 290, 1137-1140.

Klingelhoefer, F., C. Labails, E. Cosquer, S. Rouzo, L. Geli, D. Aslanian, L. L.

Olivet, M. Sahabi, H. Nouze, and P. Unternehr (2009), Crustal structure of the SW-Moroccan margin from wide-angle and reflection seismic data (the DAKHLA experiment) part A: Wide-angle seismic models, Tectonophysics, 468(1-4), 63-82.

Kobussen, A. F., W. L. Griffin, S. Y. O'Reilly, and S. R. Shee (2008), Ghosts of lithospheres past: Imaging an evolving lithospheric mantle in Southern Africa, Geology, 36, 515-518.

Koehn, D, K. Aanyu, S. Haines, and T. Sachau (2008), Rift nucleation, rift propagation and the creation of basement micro-plates within active rifts, Tectonophysics, 458, 105-116, doi:10.1016/j.tecto.2007.10.003.

König, M., and W. Jokat (2010), Advanced insights into magmatism and volcanism of the Mozambique Ridge and Mozambique Basin in the view of new potential field data, Geophys. J. Int., 180, 158-180.

Kokonyangi, J., A. B. Kampunzu, R. Armstrong, M. Yoshida, T. Okudaira, M. Arima, and D. A. Ngulube (2006), The Mesoproterozoic Kibaridebelt (Katanga, SED. R. Congo), J. Afr. Earth Sci.,46, 1-35.

Korenaga, J., and S. I. Karato (2008), A new analysis of experimental data on olivine rheology, J. Geophys. Res., 113, B02403, doi:10.1029/2007JB005100.

Kosarian, M. (2006), Lithospheric structure of North Africa and western Eurasia, PhD thesis, The Pennsylvania State University.

KRISP WORKING GROUP (1987), Structure of the Kenya rift from seismic refraction, Nature, 325, 239-242.

Kröner, A., and R. J. Stern (2004), Africa: Pan-African orogeny, in Encyclopedia of Geology, ed. by Selley R. et al., Elsevier, 1-12.

Kumar, N., H. Zeyen, and A. P. Singh (2014), 3D Lithosphere density structure of southern Indian shield from joint inversion of gravity, geoid and topography data, J. Asian Earth Sci. 89, 98-107.

Kwadiba, M. T. O. G., C. Wright, E. M. Kgaswane, R. E. Simon, and T. K. Nguuri (2003), Pn arrivals and lateral variations of Moho geometry beneath the Kaapvaal

Craton, Lithos, 71, 393-411.

Lachenbruch, A. H., and J. H. Sass, (1977), in Heat flow in the United States and the thermal regime of the crust, Am. Geophys. Union, 20, 5, doi:10.1029/GM020p0626.

Lachenbruch, A. H., and P. Morgan (1990), Continental extension, magmatism and elevation; formal relations and rules of thumb, Tectonophysics, 174, 39-62.

Laske, G., and G. Masters (1997), A global digital map of sediment thickness, Eos Trans. AGU 78, F483.

Laske, G., G. Masters, Z. Ma, and M. Pasyanos (2013), Update on CRUST1.0 a 1-degree global model of Earth's crust, Geophys. Res. Abstracts, Abstract EGU2013-2658.

Last, R. J., A. A. Nyblade, C. A. Langston, and T. J. Owens (1997), Crustal structure of the east African plateau from receiver functions and Rayleigh wave phase velocities, J. Geophys. Res., 102, 24469-24484.

Lebedev, S., and R. D. van der Hilst (2008), Global upper-mantle tomography with the automated multimode inversion of surface and S-wave forms, Geophys. J. Int., 173, 505-518.

Le Heron, D. P., and J. P. Howard (2012), Sandstones, glaciers, burrows and transgressions: the Lower Palaeozoic of Jabel az-Zalmah, Al Kufrah Basin, Libya, Sed. Geology, 245-246, 63-75, doi:10.1016/j.sedgeo.2011.12.008.

Lemoine, F. G., and 14 co-authors (1998), The development of the joint NASA GSFC and the National Imagery and Mapping Agency (NIMA) geopotential model EGM96, Goddard Space Flight Center, NASA Tech. Pub., 1998-206861.

Le Stunff, Y., and Y. Ricard (1995), Topography and geoid due to lithospheric mass anomalies, Geophys. J. Int., 122(3), 982-990, doi:10.1111/j.1365-246X.1995.tb06850.x.

Li, A., and K. Burke (2006), Upper mantle structure of southern Africa from Rayleigh wave tomography, J. Geophys. Res., 111, B10303.

Lindeque, A. S., T. Ryberg, J. Stankiewicz, M. H. Weber, and M. J. de Witt (2007),

Deep crustal seismic reflection experiment across the southern Karoo Basin, South Africa, S. Afr. J. Geol., 110(2-3), 419-438, doi:10.2113/gssajg.110.2-3.419.

Link, K., D. Koehn, M. G. Barth, K. Aanyu, and S. F. Foley (2010), Continuous cratonic crust between the Congo and Tanzania blocks in western Uganda, Int. J. Earth. Sci. (Geol Rundsch), 99, 1559-1573.

Lithgow-Bertelloni, C., and P. Silver (1998), Dynamic topography, plate driving forces, and the African superswell, Nature, 395, 269-272.

Lucassen, F., G. Franz, R. L. Romer, D. Pudlo, and P. Dulski (2008), Nd, Pb, and Sr isotope composition of Late Mesozoic to Quaternary intra-plate magmatism in NE-Africa (Sudan, Egypt): high-μ, signatures from the mantle lithosphere, Contrib. Mineral. Petr., 156(6), 765-784.

MacGregor, D. S, R. T. J. Moody, and D. D. Clark-Lowes (1998), Petroleum Geology of North Africa, Geol. Soc. Spec. Publ., 132, 7-68.

Mänttäri, I., F. Kigereigu, H. Huhma, G. S. Kock, T. de Koistinen, E. T. Kuosmanen, Y. Lahaye, M. I. Lehtonen, H. Mäkitie, T. Manninen, H. O'Brien, K. Saalmann, P. Virransalo, and A. B. Westerhof (2011), New Precambrian rock ages from Uganda, 23rd Coll. Afr. Geol. (CAG23), Abstract Vol., 260.

Maguire, P. K. H., C. J. Swain, R. Masotti, and M. A. Khan (1994), A crustal and uppermost mantle cross-sectional model of the Kenya Rift derived from seismic and gravity data, in Crustal and Upper Mantle structure of the Kenya Rift, ed. by Prodehl C. et al., Tectonophysics, 236, 217-249.

Maguire, P. K. H., G. R. Keller, S. L. Klemperer, G. D. Mackenzie, K. Keranen, S. Harder, B. O'Reilly, H. Thybo, L. Asfaw, and M. Amha (2006), Crustal structure of the northern Main Ethiopian Rift from the EAGLE controlled-source survey; a snapshot of incipient lithospheric break-up, in The Afar Volcanic Province within the East African Rift System, ed. by Yirgu G. et al., Geol. Soc. Spec. Publ., 259, 269-292.

Makris, J., A. Demnati, and J. Klussmann (1985), Deep seismic soundings in Morocco and a crust and upper mantle model deduced from seismic and gravity

data, Ann. Geophys., 3, 369-380.

Mancilla, F., D. Stich, J. Morales, J. Julià, J. Diaz, A. Pazos, D. Córdoba, J. A. Pulgar, P. Ibarra, M. Harnafi, and F. Gonzalez-Lodeiro (2012), Crustal thickness variations in northern Morocco, J. Geophys. Res., 117, B02312.

Mancilla, F., G. Booth-Rea, D. Stich, J. V. Pérez-Peña, J. Morales, J. M. Azañón, R. Martín, and F. Giaconia (2015), Slab rupture and delamination under the Betics and Rif constrained from receiver functions, Tectonophysics, 663, 225-237.

Manighetti, I., P. Tapponnier, V. Courtillot, S. Gruszow, and P. Y. Gillot (1997), Propagation of rifting along the Arabia-Somalia plate boundary: The Gulfs of Aden and Tadjoura, J. Geophys. Res., 102, 2681-2710.

Mann, P., L. Gahagan, and M. B. Gordon (2003), Tectonic setting of the world's giant oil and gas fields, in Giant oil and gas fields of the decade 1990-1999, ed. by Halbouty, M. T., AAPG Memoir, 78, 15-105.

McClusky, S., R. Reilinger, S. Mahmoud, D. Ben Sari, and A. Tealeb (2003), GPS constraints on Africa (Nubia) and Arabia plate motions, Geophys. J. Int., 155, 126-138.

McConnell, R. B. (1972), Geological development of the rift system of eastern Africa, Bull. Geol. Soc. Am., 83, 2549-2572.

McKenzie, D., and C. Bowin (1976), The relationship between bathymetry and gravity in the Atlantic Ocean, J. Geophys. Res., 81, 1903-1915.

McKenzie, D. P. (1978), Some remarks on the development of sedimentary basins, Earth Planet. Sci. Lett., 40, 25-32.

McKenzie, G. D., H. Thybo, and P. K. H. Maguire (2005), Crustal velocity structure across the Main Ethiopian Rift: Results from two-dimensional wide-angle seismic modeling, Geophys. J. Int., 162, 994-1006.

McNutt, M. K. (1998), Superswells, Rev. Geophys., 36(2), 211-244, doi:10.1029/98RG00255.

Mechie, J., K. Abu-Ayyash, Z. Ben-Avraham, R. El-Kelani, A. Mohsen, G. Rümpker, J. Saul, and M. Weber (2005), Crustal shear velocity structure across the Dead Sea Transform from two-dimensional modeling of DESERT project explosion seismic data, Geophys. J. Int. 160, 910-924.

Meier, U., A. Curtis, and J. Trampert (2007), Global crustal thickness from neural network inversion of surface wave data, Geophys. J. Int., 169, 706-722.

Meissner, R. (1986), The Continental Crust: A Geophysical Approach, Int. Geophys. Ser. Acad. Press, 34, 1-426.

Meyers, J. B., B. R. Rosendahl, C. G. A. Harrison, and Z. D. Ding (1998), Deep-imaging seismic and gravity results from offshore Cameroon Volcanic Line and speculation of African hot-lines, Tectonophysics, 284, 31-63.

Mériaux, C. A., J. C. Duarte, S. S. Duarte, W. P. Schellart, Z. Chen, F. Rosa, J. Mata, and P. Terrinha (2015), Capture of the Canary mantle plume material by the Gibraltar arc mantle wedge during slab rollback, Geophys. J. Int., 201(3), 1717-1721.

Michaut, C., and J. C. Jaupart (2004), Nonequilibrium temperatures and cooling rates in thick continental lithosphere, Geophys. Res. Lett., 31, doi:10.1029/ 2004GL021092.

Midzi, V., and L. Ottemöller (2001), Receiver function structure beneath three Southern Africa seismic broadband stations, Tectonophysics, 339, 443-454.

Milani, E. J., and De Wit. (2008), Correlations between the classic Parana' and Cape-Karoo sequences of South America and southern Africa and their basin infills flanking the Gondwanides: du Toit revisted, in West Gondwana: Pre-Cenozoic Correlations Across the South Atlantic Region, ed. by Pankhurst, R. J. et al., Geol. Soc. Publ., 294, 319-342.

Milesi, J. P., D. Frizon de Lamotte, G. de Kock, and F. Toteu (2010), Tectonic map of Africa, 1:10 000 000 scale. CCGM-CGMW, Paris.

Miller, M. S., A. A. Allam, T. W. Becker, J. F. Di Leo, and J. Wookey (2013),

Constraints on the tectonic evolution of the westernmost Mediterranean and northwestern Africa from shear wave splitting analysis, Earth Planet. Sci. Lett., 375, 234-243.

Miller, M. S., L. O'Driscoll, A. J. Butcher, and C. Thomas (2015), Imaging Canary Island hotspot material beneath the lithosphere of Morocco and southern Spain, Earth Planet. Sci. Lett., 431,186-194.

Mohorovičić, A. (1910), "Epicenters of earthquakes in Croatia and Slavonia (Epicentra potresa u Hrvatskoj i Slavoniji)", Yearly report of the Zagreb meteorological observatory for the year 1909.

Mohr, P., and B. Zanettin (1988), The Ethiopian flood basalt province, in Continental Flood Basalts, ed. by Macdougall, J.D., Kluwer, Dordrecht, 63-110.
Molnar, P., P. C. England, and C. H. Jones (2015), Mantle dynamics, isostasy, and the support of high terrain, J. Geophys. Res. Solid Earth, 120, 1932-1957.

Mooney, W. D., G. Laske, and G. Masters (1998), CRUST-5.1: a global crustal model at 5º x 5º, J. Geophys. Res., 103, 727-747.

Morelli, C., and R. Nicolich (1990), A cross section of the lithosphere along the European Geotraverse Southern Segment (from the Alps to Tunisia), Tectonophysics, 176, 229-243.

Morley, C. K. (1999), Influence of preexisting fabrics on rift structure, in Geoscience of Rift Systems Evolution of East Africa, ed. by Morley, C. K., AAPG Studies in Geology, 44, 151-160.

Morgan, P. (1984), The thermal structure and thermal evolution of the continental lithosphere, in Structure and Evolution of the Continental Lithosphere, ed. By Pollack, H. N., and V. R. Murthy, Phys. and Chem. Earth, 15, 107-193.

Morgan, P., and J. H. Sass (1984), Thermal regime of continental lithosphere, J. Geodynam., 1, 137-151.

Morley, C. K. (1999), Influence of preexisting fabrics on rift structure, in Geoscience of Rift Systems Evolution of East Africa, ed. by Morley, C. K., Am. Assoc. Petr. Geol. Stud. Geol., 44, 151-160.

Moucha, R., and A. M. Forte (2011), Changes in African topography driven by mantle convection, Nature, 4(10), 707-712.

Nair, S. K., S. S. Gao, K. H. Liu, and P. G. Silver (2006), Southern African crustal evolution and composition: constraints from receiver function studies, J. Geophys. Res., 111, B02304.

Nataf, H. C., and Y. Ricard (1996), 3SMAC: an a priori tomographic model of the upper mantle based on geophysical modeling, Phys. Earth. Planet. Int., 95, 101-122.

Ngako, V., E. Njonfang, F. T. Aka, P. Affaton, and J. M. Nnange (2006), The North-South Paleozoic to Quaternary trend of alkaline magmatism from Niger-Nigeria to Cameroon: complex interaction between hotspots and Precambrian faults, J. Afr. Earth Sci., 45, 241-256.

Nguuri, T. K., J. Gore, D. E. James, S. J. Webb, C. Wright, T. G. Zengeni, Gwavava, J. A. Snoke, and Kaapvaal Seismic Group (2001), Crustal structure beneath southern Africa and its implications for the formation and evolution of the Kaapvaal and Zimbabwe cratons, Geophys. Res. Lett., 28, 2501-2504.

Ni, S., E, Tan, M. Gurnis, and D. Helmberger (2002), Sharp sides to the African superplume, Science, 296, 1850-1852.

Niu, F., and D. E. James (2002), Fine structure of the lowermost crust beneath the Kaapvaal Craton and its implications for crustal formation and evolution, Earth Planet. Sci. Lett., 200, 121-130.

Nocquet, J. M., and E. Calais (2003), The crustal velocity field in Western Europe from permanent GPS array solutions, 1996-2001, Geophys. J. Int., 154, 72-88.

Nolet, G. R., R. Montelli, G. Masters, F. A. Dahlen, and S. Hung, (2003), Finite frequency tomography shows a variety of plumes, Geophys. Res. Abstr., 5, 03146.

Nyblade, A. A., and S. W. Robinson (1994), The African Superswell, Geophys. Res. Lett. 21, 765-768.

Nyblade, A. A., and C. A. Langston (2002), Broadband seismic experiments probe the East African Rift, Eos Trans. AGU, 83, 405-408, doi:10.1029/2002EO000296.

Nyblade, A. A., and N. Sleep (2003), Long lasting epeirogenic uplift from mantle plumes and the origin of the Southern African Plateau, Geochem. Geophys. Geosyst., 4(12), 1105.

Okereke, C. S. (1984), A gravity study of the lithospheric structure beneath the West Africa rift system in Nigeria and Cameroon, PhD Thesis, Univ. of Leeds, UK, 272p.

Oldenburg, D. W. (1974), Inversion and interpretation of gravity anomalies, Geophysics, 39, 526-536.

O'Reilly, S. Y., and W. L Griffin (2010), The continental lithosphere-asthenosphere boundary. Can we sample it?, Lithos, 120, 1-13.

O'Reilly, S. Y., and W. L Griffin (2013), Moho vs. Crust-Mantle Boundary: Evolution of an idea, Tectonophysics, 609, 535-546.

Pail, R., H. Goiginger, W. D. Schuh, E. Höck, J. M. Brockmann, T. Fecher, T. Gruber, T. Mayer-Gürr, J. Kusch, A. Jgi, and D. Rieser (2010), Combined satellite gravity field model GOCO01S derived from GOCE and GRACE, Geophys. Res. Lett., 37, L20314.

Palomeras, I., S. Thurner, A. Levander, K. Liu, A. Villaseñor, R. Carbonell, and M. Harnafi (2014), Finite-frequence Rayleigh wave tomography of the western Mediterranean: Mapping its lithospheric structure, Geochem. Geophys. Geosyst., 15, 140-160.

Parker, R. L. (1973), The rapid calculation of potential anomalies, Geophys. J. R. Astron. Soc., 31, 447-455.

Parsiegla, N., J. Stankiewicz, K. Gohl, T. Ryberg, and G. Uenzelmann-Neben (2009), Southern African continental margin: Dynamic processes of a transform margin, Geochem. Geophys. Geosyst., 10, Q03007, doi:10.1029/2008GC002196.

Pasyanos, M. E., and A. A. Nyblade (2007), A top to bottom lithospheric study of Africa and Arabia, Tectonophysics, 444, 27-44.

Pasyanos, M. E. (2010), Lithospheric thickness modeled from long period surface wave dispersion, Tectonophysics, 481, 38-50, doi:10.1016/j.tecto.2009.02.023.

Pasyanos, M. E., T. G. Masters, G. Laske, and Z. Ma (2014), LITHO1.0: An updated crust and lithospheric model of the Earth, J. Geophys. Res., 119(3), 2153-2173, doi:10.1002/2013JB010626.

Pavlis, N. K., S. A. Holmes, S. C. Kenyon, and J. K. Factor (2012), The development and evaluation of the Earth Gravitational Model 2008 (EGM2008), J. Geophys. Res., 117, B04406.

Pearson, D. G., R. W. Carlson, S. B. Shirey, F. R. Boyd, and P. H. Nixon (1995), Stabilisation of Archaean lithospheric mantle: A Re-Os isotope study of peridotite xenoliths from the Kaapvaal craton, Earth Planet. Sci. Lett., 15, 341-357.

Pérez-Gussinyé, M., M. Metois, M. Fernàndez, J. Vergés, J. Fullea, and A. R. Lowry (2009), Effective elastic thickness of Africa and its relationship to other proxies for lithospheric structure and surface tectonics, Earth Planet. Sci. Lett., 287(1-2), 152-167.

Pik, R., B. Marty, and D. R. Hilton (2006), How many mantle plumes in Africa? The geochemical point of view, Chem. Geol., 226, 100-114.

Plomerova, J., D. Kouba, and V. Babuska (2002), Mapping the lithosphere - asthenosphere boundary through changes in surface-wave anisotropy, Tectonophysics, 358, 175-185.

Pollack, H. N., and D. S. Chapman (1977), On the regional variation of heat flow, geotherms, and lithospheric thickness, Tectonophysics, 38, 279-296.

Pontevivo, A., and H. Thybo (2006), Test of the upper mantle low-velocity layer in Siberia with surface waves, Tectonophysics 416, 113-131.

Pratt, J. H. (1855), On the attraction of the Himalaya Mountains and of the regions beyond the plump-line in India, Philo. Trans. R. Soc. London, 145, 53.

Priestley, K. (1999), Velocity structure of the continental upper mantle: evidence from southern Africa, Lithos, 48, 45-56.

Priestley, K., and D. McKenzie (2006), The thermal structure of the lithosphere from shear wave velocities, Earth Planet. Sci. Lett., 244, 285-301.

Priestley, K., D. McKenzie, E. Debayle, and S. Pilidou, (2008), The African upper

mantle and its relationship to tectonics and surface geology, Geophys. J. Int., 175, 1108-1126.

Priestley, K., and F. Tilmann (2009), Relationship between the upper mantle high velocity seismic lid and the continental lithosphere, Lithos, 109(1-2), 112-124.

Priestley, K., and D. McKenzie (2013), The relationship between shear wave velocity, temperature, attenuation and viscosity in the shallow part of the mantle, Earth Planet. Sci. Lett., 381, 78-91.

Prodehl, C., B. Jacob, H. Thybo, E. Dindi, and R. Stangl (1994), Crustal structure on the northeastern flank of the Kenya rift, in: Crustal and Upper Mantle Structure of the Kenya Rift, ed. by Prodehl, C. et al., Tectonophysics, 236, 271-290.

Prodehl, C., J. R. R. Ritter, M. Mechie, G. R. Keller, M. A. Khan, B. Jacob, K. Fuchs, I. O. Nyambok, J. D. Obel, and D. Riaroh (1997), The KRISP 93/94 lithospheric investigations of southern Kenya-The experiments and their main results, Tectonophysics, 278, 121-147.

Pysklywec, R. N., and J. X. Mitrovica (1999), The role of subduction induced subsidence in the evolution of the Karoo Basin, J. Geol., 107, 155-164.

Rabbel, W., M. Kaban, and M. Tesauro (2013), Contrasts of seismic velocity, density and strength across the Moho, Tectonophysics, 609, 437-455.

Reguzzoni, M., D. Sampietro, and F. Sans (2013), Global Moho from the combination of the CRUST2.0 model and GOCE data, Geophys. J. Int., 195(1), 222-237.

Reid, A. B., J. Ebbing, and S. J. Webb (2012), Comment on ‘A crustal thickness map of Africa derived from a global gravity field model using Euler deconvolution’ by Tedla, G. E., M. van der Meijde, A. A. Nyblade and F. D. van der Meer, Geophys. J. Int., 189(3), 1217-1222, doi:10.1111/j.1365-246X.2012.05353.x.

Reusch, A. M., A. A. Nyblade, D. A. Wiens, P. J. Shore, B. Ateba, C. T. Tabod, and J. M. Nnange (2010), Upper mantle structure beneath Cameroon from body wave tomography and the origin of the Cameroon Volcanic Line, Geochem. Geophys. Geosyst., 11, Q10W07.

Ricard, Y., M. Richards, C. Lithgow-Bertelloni, and Y. Le Stuenff (1993), A geodynamic model of mantle density heterogeneity, J. Geophys. Res., 98, 21895-21909.

Rihm, R., J. Makris, and L. Möller (1991a), Seismic surveys in the northern Red Sea: asymmetric crustal structure, Tectonophysics, 198, 279-295.

Rihm, R., J. Makris, Y. A. Izzeldin, M. Bobsien, K. Meier, P. Junge, T. Noman, and W. Warsi (1991b), Contrasting structural styles of the eastern and western margins of the southern Red Sea: the 1988 SONNE experiment, Tectonophysics, 198, 329-353.

Ring, U. (1994), The influence of preexisting crustal anisotropies on the evolution of the Cenozoic Malawi rift (East African rift system), Tectonics, 13, 313-326.

Ritsema, J., H. J. van Heijst, and J. H. Woodhouse (1999), Complex shear velocity structure imaged beneath Africa and Iceland, Science, 286, 1925-1928.

Ritsema J., and H. J. van Heijst (2000), New seismic model of the upper mantle beneath Africa, Geology, 28, 63-66.

Ritsema, J., and R. Allen (2003), The elusive mantle plume, Earth Planet. Sci. Lett., 207, 1-12.

Ritzwoller, M., N. Shapiro,, M. Barmin, and A. Levshin (2002), Global surface wave diffraction tomography, J. Geophys. Res., 107(B12), 2335.

Robert, A., M. Fernàndez, I. Jiménez-Munt, and J. Vergés (2015), Lithospheric structures in Central Eurasia derived from elevation, geoid anomaly and a thermal analysis, Geol. Soc. Spec. Publ., 427, doi.org/10.1144/SP427.10.

Roberts, D. G., and A. W. Bally (2012), Regional geology and tectonics: Phanerozoic passive margins, cratonic basins and global tectonic maps, Burlington: Elsevier Science.

Rogers, N., R. McDonald, J. G. Fitton, R. George, M. Smith, and B. Barreiro, (2000), Two mantle plumes beneath the East African rift system: Sr, Nd and Pb isotope evidence from Kenya Rift basalts, Earth Planet. Sci. Lett., 176, 387-400.

Rooney, T. O., B. B. Hanan, D. W. Graham, T. Furman, J. Blichert-Toft, and J. G.

Schilling (2012), Upper Mantle Pollution during Afar Plume-Continental Rift Interaction, J. Petrol., 53, 365-389.

Root, B. C., W. van der Wal, P. Novák, J. Ebbing, and L. L. A. Vermeersen (2014), Glacial isostatic adjustment in the static gravity field of Fennoscandia, J. Geophys. Res. Solid Earth, 120, 503-518, doi:10.1002/2014JB011508.

Rosenbaum, G., and G. S. Lister (2004), Neogene and Quaternary rollback evolution of the Tyrrhenian Sea, the Apennines, and the Sicilian Maghrebides, Tectonics, 23, TC1013.

Royer, J. Y., and M. F. Coffin (1992), Jurassic to Eocene plate tectonic reconstructions in the Kerguelen plateau region, Proc. Ocean Drill. Program Sci. Results, 120, 917-928.

Rudnick, L. R., and A. A. Nyblade (1999), The thickness and heat production of Archean lithosphere: Constraints from xenolith thermobarometry and surface heat flow, in Mantle Petrology: Field Observations and High Pressure Experimentation: A Tribute to Francis R. (Joe) Boyd, ed. by Y. Fei, Y. et al. Chem. Soc. Spec. Publ., 6, 3-12.

Rychert, C. A., and P. M. Shearer, P.M (2009), A global view of the lithosphere-asthenosphere boundary, Science, 324, doi:10.1126/science.1169754.

Sandvol, E., D. Seber, A. Calvert, and M. Barazangi, (1998), Grid search modeling of receiver functions: Implications for crustal structure in the Middle East and North Africa, J. Geophys. Res., 103, 26899-26917.

Sandwell, D. T., and W. H. F. Smith (1997), Marine gravity anomaly from Geosat and ERS 1 satellite altimetry, J. Geophys. Res., 102(B5), 10039-10054.

Savage, B., and P. G. Silver (2008), Evidence for a compositional boundary within the lithospheric mantle beneath the Kalahari craton from S receiver functions, Earth Planet. Sci. Lett., 272, 600-609.

Schilling, J. G. (1973), Afar mantle plume: rare earth evidence, Nature, 242, 2-5.

Schmitz, M. D., and S. A. Bowring (2004), Lower crustal granulite formation during Mesoproterozoic Namaqua-Natal collisional orogenesis, southern Africa, S. Afr. J.

Geol., 107, 175-190.

Schoene, B., M. J. deWit, and S. A. Bowring (2008), Mesoarchean assembly and stabilization of the eastern Kaapvaal craton: A structural-thermochronological perspective, Tectonics, 27, TC5010.

Sebai, A., E. Stutzmann, J. P. Montagner, D. Sicilia, and E. Beucler (2006), Anisotropic structure of the African upper mantle from Rayleigh and Love wave tomography, Phys. Earth Planet. Int., 155, 48-62.

Sengör, A. M. C., and K. Burke (1978), Relative timing of rifting and volcanism on Earth and its tectonic implications, Geophys. Res. Lett., 5, 419-421, doi:10.1029/GL005i006p00419.

Shang, C. K., G. Morteani, M. Satir, and H. Taubald (2010), Neoproterozoic continental growth prior to Gondwana assembly: constraints from zircon-titanite geochronology, geochemistry and petrography of ring complex granitoids, Sudan, Lithos, 118, 61-81.

Shapiro, N. M., and M. H. Ritzwoller (2002), Monte-Carlo inversion for a global shear velocity model of the crust and upper mantle, Geophys. J. Int., 151(1), 88-105.

Simiyu, S. M., and G. R. Keller (1997), An integrated analysis of lithospheric structure across the East African plateau based on gravity anomalies and recent seismic studies, Tectonophysics, 278, 291-313.

Simmons, N. A., A. M. Forte, and S. P. Grand (2007), Thermo-chemical structure and dynamics of the African super-plume, Geophys. Res. Lett., 34, L02301.

Simmons, N., A. Forte, and S. P. Grand (2009), Joint seismic, geodynamic and mineral physical constraints on three-dimensional mantle heterogeneity: Implications for the relative importance of thermal versus compositional heterogeneity, Geophys. J. Int., 177, 1284-1304.

Soller, D. R., R. D. Ray, and R. D. Brown (1982), A new global crustal thickness model, Tectonics, 1, 125-149.

Spada, M., I. Bianchi, E. Kissling, A. Piana Agostinetti, and S. Wiemer (2013),

Combining controlled-source seismology and receiver function information to derive 3-D Moho topography for Italy, Geophys. J. Int., 194(2), 1050-1068.

Spakman, W., and R. Wortel (2004), A tomographic view on western Mediterranean geodynamics, in The Transmed Atlas, the Mediterranean Region from Crust to Mantle, ed. By Cavazza, W. et al., 31-52, Springer, Berlin.

Spieker, K., I. Wölbern, C. Thomas, M. Harnafi, and L. E. Moudnib (2014), Crustal and upper mantle structure beneath the western Atlas Mountains in SW Morocco derived from receiver functions, Geophys. J. Int., 198(3), 1474-1485.

Stankiewicz, J., T. Ryberg, N. Parsiegla, K. Gohl, R. Trumbull, and M. Weber (2008), Crustal structure of the Southern Margin of the African Plate: Results from Geophysical Experiments, J. Geophys. Res., 113, B10313.

Steinhart, J. (1967), Mohorovičićic discontinuity, Int. Dict. Geophys., 2. 991-994.

Stuart, G. W., and T. G. Zengeni (1987), Seismic crustal structure of the Limpopo mobile belt, Tectonophysics, 144, 323-335.

Stuart, G. W., I. D. Bastow, and C. J. Ebinger (2006), Crustal structure of the Northern Main Ethiopian rift from receiver function studies, in The Afar Volcanic Province within the East African Rift System, ed. by Yirgu, G. et al., Geol. Soc. Spec. Publ., 259, 253-267.

Tadili, B., M. Ramdani, B. Sari, K. Chapochnikov, and A. Bellot (1986), Structure de la croute dans le nord du Maroc, Ann. Geophys., 4 (1), 99-104.

Tedla, G. E., M. van der Meijde, A. A. Nyblade, and F. van der Meer (2011), A crustal thickness map of Africa derived from a global gravity field model using Euler deconvolution, Geophys. J. Int., 187, 1-9.

Teixell A., P. Ayarza, H. Zeyen, M. Fernàndez, and M. L. Arboleya (2005), Effects of mantle upwelling in a compressional setting: the Atlas Mountains of Morocco, Terra Nova, 17, 456-461.

Tenzer R., W. Chen, D. Tsoulis, M. Bagherbandi, L. E. Sjöberg, P. Novák, and S. Jin (2015), Spectral and spatial characteristics of the refined CRUST1.0 gravity field, Surv. Geophys., 36, 139-165.

Thorpe, R. S. and K. Smith (1974), Distribution of Cenozoic volcanism in Africa, Earth Planet. Sci. Lett., 22, 91- 95.

Tokam, A. P. K., C. T. Tabod, A. A. Nyblade, J. Julià, D. A. Wiens, and M. E. Pasyanos (2010), Structure of the crust beneath Cameroon, West Africa, from the joint inversion of Rayleigh wave group velocities and receiver functions, Geophys. J. Int., 183(2), 1061-1076.

Torne, M., M. Fernàndez, J. Vérges, C. Ayala, M. C. Salas, I. Jimenez-Munt, and G. G. Buffet (2015), Crustal and mantle lithosphere structure from potential field and thermal analysis, Tectonophysics, 663, 419-433.

Trampert, J., and J. Woodhouse (2003), Global anisotropic phase velocity maps for fundamental mode surface waves between 40 and 150 s, Geophys. J. Int., 154(1), 154-165.

Tugume, F., A. A. Nyblade, J. Julia, and M. van der Meijde (2013), Crustal shear wave velocity structure and thickness for Archean and Proterozoic terranes in Africa and Arabia from modeling receiver functions, surface wave dispersion, and satellite gravity data, Tectonophysics, 609, 250-266.

Turcotte, D. L., and G. Schubert (2002), Geodynamics: Applications of Quantum Physics to Geological Problems, John Wiley and Sons, New York, 456p.

van der Meijde M., S. van der Lee, and D. Giardini (2003), Crustal structure beneath broad-band seismic stations in the Mediterranean region, Geophys. J. Int., 152, 729-739, doi:10.1046/j.1365-246X.2003.01871.x.

van der Meijde, M., and A. A. Nyblade (2014), Reply to “Comment on ‘A crustal thickness map of Africa derived from a global gravity field model using Euler deconvolution”’. In: Geophys. J. Int., 196(1), 96-99, doi:10.1093/gji/ggt450.

van der Meijde, M., I. E. A. M. Fadel, P. Ditmar, and M. Hamayun (2015), Uncertainties in crustal thickness models for data sparse environments: A review for South America and Africa, J. Geodyn., 84, 1-18.

Vening Meinesz, F. A. (1931), Une nouvelle methode pour la reduction isostatique regionale de l’intensite de la pesanteur, Bull. Géodésique, 29, 33-51.

Vening Meinesz F. A. (1940), Fundamental Tables for Regional Isostatic Reduction of Gravity Values, Publ. Netherlands Acad. Sci., 1, 1-44.

Vergés, J., and F. Sàbat (1999), Constraints on the Neogene Mediterranean kinematic evolution along a 1000 km transect from Iberia to Africa, in The Mediterranean Basins: Tertiary Extension within the Alpine Orogen, ed. by Durand, B. et al., Geol. Soc. Spec. Publ., 156, 63-80.

Vergés, J., and M. Fernàndez (2012), Tethys-Atlantic interaction along the Iberia-Africa plate boundary: The Betic-Rif orogenic system, Tectonophysics, 579, 144-172.

Vilà, M., M. Fernàndez, and I. Jiménez-Munt (2010), Radiogenic heat production variability of some common lithological groups and its significance to lithospheric thermal modeling, Tectonophysics, 490, 152-164.

Villeneuve, M. (2005), Paleozoic basins in West Africa and the Mauritanide thrust belt, J. Afr. Earth. Sci., 43, 166-195.

Vinnik, L., S. Oreshin, G. Kosarev, S. Kiselev, and L. Makeyeva (2009), Mantle anomalies beneath southern Africa: Evidence from seismic S and P receiver functions, Geophys. J. Int., 179(1), 279-298.

Visser, J. N. J. (1997), A review of the Permo-Carboniferous glaciation in Africa, in Deglaciation and Global Changes: Quaternary, Permo-Carboniferous and Proterozoic, ed. by Martini, I. P., Oxford Univ. Press, 169-191.

Waldhauser, F., E. Kissling, J. Ansorge, and S. Mueller (1998), Three-dimensional interface modelling with two-dimensional seismic data: the Alpine crust-mantle boundary, Geophys. J. Int., 135, 264-278.

Wang, Y., L. Wen, and D. Weidner (2008), Upper mantle SH- and P-velocity structures and compositional models beneath southern Africa, Earth Planet. Sci. Lett., 267, 596-608.

Waters, C. N., and D. I. Schofield (2004), Contrasting Late Neoproterozoic to Ordovician successions of the Taoudeni Basin, Mauritania and Souss Basin, Morocco: the influence of eustatic versus tectonic controls on sedimentation, J. Afr.

Earth Sci., 39, 301-309.

Watts, A. B. (2001), Isostasy and Flexure of the Lithosphere, Cambridge, Cambridge University Press, 458p.

Webb, S. J., R. G. Cawthorn, T. Nguuri, and D. James (2004), Gravity modeling of Bushveld Complex connectivity supported by Southern African Seismic Experiment results, S. Afr. J. Geol., 107, 207-218.

Weeraratne, D., D. Forsyth, K. Fischer, and A. A. Nyblade (2003), Evidence for an upper mantle plume beneath the Tanzanian craton from Rayleigh wave tomography, J. Geophys. Res., 108(B9), 2427, doi:10.1029/2002JB002273.

Wigger, P., G. Asch, P. Giese, W. D. Heinsohn, S. O. El Alami, and F. Ramdani (1992), Crustal structure along a traverse across the Middle and High Atlas mountains derived from seismic refraction studies, Geol. Rundschau, 81(1), 237-248.

Willmore, P. L., A. L. Hales, and P. G. Gane (1952), A seismic investigation of crustal structure in the western Transvaal, Bull. Seis. Soc. Am., 42, 53-80.

Wilson, M., and R. Guiraud (1992), Magmatism and Rifting in Western and Central Africa, from Late Jurassic to Recent Times, Tectonophysics, 213, 203-225.

Wittlinger, G., and V. Farra (2007), Converted waves reveal a thick and layered tectosphere beneath the Kalahari super-craton, Earth Planet. Sci. Lett., 254, 404-415.

Wölbern, I., G. Rümpker, A. Schumann, and A. Muwanga (2010), Crustal thinning beneath the Rwenzori region, Albertine rift, Uganda, from receiver-function analysis, Int. J. Earth Sci., 99, 1545-1557.

Woodhouse, J. H., and A. M. Dziewonski (1984), Mapping the upper mantle: Three dimensional modeling of Earth structure by inversion of seismic waveforms, J. Geophys. Res., 89, 5953-5986.

Wopfner, H. (2002), Tectonic and climatic events controlling deposition in Tanzanian Karoo basins, J. Afr. Earth. Sci., 34, 167-177.

Wortel, M. J. R., and W. Spackman (2000), Subduction and slab detachment in the Mediterranean-Carpathian region, Science, 290, 1910-1917.

Wright, J. A., and J. Hall (1990), Deep seismic profiling in the Nosop Basin, Botswana: cratons, mobile belts and sedimentary basins, Tectonophysics, 173, 333-343.

Wright, C., E. M. Kgaswane, M. T. O. Kwadiba, R. E. Simon, T. K. Nguuri, and R. McRae-Samuel (2003), South African seismicity, April 1997-April 1999, and regional variations in the composition of the crust and uppermost mantle, Lithos, 71, 369-392.

Youssof, M., H. Thybo, I. M. Artemieva, and A. Levander (2013), Moho depth and crustal composition in Southern Africa, Tectonophysics, 609, 267-287.

Zeyen, H., P. Ayarza, M. Fernàndez, and A. Rimi (2005), Lithospheric structure under the western African-European plate boundary: A transect across the Atlas Mountains and the Gulf of Cadiz, Tectonics, 24, doi:10.1029/2004TC001639.

Zhao, D. (2001), Seismic structure and origin of hotspots and mantle plumes, Earth Planet. Sci. Lett., 192, 251-265.

Zhou, Y., G. Nolet, F. A. Dahlen, and G. Laske (2006), Global upper-mantle structure from finite-frequency surface-wave tomography, J. Geophys. Res.,111, B04304, doi:10.1029/2005JB003677.